Physics – Uspekhi **56** (5) 429 – 464 (2013)

REVIEWS OF TOPICAL PROBLEMS PACS numbers: 52.35.Mw, 52.38.Ph, 52.59.Ye

Relativistic mirrors in plasmas. Novel results and perspectives

S V Bulanov, T Zh Esirkepov, M Kando, A S Pirozhkov, N N Rosanov *

DOI: 10.3367/UFNe.0183.201305a.0449

Contents

S V Bulanov Kansai Photon Science Institute, Japan Atomic Energy Agency, 8-1-7 Umemidai, Kizugawa-shi, Kyoto-fu 619-0215, Japan
Tel. +81 774-71-3005
Fax +81 774-71-3316
E-mail: bulanov.sergei@jaea.go.jp
Prokhorov Institute of General Physics, Russian Academy of Sciences, ul. Vavilova 38, 119991 Moscow, Russian Federation
T Zh Esirkepov, M Kando, A S Pirozhkov Kansai Photon Science Institute, Japan Atomic Energy Agency, 8-1-7 Umemidai, Kizugawa-shi, Kyoto-fu 619-0215, Japan
N N Rosanov Vavilov State Optical Institute, Kadetskaya liniya V.O. 5/2, 199053 Saint Petersburg, Russian Federation;
Saint Petersburg National Research University of Information Technologies, Mechanics, and Optics, Kronverkskii prosp. 49, 197101 Saint Petersburg, Russian Federation;
Ioffe Physical-Technical Institute, Russian Academy of Sciences, ul. Politekhnicheskaya 26, 194021 Saint Petersburg, Russian Federation
E-mail: nrosanov@yahoo.com

Received 17 July 2012
Uspekhi Fizicheskikh Nauk **183** (5) 449 – 486 (2013)
DOI: 10.3367/UFNr.0183.201305a.0449
Translated by S V Bulanov; edited by A M Semikhatov

Abstract. Relativistic flying mirrors in plasmas are thin, dense electron or electron–ion layers accelerated by high-intensity electromagnetic waves to velocities close to the speed of light in the vacuum; in nonlinear media, refractive index modulations are induced by a strong electromagnetic wave. The reflection of the electromagnetic wave from the relativistic mirror results in its energy and frequency changing. In the counter-propagation configuration, the frequency of the reflected wave is multiplied by the factor proportional to the gamma-factor squared. This scientific area promises the development of sources of ultrashort X-ray pulses in the attosecond range. The expected intensity will reach the level at which the effects predicted by nonlinear quantum electrodynamics start to play a key role. In the co-propagating configuration, the energy of the electromagnetic wave is transferred to the ion energy, providing a highly efficient acceleration mechanism.

1. Introduction

The sources of electromagnetic radiation from microwaves to X-rays and gamma rays are in high demand for various

* Also transliterated as N N Rozanov in some sources.

applications, as well as due to fundamental interest. Currently, the brightest X-ray radiation is generated by synchrotron sources during ultrarelativistic electron motion in a magnetic field. A new generation of free-electron lasers, which use ultrarelativistic electrons produced by linear accelerators of charged particles, can emit X-ray photon beams with a brightness several orders of magnitude higher than that of X-rays produced by synchrotrons. The Linac Coherent Light Source (LCLS) at Stanford University uses 14 GeV energy electrons from the kilometer-long linear electron accelerator. In the process of electron beam interaction with the ondulator (a system of periodically located magnets), electrons emit pulses of coherent X-ray radiation with the photon energy equal to 8 keV, the pulse length from 1 to 200 fs, and the intensity of the order of 10^{20} W cm^{-2}.

The maximal energy of charged particles that can be achieved under conditions on Earth is 7 TeV, which is the energy of protons accelerated by the Large Hadron Collider (LHC) at CERN. With a size of 27 km, the LHC can provide the hadron beam luminosity (the reaction rate divided by the cross section) equal to 10^{34} cm^{-2} s^{-1}, which exceeds the luminosity of beams generated by the previous generation of accelerators by two orders of magnitude. Such luminosity was one of main reasons that allowed the discovery of the Higgs boson.

Each new generation of accelerators aimed at basic research is characterized by parameters greatly exceeding the ones of the previous generation. However, ultimately, there are questions of the accelerator size and cost. As regards the question of the maximum achievable size (and the maximum energy of charged particles), Enrico Fermi pointed out in the middle of the 1950s that the maximum energy would be approximately 10^{15} eV for an accelerator length equal to the circumference of Earth's equator — the maximal accelerator size on Earth. This follows from the requirement that the amplitude of the accelerating electric field not cause a vacuum breakdown.

In the middle of the 1950s in the USSR, Ya B Fainberg, A M Budker, and V I Veksler proposed several methods of collective acceleration of charged particles. These methods are based on the idea of using electric fields excited in plasma media, which can provide a substantially higher acceleration rate, in turn resulting in a decrease in the accelerator size. In particular, Veksler considered the charged particle acceleration by the radiation pressure of a strong electromagnetic wave acting on an electron–ion bunch [1].

The idea of transferring the electromagnetic wave momentum to matter was formulated by Lebedev and Eddington [2, 3]. There is also a strong analogy between the radiation acceleration of charged particles and the 'light sail', proposed by Zander for propulsion of spacecraft intended for interplanetary and interstellar travel [4].

The work by Veksler had a strong influence on the development of plasma physics and charged particle acceleration methods (see, e.g., [5]). For a plasma target with a size smaller than the electromagnetic wave length, the radiation pressure force acting on it is proportional to the square of the electric charge of the target. When an electromagnetic wave interacts with a substantially large target, the radiation pressure force does not depend on the electric charge and becomes equal to the radiation pressure times the irradiated surface area. In the limit of relativistic ion energies, the acceleration process is similar to light interaction with a receding relativistic mirror. Due to the double Doppler effect, the energy of the reflected light is much lower than the energy of the wave incident on the mirror. The electromagnetic energy is therefore transferred to the ions with high efficiency. A compact ion accelerator of this type finds application in nuclear physics [6], controlled fusion [7], and medicine [8].

As a result of the electromagnetic wave reflection by a counter-propagating relativistic mirror (in the head-on wave–mirror collision configuration), the reflected electromagnetic pulse is compressed in the longitudinal direction and its carrier frequency is upshifted, as was shown by Einstein [9], i.e., in this case, the mirror transfers momentum to the electromagnetic field. This regime is of substantial interest for developing compact sources of coherent radiation in the ultraviolet and X-ray range of photon energies.

There are a number of publications discussing various aspects of light interaction with relativistic mirrors, beginning with papers on the interpretation of the Michelson–Morley experiments and on radiolocation problems and ending with those devoted to quantum field theory. As an example, we note articles by Davies and Fulling on the calculation of the properties of radiation emitted by an accelerated mirror [10], on a discussion of its relation to the Hawking effect [11] and Unruh radiation [12], and paper [13] on the nonstationary Casimir effect. As regards applications, the electromagnetic field intensification and the frequency upshift are attractive for research on the development of sources of radiation with tunable parameters. It is therefore not surprising that the question of relativistic mirror formation in laboratory conditions has been raised repeatedly in the past [14–16]. Currently, it is also attracting much attention. First of all, relativistic electron beams [17, 18] and ionization fronts propagating with a relativistic speed [19–25] have been considered as candidates for such mirrors.

Experimental results on relativistic mirror realization in the case of ionization waves propagating in configurations with a static inhomogeneous electric field have been reported in a number of papers. During the interaction with the static electric field, the ionization wave is converted into an electromagnetic wave [23]. In the experiments presented in Refs [24, 25], the frequency of the emitted wave is in the terahertz range (the 1 THz frequency corresponds to the wave period equal to 10^{-12} s). The frequency upshift of the radiation reflected by the ionization front formed by the oblique incidence of the ionizing radiation on the target was observed in Ref. [26]. The authors of Ref. [27] discuss the possibility of radar detection of ultra-high-energy cosmic rays by using electromagnetic wave reflection at the front of the ionized region produced by extensive air showers generated by cosmic rays.

The typical parameters of relativistic electron beams and ionization waves — the front width and the electron density — realized in experimental conditions were such that the electromagnetic wave frequency corresponded to the microwave range. For the reflection of electromagnetic radiation in the optical range of the wave frequency, the electron density has to be significantly higher than the density that can be achieved in electron beams from conventional accelerators.

The question arises as to whether it is possible to generate a relativistic mirror of a sufficiently high quality for efficient reflection of light, which can move with large velocity in order to provide a significant frequency upshift to the photon

energy in the X-ray range. The answer to this question can be found in the field of the physics of nonlinear processes in relativistic laser plasmas.

Progress in laser technologies resulted in the development of laser facilities providing laser radiation with an intensity ensuring the relativistic regime of laser–matter interaction, which allowed developing compact sources of hard electromagnetic radiation and compact accelerators of charged particles that are used, in particular, for studying fundamental physics and processes of key importance for astrophysics. Discussions of the results obtained in these fields can be found in numerous recently published review articles (see, e.g., [28–33]).

Under the conditions typical for the interaction of high-intensity electromagnetic waves with plasmas, the nonlinear character of this interaction results in the formation of electron density modulations in the form of high-density bunches and thin layers moving with a relativistic velocity. Interaction of the electromagnetic radiation with these relativistic objects can be regarded as the wave reflection by relativistic mirrors [34, 35], which is accompanied by a relativistic frequency shift and change in the reflected wave amplitude. This is the underlying mechanism of high-order harmonic generation in relativistic collisionless plasma, which is based on the oscillating relativistic mirror concept [36] (see review article [37] and the references therein), of the generation of attosecond pulses of electromagnetic radiation [38–40], and of frequency upshift and wave intensification [35, 41–46]. The ultimate goal of these studies is the development of a compact source of high-intensity X-ray radiation, which is required by a broad range of applications, from molecular imaging [47], which is of high interest for medicine and biology, to the diagnostics of thermonuclear plasmas and experiments on laboratory astrophysics [48] and the experimental study of nonlinear effects of quantum electrodynamics [49].

2. Reflection of an electromagnetic wave from a relativistic mirror

2.1 Uniformly moving mirror

The change in the frequency and amplitude of an electromagnetic wave reflected by a moving mirror occurs due to the double Doppler effect. The corresponding theory of light reflection from a mirror moving in the vacuum with an arbitrary (subluminal) velocity v_M ($v_M < c$, where c is the speed of light in the vacuum) is formulated in Einstein's paper on the special theory of relativity [9]. It presents a classic illustration of an application of the Lorentz transformation formalism for solving problems of electrodynamics.

The process of an electromagnetic wave reflection from a relativistic mirror is characterized by several remarkable features. According to Ref. [9] (see also [50]), the frequency of a reflected wave depends on the incidence angle and the mirror velocity as

$$\omega_r = \omega_0 \frac{1 + 2\beta_M \cos\theta_0 + \beta_M^2}{1 - \beta_M^2}, \qquad (1)$$

where ω_0 and ω_r are the frequency of the light incident on the mirror and the frequency of reflected waves, θ_0 is the incidence angle, and $\beta_M = v_M/c$ is the mirror velocity normalized to the speed of light in the vacuum. The reflection angle θ_r is related to the incidence angle as

$$\sin\theta_r = \frac{\omega_0}{\omega_r}\sin\theta_0 = \frac{(1-\beta_M^2)\sin\theta_0}{1 + 2\beta_M\cos\theta_0 + \beta_M^2}. \qquad (2)$$

During the wave–mirror interaction, the ratio of the amplitude of the electric field to its frequency is constant:

$$\frac{E_r}{\omega_r} = \frac{E_0}{\omega_0}. \qquad (3)$$

Here and below, indices '0' and 'r' denote the parameters of the radiation incident on the mirror and reflected in the laboratory frame.

Depending on whether the wave and mirror are co-propagating ($\beta_M < 0$) or counter-propagating ($\beta_M > 0$) in the laboratory frame, we have either frequency downshift or frequency upshift, stretching or compression of the electromagnetic pulse, and a decrease or increase in the wave energy. In the simplest configuration of normal incidence of the wave on the mirror ($\theta_0 = 0$), expression (1) yields

$$\omega_r = \omega_0 \frac{1+\beta_M}{1-\beta_M} = \omega_0(1+\beta_M)^2\gamma_M^2,$$

where $\gamma_M = (1-\beta_M^2)^{-1/2}$ is the relativistic gamma-factor of the mirror. In the ultrarelativistic limit $\gamma_M \gg 1$, the reflected wave frequency is higher (lower) by a factor $\approx 4\gamma_M^2$. The reflected wave energy changes accordingly.

2.2 Accelerated mirror

We consider the wave reflection from an accelerated mirror in the case of normal incidence. The incident and reflected waves are described by the transverse component of the vector potential $A(x,t) = A_0(t - x/c) + A_r(t + x/c)$. The mirror coordinate at time t is determined by the equation $\mathcal{M}(x,t) = \text{const}$, i.e., the mirror is located at the point $x = x_M(t)$ (Fig. 1a).

The solution of the wave equation with the boundary conditions $A(x_M(t), t) = 0$ at $x = x_M(t)$ can be written in the form [51]

$$A(x,t) = A_0\left[\exp(-i\omega_0 v) - \exp\left(-i\int^u \omega_r(u)\,du\right)\right], \qquad (4)$$

where the coordinates u and v are

$$u = t - \frac{x}{c}, \qquad v = t + \frac{x}{c}. \qquad (5)$$

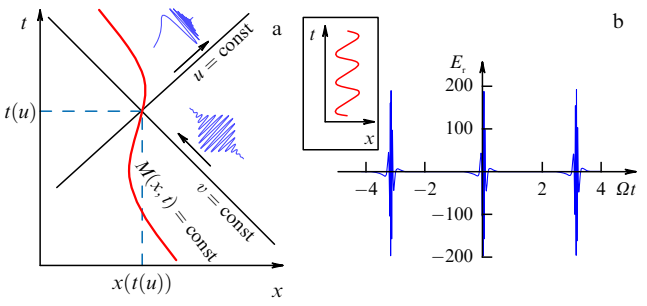

Figure 1. (a) Mirror coordinates (x,t) as functions of the variable $u = t - x/c$, with $v = t + x/c$. b) The electric field of the wave reflected from the oscillating mirror with $\Omega/\omega_0 = 1$ and $a = 10$. The inset shows the oscillating mirror position in the (x,t) plane.

The reflected-wave phase $\psi_r(u) = \int^u \omega_r(u)\,\mathrm{d}u$ is given by $\psi_r(u) = \omega_0(2t(u) - u)$, which follows from Eqns (5) and the relation $\psi_r(u)/\omega_0 = 2t(u) - u = u + 2x(t(u))/c$. From Eqns (5), we obtain the dependence of the time $t(u)$ on the coordinate u of the intersection of lines $u = \text{const}$ and $v = \text{const}$, with the mirror trajectory given by $t(u) = u + x_M(t(u))/c$. Here, $x_M(t(u))$ is the coordinate of the intersection point (see Fig. 1a). From these relations, it also follows that $\omega_0 v = \psi_r(u)$. Differentiating this expression with respect to time, we find

$$\psi_r'(u) = \omega_0 \frac{1 + \beta_M(u)}{1 - \beta_M(u)}\,, \tag{6}$$

where $\beta_M(u) = \mathrm{d}x_M(t(u))/c\,\mathrm{d}t$ is the mirror velocity normalized to c. The derivative of the phase with respect to u in Eqn (6) is nothing more than the frequency of the reflected wave, ω_r.

Differentiating expression (4) with respect to time, we can find a relation between the electric field $E = -(\partial A/\partial t)/c$ in the incident and reflected waves:

$$E_r = -E_0 \frac{1 + \beta_M(t)}{1 - \beta_M(t)}\,, \tag{7}$$

where $\beta_M(t) \equiv \beta_M(u(t))$, which corresponds to relation (3).

In the case of a mirror moving with a constant velocity, i.e., for $x_M(t) = v_M t$, expressions (6) and (7) are equivalent to Eqn (1) for $\theta_0 = 0$ and Eqn (3) for the electric field.

When the mirror moves with a uniform acceleration w_M, the dependence of its coordinate on time is given by $x_M(t) = (c/w_M)(m^2c^2 + w_M^2 t^2)^{1/2}$ [52]. In this case, the frequency of light reflected from the uniformly accelerated mirror, in the limit $t \to \infty$, increases proportionally to the square of the time of positive acceleration, $w_M > 0$, and decreases inversely proportional to the square of the time of negative acceleration, $w_M < 0$:

$$\omega_r = \omega_0 \frac{\sqrt{m^2c^2 + w_M^2 t^2} + w_M t}{\sqrt{m^2c^2 + w_M^2 t^2} - w_M t} \underset{t\to\infty}{\approx} \begin{cases} \dfrac{4\omega_0 w_M^2 t^2}{m^2c^2}\,, & w_M > 0\,, \\ \dfrac{\omega_0 m^2 c^2}{4 w_M^2 t^2}\,, & w_M < 0\,. \end{cases} \tag{8}$$

The amplitude of the reflected wave increases (decreases) in a similar way. In Refs [45, 53], these dependences were respectively obtained by integrating the wave equation along the characteristics and by using the Rindler transformation to the accelerated frame of reference.

2.3 Oscillating mirror

When a wave is reflected from a relativistic mirror, its frequency spectrum extends to the high-frequency range [36] and the wave breaks up into short wave packets. According to Eqn (6), the wave frequency increases by a factor approximately equal to $4\gamma_M^2$. The maximum electric field increases by the same factor according to Eqn (7).

As an illustration of this process, we consider a thin electron layer oscillating under the action of a linearly polarized electromagnetic wave with the electric field parallel to the y axis:

$$E_y = E_0 \cos\left[\Omega\left(t + \frac{x}{c}\right)\right].$$

The second electromagnetic wave is reflected from the electron layer as from the mirror. To describe the electron layer motion, we use the results of an exact solution of the problem of electric charge dynamics in the field of an electromagnetic wave [52], which yields parametric dependences of the charge coordinates and momentum components on time:

$$\begin{aligned} &x = \frac{a_0^2}{4(2 + a_0^2)} \sin 2\eta\,, \qquad y = \frac{a_0}{\sqrt{1 + a_0^2/2}} \cos\eta\,, \\ &t = \eta + \frac{a_0^2}{4(2 + a_0^2)} \sin 2\eta\,, \qquad p_x = \frac{a_0^2}{4\sqrt{1 + a_0^2/2}} \cos 2\eta\,, \\ &p_y = a \sin\eta\,, \qquad z = 0\,, \qquad p_z = 0\,. \end{aligned} \tag{9}$$

Here, the coordinates and time are normalized to c/Ω and Ω^{-1}, $\eta = \Omega v$, the momentum is measured in $m_e c$ units, and the normalized amplitude of the wave is $a_0 = eE_0/m_e\Omega c$.

Using solution (9), we can calculate the phase and frequency of the reflected wave and find the electric field $E_r(t) = \omega_0^{-1}\psi_r'(t)\cos(\psi_r(t))$, which is shown in Fig. 1b in the case of a constant-amplitude incident wave. The reflected radiation is given by a sequence of wave packets with the frequency approximately equal to $\omega_0 a_0^2/2$ in the limit $a_0 \gg 1$ and with the wave packet duration $\approx 2\pi/\Omega a_0$. Here, we assume that the second wave propagates in the direction opposite to the direction of the wave that drives the mirror oscillations.

If the second wave and the wave driving the mirror oscillations propagate in the same direction, then the electric field in the reflected wave is given by a sequence of short pulses with the width $\approx \pi/a_0\Omega$ with no high-frequency component. We note that the generation of ultrashort electromagnetic pulses under similar conditions was observed in computer simulations of the relativistically strong electromagnetic wave interaction with an overdense plasma target [38].

3. Fundamentals of the parametric Doppler effect theory

If the mirror moves not in the vacuum but in a continuous medium, then the Doppler effect acquires novel properties, first of all due to the frequency dispersion of the medium.

The parametric Doppler effect corresponds to the media that are not moving, in which the electromagnetic radiation is reflected from or scattered by the moving inhomogeneities of the medium [54, 55]. The medium dispersion effects in the case of a moving source and detector lead to the complex Doppler effect, found by Frank [56]. For a moving mirror, this means that several frequencies in the reflected radiation can correspond to a single frequency in the incident wave. The Doppler shift of the wave reflected from the shock wave front has been analyzed in Refs [57, 58]. Finally, in [59], the authors considered the problem of the Doppler transformation of the frequency of relatively weak radiation reflected by a high-intensity pulse of self-induced transparency in the gas of three-level atoms.

In this section, we present a detailed discussion of the parametric Doppler effect for a small-amplitude wave reflection from medium modulations moving with a relativistic velocity [57, 60–66]. We consider the propagation of weak radiation in a nonstationary medium with the dielectric permittivity ε and the magnetic permeability μ, both depen-

dent on time and coordinates. We assume that the modulations move with the velocity v_M in the positive ($v_M > 0$) and negative ($v_M < 0$) direction along the x axis.

Fast moving (relativistic) modulations can be induced in nonlinear media by high-intensity laser pulses or by temporal solitons. The fast-response medium with a cubic nonlinearity can be considered as an example. In fact, we can disregard the specific origin of a moving inhomogeneity and analyze the linear problem of weak radiation reflection from a given inhomogeneity. This approximation is valid if we can neglect the energy depletion of the high-intensity pulse driving the inhomogeneity.

We further assume that the electromagnetic radiation is linearly polarized, with the electric and magnetic fields given by $\mathbf{E} = E\mathbf{e}_y$ and $\mathbf{H} = H\mathbf{e}_z$, where $\mathbf{e}_y$ and $\mathbf{e}_z$ are unit vectors along the y and z axis. In this case, the Maxwell equations reduce to the form

$$\partial_x H = -\frac{1}{c}\frac{\partial D}{\partial t}\,, \qquad \partial_x E = -\frac{1}{c}\frac{\partial B}{\partial t}\,, \tag{10}$$

where $D = E + 4\pi P = \hat{\varepsilon}E$ and $B = H + 4\pi M = \hat{\mu}H$ are the electric and magnetic inductions. The operator form of $\hat{\varepsilon}$ and $\hat{\mu}$ reflects the dependence of the dielectric permittivity ε and the magnetic permeability μ on frequency (this is the frequency dispersion). At the discontinuities of the medium modulations moving with the velocity $v_M = c\beta_M$, we have boundary conditions corresponding to the continuity of the functions [69]

$$E - \beta_M B\,, \qquad H - \beta_M D\,. \tag{11}$$

In the medium regions where the dielectric permittivity and the magnetic permeability do not depend on the coordinate, Maxwell equations (10) have a solution in the form of plane waves. Below, we consider regimes in which the radiation field consists of several monochromatic plane waves with complex wave numbers k and frequencies ω (the meaning of a complex frequency is explained below). The dispersion equation, which gives a relation between the wave number and the wave frequency, can be written in the standard way:

$$k^2c^2 = \omega^2\varepsilon\mu\,. \tag{12}$$

To find the wave number from Eqn (12), we must specify the sign of the square root. When the wave has the energy flux averaged over the optical period (the Poynting vector) along the positive direction of the x axis and the field components are proportional to $\exp(\mathrm{i}kx - \mathrm{i}\omega t)$, we have

$$kc = \omega\mu Y\,, \tag{13}$$

where we introduce the inverse impedance

$$Y = \sqrt{\frac{\varepsilon}{\mu}}\,, \qquad \mathrm{Re}\, Y \geqslant 0\,. \tag{14}$$

In these relations, the dielectric permittivity ε and the magnetic permeability μ of the medium can also be complex functions. Evidently, for a wave carrying the energy in the opposite direction, the wave number has the sign opposite to that in (13).

3.1 Asymptotic behavior of the field and the Doppler frequency shift

We assume that the inhomogeneity is localized in space. In this case, there is no inhomogeneity in the region of the medium at $x \to -\infty$, where the medium is homogeneous and the radiation has the form of a superposition of incident and reflected plane waves. In what follows, we distinguish between the cases of counter-propagating and co-propagating interaction. We show that in order to find the frequency shift under the conditions of the parametric Doppler effect, it suffices to know the dispersion properties of the medium in the homogeneous region and the velocity of the inhomogeneities.

3.2 Regime of homogeneous plane waves

We assume that the field configuration is given by a plane monochromatic wave propagating in the direction normal to the inhomogeneity, which is moving along the x axis. Indices 0 and r denote the incident and reflected waves. In the homogeneous region, at $x \to \infty$, the asymptotic representation of the radiation fields has the form

$$\begin{aligned}
E &= E_0 \exp\left[\mathrm{i}(k_0 x - \omega_0 t)\right] + E_\mathrm{r} \exp\left[\mathrm{i}(-k_\mathrm{r} x - \omega_\mathrm{r} t)\right],\\
H &= Y_0 E_0 \exp\left[\mathrm{i}(k_0 x - \omega_0 t)\right] - Y_\mathrm{r} E_\mathrm{r} \exp\left[\mathrm{i}(-k_\mathrm{r} x - \omega_\mathrm{r} t)\right],\\
D &= \varepsilon_0 E_0 \exp\left[\mathrm{i}(k_0 x - \omega_0 t)\right] + \varepsilon_\mathrm{r} E_\mathrm{r} \exp\left[\mathrm{i}(-k_\mathrm{r} x - \omega_\mathrm{r} t)\right],\\
B &= n_0 E_0 \exp\left[\mathrm{i}(k_0 x - \omega_0 t)\right] - n_\mathrm{r} E_\mathrm{r} \exp\left[\mathrm{i}(-k_\mathrm{r} x - \omega_\mathrm{r} t)\right].
\end{aligned} \tag{15}$$

Here, we use the inverse impedance given by Eqn (14) and introduce the refractive indices $n_{0,\mathrm{r}} = \mu_{0,\mathrm{r}} Y_{0,\mathrm{r}}$, assuming that $\varepsilon_{0,\mathrm{r}}\mu_{0,\mathrm{r}} > 0$ for incident and reflected waves, as well as the wave numbers of these waves $k_{0,\mathrm{r}} = (\omega_{0,\mathrm{r}}/c)n_{0,\mathrm{r}}$. The wave frequencies are different due to the Doppler effect. We first consider the case of a head-on interaction where the wave number of the reflected wave k_r is positive.

Expressions (15) are valid up to the inhomogeneity boundary moving with the velocity v_M. It is convenient to use a step function to approximate the inhomogeneity profile. At the boundary of the first step, i.e., at $x = x_b = v_M t$, the functions determined by Eqns (11) are continuous. Their continuity implies that at $x = v_M t$, the exponents in Eqns (15) should be the same. This yields a relation between the frequencies in the incident and reflected waves:

$$\omega_0(1 + \beta_M n_0) = \omega_\mathrm{r}(1 - \beta_M n_\mathrm{r})\,. \tag{16}$$

In Eqn (16), the incident wave frequency ω_0 and the refractive index value n_0 at this frequency are known. Using this fact, we can use Eqn (16) to find the frequency of the reflected wave ω_r for which we should additionally specify the velocity of the inhomogeneity motion v_M and the dispersion, i.e., the dependence $n_\mathrm{r}(\omega_\mathrm{r})$. But it is more convenient to rewrite Eqn (16) in the form

$$\beta_M = \frac{\omega_0 - \omega_\mathrm{r}}{\omega_0 n_0 + \omega_\mathrm{r} n_\mathrm{r}}\,. \tag{17}$$

In this equation, with an arbitrary dispersion, it suffices to vary the reflected wave frequency ω_r and to find the velocity of the inhomogeneity motion v_M. Although the function $v_M(\omega_\mathrm{r})$ is single-valued according to Eqn (17), the inverse function $\omega_\mathrm{r}(v_M)$ can be multi-valued, which corresponds to the complex Doppler effect. In that case, the equation for the frequency corresponding to a certain value of the velocity of the inhomogeneity motion can have several solutions or no solutions at all.

To illustrate our results, we consider an unmagnetized medium with the magnetic permeability $\mu = 1$ and the frequency dispersion corresponding to the collisionless plasma in the transparency domain:

$$\varepsilon(\omega) = 1 - \frac{\omega_{\rm pe}^2}{\omega^2}\,, \qquad \omega^2 > \omega_{\rm pe}^2\,. \tag{18}$$

In the case under consideration, the refractive index is less than unity, $n(\omega) = \sqrt{\varepsilon(\omega)} < 1$, i.e., the phase velocity $v_{\rm ph}(\omega) = c/n(\omega)$ is greater than the speed of light in the vacuum c in all the transparency domain. We can write Eqn (17) in the form

$$\beta_{\rm M} = \frac{\omega_0 - \omega_{\rm r}}{\sqrt{\omega_0^2 - \omega_{\rm pe}^2} + \sqrt{\omega_{\rm r}^2 - \omega_{\rm pe}^2}}\,, \qquad \omega_{0,\,{\rm r}}^2 > \omega_{\rm pe}^2\,, \tag{19}$$

whence it follows that for the frequency $\omega_{\rm r}$ ranging in the transparency domain from $\omega_{\rm pe}$ to ∞, the velocity $v_{\rm M}$ decreases monotonically from

$$v_{\rm M,\,max} = c\sqrt{\frac{\omega_0 - \omega_{\rm pe}}{\omega_0 + \omega_{\rm pe}}} < c \tag{20}$$

to $-c$, vanishing at $\omega_{\rm r} = \omega_0$. The inverse dependence $\omega_{\rm r}(v_{\rm M})$ in this frequency range is also a single-valued function corresponding to a monotonic decrease of the reflected radiation frequency. At the same time, there is a subluminal interval of the velocities of the inhomogeneity motion

$$v_{\rm M,\,max} \leqslant v_{\rm M} < c\,, \tag{21}$$

to which no real frequency value corresponds. For the velocity in the range given by Eqn (21), Eqn (19) does not have a real-valued solution $\omega_{\rm r}$. In other words, under condition (19), or $\omega_0 < \omega_{\rm min}$, where

$$\omega_{\rm min} = \begin{cases} \dfrac{1+\beta_{\rm M}^2}{1-\beta_{\rm M}^2}\,\omega_{\rm pe}\,, & v_{\rm M} > 0\,, \\ \omega_{\rm pe}\,, & v_{\rm M} < 0\,, \end{cases} \tag{22}$$

the reflected radiation is not a monochromatic wave with a real-valued frequency. A straightforward calculation shows that under this condition, the reflection with a complex-valued frequency does not exist either (see the discussion below).

The dependence of the reflected radiation frequency on the frequency of the incident wave for a given velocity of the inhomogeneity motion is given by

$$\beta_{\rm M}\omega_{\rm r} = \frac{1}{1-\beta_{\rm M}^2}\left[(1-\beta_{\rm M}^2)\omega_0 - 2\beta_{\rm M}\sqrt{\omega_0^2 - \omega_{\rm pe}^2}\,\right], \qquad \omega_0 > \omega_{\rm min}\,. \tag{23}$$

According to Eqn (23), the reflected radiation frequency $\omega_{\rm r}$ monotonically increases with the increase in the incident wave frequency ω_0.

In Fig. 2, we show domain I in the plane of parameters $(\beta_{\rm M}, \omega_0/\omega_{\rm pe})$, which corresponds to the above regime of head-on interaction. This regime can be realized for arbitrary negative and for not very large positive values of the inhomogeneity velocity. As the analysis in Ref. [67] shows, when the inhomogeneity motion velocity and the incident wave frequency enter domain II (see Fig. 2), the 'reflected' wave is characterized by a negative value of the wave number $k_{\rm r}$, i.e., the energy flux of this wave is in the same direction as

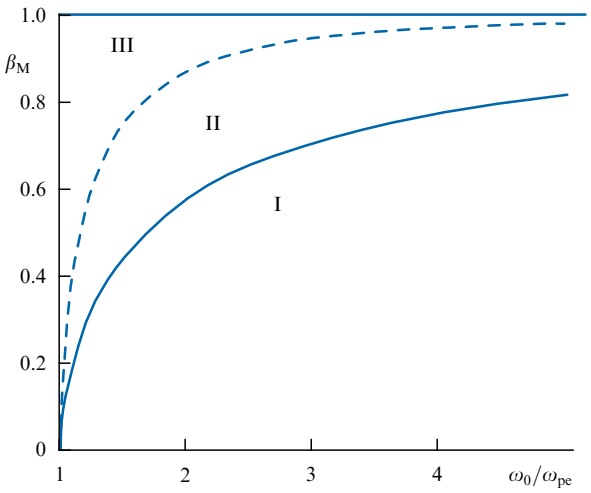

Figure 2. Subdivision of the plane of parameters — the inhomogeneity motion velocity $\beta_{\rm M} = v_{\rm M}/c$ and the incident wave frequency $\omega_0/\omega_{\rm pe}$ — into three domains corresponding to different regimes of the wave reflection: I, reflection in the counter-propagating configuration; II, reflection in the co-propagating configuration; III, the 'no-reflection' regime.

the incident radiation. The upper limit of the inhomogeneity velocity in this regime is determined by the condition $v_{\rm M}/c = (1 - \omega_{\rm pe}^2/\omega_0^2)^{1/2}$. Above this limit, there are no solutions describing the monochromatic wave reflection from a moving inhomogeneity. The 'no-reflection' regime corresponds to domain III in Fig. 2.

The physical meaning of 'exotic' regimes can be elucidated if we consider the reflection of a quasimonochromatic radiation, i.e., the reflection of a finite-length optical pulse carrying a large number of optical oscillations [67] (see Section 3.3 below) instead of the monochromatic wave interaction with a moving inhomogeneity.

The co-propagating reflection regime (corresponding to domain II in Fig. 2) occurs because the carrier frequency of the pulse decreases during reflection of the wave from the receding inhomogeneity, which for the dispersion given by (18) results in a decrease in the wave group velocity to the limit below the velocity of the inhomogeneity motion.

Next, the 'no-reflection' regime corresponding to domain III in Fig. 2 is realized when the group velocity of the incident wave is less than the velocity of the inhomogeneity. In this case, the incident electromagnetic pulse does not catch up with the moving inhomogeneity region. It is obvious that this conclusion is valid for the reflection of the main part of the wave packet, because a finite-length pulse always contains a small contribution from the high-frequency radiation reflected by a moving inhomogeneity. We note that the superluminal inhomogeneity emits Vavilov–Cherenkov radiation [68]. Under the conditions of weak dissipation, this leads to the optical phase conjugation phenomenon [69].

In the foregoing, we neglected the effects of spatial dispersion, i.e., the refractive index dependence on the coordinates (on the wave number). These effects become important in the limit where the refractive index of the medium vanishes, which corresponds to the inhomogeneity velocity $v_{\rm M} = v_{\rm M,\,max}$. Taking the spatial dispersion effects into account, we can describe phenomena such as the longitudinal (plasma) wave generation and Landau damping in collisionless plasmas. We note that in the case of oblique

incidence configurations, a transformation of the transverse wave energy into the energy of plasma waves accompanied by electromagnetic wave absorption becomes possible [70].

3.3 Regime of inhomogeneous plane waves

Here, in contrast to the previous subsection, we allow the wave number of plane waves to be complex, which can be realized either in dissipative media or in an optically transparent medium in the regime of total internal reflection, e.g., in the limit of a sufficiently low frequency for wave dispersion (18). We use a complex form of the field representation with the time dependence $\exp(-\mathrm{i}\omega t)$. We consider the case where the inhomogeneity region is localized at $x > x_\mathrm{b} = v_\mathrm{M} t$. Then in the region $x < x_\mathrm{b}$ where the medium is homogeneous, the dependence on time and the coordinate of the incident wave is given by $\exp(\mathrm{i}k_0 x - \mathrm{i}\omega_0 t)$. The reflected wave is described by $\exp(-\mathrm{i}k_\mathrm{r} x - \mathrm{i}\omega_\mathrm{r} t)$. Here, the wave numbers $k_{0,\mathrm{r}} = k(\omega_{0,\mathrm{r}})$ are determined from Eqns (13) and (14).

A condition for the exponents similar to that in Eqn (16) follows from the requirement of the continuity of the electric and magnetic field combinations determined by Eqns (11). This is equivalent to the condition that the phases of the incident and reflected waves are equal to each other at $x = x_\mathrm{b}$:

$$k_\mathrm{r} v_\mathrm{M} = \omega_0 - \omega_\mathrm{r} - k_0 v_\mathrm{M} \,. \tag{24}$$

The condition equivalent to (17) now has a complex form resulting in two equations

$$v_\mathrm{M} = \mathrm{Re}\,\frac{\omega_0 - \omega_\mathrm{r}}{k_0 + k_\mathrm{r}} \,, \qquad \mathrm{Im}\,\frac{\omega_0 - \omega_\mathrm{r}}{k_0 + k_\mathrm{r}} = 0 \,. \tag{25}$$

Taking Eqns (11) and (12) into account, we conclude that expressions (25) are the equations for the reflected wave frequency ω_r. Squaring Eqn (24), we obtain

$$(1 - \beta_\mathrm{M}^2 n_\mathrm{r}^2)\omega_\mathrm{r}^2 - 2(\omega_0 - k_0 v_\mathrm{M})\omega_\mathrm{r} + (\omega_0 - k_0 v_\mathrm{M})^2 = 0 \,. \tag{26}$$

Equations (26) and (17) allow determining the reflected wave frequency ω_r. But these two equations are not equivalent to each other, because the solution of Eqn (26) contains extra roots. Hence, a solution of Eqn (26) must be proved to be relevant, e.g., by using conditions (25).

The possibility of a complex frequency of the reflected wave, which follows from Eqn (26), is an important property of the parametric Doppler effect, whose physical meaning is elucidated by analyzing the time dependence of the wave amplitude. On the boundary of a moving inhomogeneity, the wave is given by

$$\exp\left[-v_\mathrm{M}\,\mathrm{Im}\,(k_0)t\right] \exp\left[-\mathrm{i}\omega_0 t + v_\mathrm{M}\,\mathrm{Re}\,(k_0)t\right] . \tag{27}$$

The real parts of the incident, A_0, and reflected, A_r, waves at the boundary are proportional to the first exponential in Eqn (27). Accordingly, they exponentially decay if $v_\mathrm{M} > 0$, taking into account that $\mathrm{Im}\,k_0 > 0$, or increase with time if $v_\mathrm{M} < 0$. This can be explained as follows. In the regime of inhomogeneous waves propagating in an unbounded medium, the wave amplitude A_0 increases as $x \to \infty$ unlimitedly. A more realistic formulation of the problem under consideration requires taking a finite length of the medium with dispersion into account, i.e., considering, for example, wave incidence from the vacuum region on the medium boundary located at $x = x_0 < x_\mathrm{b}$. At the boundary, we can assume the amplitude of the wave penetrating into the medium with dispersion to be equal to $A_{0,0} = A_0(x = x_0)$. But inside the medium, the amplitude A_0 exponentially decreases with x due to the wave absorption and/or total internal reflection. Hence, the wave amplitude at the medium boundary $x = x_\mathrm{b} = v_\mathrm{M} t$ exponentially decays for $v_\mathrm{M} > 0$ (the distance between the boundary of the inhomogeneity region and the position where the wave enters the medium increases) or exponentially increases for $v_\mathrm{M} < 0$ (the distance between the boundary of the inhomogeneity region x_b and the position where the wave enters the medium decreases).

3.4 Pulse reflection

If the incident radiation can be represented by a pulse with a narrow frequency spectrum with a carrier frequency ω_0, then, in the regime of counter-propagation, the reflected wave frequency ω_r is determined by Eqn (16), the pulse propagation velocity is equal to the group velocity $v_\mathrm{g} = 1/(\mathrm{d}k/\mathrm{d}\omega)|_{\omega=\omega_0}$, and the ratio of the reflected to the incident pulse lengths is

$$q = \left.\frac{\mathrm{d}\omega_\mathrm{r}}{\mathrm{d}\omega_0}\right|_{\omega=\omega_0} = \frac{1}{1-\beta_\mathrm{M}^2}\left[1 + \beta_\mathrm{M}^2 - 2\beta_\mathrm{M}\left(1 - \frac{\omega_\mathrm{pe}^2}{\omega_0^2}\right)\right] . \tag{28}$$

This expression is obtained for dispersion equation (18). Equation (28) shows the possibility of a substantial shortening of the electromagnetic pulse length, accompanied by an upshift of its carrier frequency.

3.5 Reflection coefficient

The coefficient of wave reflection from a moving inhomogeneity is essentially determined by the inhomogeneity spatial profile. The differential equations for the amplitudes of waves propagating in opposite directions have been obtained in Refs [61] and [62], where the wave cross-scattering on the medium inhomogeneity regions was taken into account. It follows from these equations that the amplitude coefficient of the wave reflection from a weak inhomogeneity with the inverse impedance Y is given by

$$\begin{aligned}
\rho &\approx \frac{1}{Y_0^{(+)} + Y_0^{(-)}} \frac{1 - \beta_\mathrm{M} n_0^{(+)}}{1 + \beta_\mathrm{M} n_0^{(-)}} \\
&\times \int_{-\infty}^{+\infty} Y^{(+)}(x) \exp\left[\mathrm{i}(k_0^{(+)} + k_0^{(-)})x\right] \mathrm{d}x \\
&\approx \mathrm{i}\,\frac{k_0^{(+)} + k_0^{(-)}}{Y_0^{(+)} + Y_0^{(-)}} \frac{1 - \beta_\mathrm{M} n_0^{(+)}}{1 + \beta_\mathrm{M} n_0^{(-)}} \\
&\times \int_{-\infty}^{+\infty} \delta Y^{(+)}(x) \exp\left[\mathrm{i}(k_0^{(+)} + k_0^{(-)})x\right] \mathrm{d}x \,,
\end{aligned} \tag{29}$$

where the index '0' denotes the characteristics of an unperturbed homogeneous medium and the indices '$\pm$' are used for incident and reflected waves. The last expression in Eqn (29) was established for a localized inhomogeneity, which has the inverse impedance values $Y^{(+)}(-\infty) = Y^{(+)}(+\infty)$ and $\delta Y^{(+)}(x) = Y^{(+)}(x) - Y^{(+)}(\infty) \to 0$ at $x \to \pm\infty$. For example, in the case of a medium inhomogeneity with the inverse impedance variation equal to $\delta Y^{(+)}(x) = \delta Y_0^{(+)} \cosh^{-2}(x/l_\mathrm{s})$ and with the width l_s, Eqn (29) yields

$$\rho \approx \frac{\mathrm{i}\pi\left[(k_0^{(+)} + k_0^{(-)})l_\mathrm{s}\right]^2}{\sinh\left[\pi(k_0^{(+)} + k_0^{(-)})l_\mathrm{s}/2\right]} \frac{\delta Y_0^{(+)}}{Y_0^{(+)} + Y_0^{(-)}} \frac{1 - \beta_\mathrm{M} n_0^{(+)}}{1 + \beta_\mathrm{M} n_0^{(-)}} \,. \tag{30}$$

The first fraction in the right-hand side of Eqn (30) describes the decrease in the reflection coefficient due to the finite width of the front. As we see, the reflection coefficient decreases exponentially if the inhomogeneity width w is much larger than the wavelength of the incident wave $\lambda_0 = 2\pi/(k_0^{(+)} + k_0^{(-)})$. The second fraction corresponds to the well-known Fresnel reflection from a sharp boundary inhomogeneity, $r \propto \delta\varepsilon/\varepsilon_0$. For the conditions under consideration, this factor is small. Finally, the third fraction represents a resonance growth of the reflection coefficient when the inhomogeneity velocity approaches the phase velocity of the wave in the medium.

Relativistic flying mirrors can be formed not only in collisionless plasmas but also in various nonlinear optical media. In particular, they can be generated in media with a fast-response Kerr nonlinearity, when the refractive index is proportional to the radiation intensity I. As an example, we can consider a high-intensity laser pulse or a soliton propagating with a velocity v_M. The electromagnetic pulse induces a refractive index modulation propagating with the same velocity v_M. For a counter-propagating weak electromagnetic wave, the refractive index inhomogeneity plays the role of a relativistic flying mirror. In such a configuration of the 'optical collider', the frequency and intensity of the weak electromagnetic wave can be upshifted significantly due to the parametric Doppler effect.

To conclude this section, we note that if a high-intensity laser pulse induces a frequency-dependent inhomogeneity of the dielectric permittivity $\hat{\varepsilon}$ and the magnetic permeability $\hat{\mu}$ moving with a relativistic velocity, then the reflected relatively weak radiation undergoes a Doppler frequency shift. Due to the frequency dispersion, the refractive index depends on the wave frequency, $n_r = n_r(\omega_r)$. Equation (16) is an implicit equation [as opposed to explicit equation (18)], from which the frequency of the reflected wave ω_r can be found. The incident wave can propagate either in the direction of the inhomogeneity motion or in the opposite direction. In general, the equation may not have a solution or may have several different solutions. This phenomenon corresponds to the parametric Doppler effect [56], when, for a given incident wave frequency, several reflected waves with different frequencies can exist or regimes can be realized where the reflection of a monochromatic wave is impossible [56].

We note that in the case of inhomogeneous electromagnetic waves with a complex wave number, due to wave absorption or due to total internal reflection, the reflected wave frequency can be complex. This corresponds to the exponential growth or decay of the wave amplitude. There is a possibility of the wave frequency upshift by a factor much larger than unity, not only in relativistic plasmas but also in optical media with fast-response nonlinearities. The reflection coefficient value can be significantly enhanced due to the Bragg effect in the course of reflection from a periodic sequence of isolated inhomogeneity regions [71].

4. Nonlinear electromagnetic and plasma waves

This section contains a summary of the properties of nonlinear electromagnetic and plasma waves in collisionless plasmas, which are to be used below.

Small-amplitude electromagnetic and plasma waves can be described in the linear approximation framework as waves propagating in the plasma without interacting with each other and with their frequencies independent of the wave amplitude. The longitudinal (plasma) wave frequency $\omega_{pe} = \sqrt{4\pi n e^2/m_e}$ does not depend on the wave vector, whence it follows that its group velocity vanishes. The phase velocity of the plasma wave is given by $v_{ph} = \omega_{pe}/k$, while the group velocity is $v_g = \partial\omega/\partial k = \partial\omega_{pe}/\partial k = 0$. The dispersion equation giving the relation between the frequency and the wave number of the transverse (electromagnetic) wave is $\omega = (k^2c^2 + \omega_{pe}^2)^{1/2}$, whence for the phase and group velocities we have $v_{ph}v_g = c^2$ (see Ref. [72]).

For finite-amplitude waves, an exact solution describing wave propagation in cold collisionless plasmas was found in Ref. [72]. The use of the hydrodynamics approximation for describing the electron and ion component dynamics and Maxwell equations for a self-consistent electromagnetic field allowed deriving the system of equations for coupled electromagnetic and plasma waves. This system of equations has the form [72–75]

$$\frac{\partial^2 \mathbf{A}}{\partial t^2} - \Delta\mathbf{A} + \frac{\partial \nabla\varphi}{\partial t} = n_\alpha \mathbf{v}_\alpha - n_e \mathbf{v}_e \,, \tag{31}$$

$$\Delta\varphi = n_e - n_\alpha \,, \tag{32}$$

$$\frac{\partial n_\beta}{\partial t} + n_\beta \nabla \mathbf{v}_\beta = 0 \,, \tag{33}$$

$$\frac{\partial \mathbf{P}_\beta}{\partial t} = -\nabla(\rho_\beta\varphi + \gamma_\beta) + \mathbf{v}_\beta \times \nabla \times \mathbf{P}_\beta \,, \tag{34}$$

where the indices e and α denote the electron and ion components, and the index β can be either e or α. The generalized momentum $\mathbf{P}_\beta$ and the relativistic gamma-factor γ_β are related to the particle momentum $\mathbf{p}_\beta$ and the vector potential $\mathbf{A}$ as $\mathbf{P}_\beta = \mathbf{p}_\beta + \rho_\beta \mathbf{A}$ and $\gamma_\beta = (1 + |\mathbf{p}_\beta|^2)^{1/2}$. The parameter ρ_β is equal to $em_\alpha/e_\alpha m_e$. The velocity of an electron (ion) fluid element is $\mathbf{v}_\beta = \mathbf{p}_\beta/\gamma_\beta$. In this system of equations, the variables are normalized as follows. The units of length and time are c/ω_{pe} and ω_{pe}^{-1}, velocity is normalized to c, momentum to $m_\beta c$, the vector and electrostatic potential to $m_e c/e$, and density to n_0.

In an ansatz corresponding to one-dimensional geometry, the dependence of all functions on the time t and coordinate x is assumed to be of the form $X = x - v_g t$ and $\tau = t - v_g x$, which corresponds to a plane wave propagating with a constant velocity. For simplicity, we assume below that $e_\alpha = |e|$, i.e., $\rho_\beta \equiv -\rho = -m_e/m_\alpha$. Equations for the electromagnetic $A_y + iA_z = a(X)\exp(i\omega\tau)$ and electrostatic $\varphi = \varphi(X)$ potentials can be rewritten in the form [72–75]

$$\varphi'' = \frac{\beta_g}{1-\beta_g^2}\left(\frac{\psi_e}{R_e} - \frac{\psi_\alpha}{R_\alpha}\right), \tag{35}$$

$$a'' + \omega^2 a = a\,\frac{\beta_g}{1-\beta_g^2}\left(\frac{1}{R_e} - \frac{\rho}{R_\alpha}\right), \tag{36}$$

where the prime denotes differentiation with respect to X and $\beta_g = v_g/c$ is the group velocity of the electromagnetic wave normalized to the speed of light in the vacuum c, equal to the phase velocity of the plasma wave. We have also introduced the functions

$$\psi_e = \Gamma_e + \varphi \,, \qquad \psi_\alpha = \Gamma_\alpha - \rho\varphi \,,$$
$$R_e = \sqrt{\psi_e^2 - (1-\beta_g^2)(1+a^2)} \,,$$
$$R_\alpha = \sqrt{\psi_\alpha^2 - (1-\beta_g^2)(1+\rho^2 a^2)} \,,$$

where the constants Γ_e and Γ_α are determined by the boundary conditions. For example, if the field has a constant

amplitude ($a = a_0,\ \varphi = 0$) and the plasma is at rest at $x \to \pm\infty$, then $\Gamma_e = (1 + a_0^2)^{1/2}$ and $\Gamma_\alpha = (1 + \rho^2 a_0^2)^{1/2}$.

The density and the relativistic Lorentz factors of the electron and ion components ($\beta = e, \alpha$) are equal to

$$n_\beta = \beta_\beta \frac{\psi_\beta - \beta_\beta R_\beta}{R_\beta(1 - \beta_g^2)}, \qquad \gamma_\beta = \frac{\psi_\beta - \beta_g R_\beta}{1 - \beta_g^2}. \tag{37}$$

System of equations (35) and (36) has the integral [75]

$$\frac{1 - \beta_g^2}{2}(a'^2 + \omega^2 a^2) + \frac{1}{2}\varphi'^2 + \frac{\beta_g}{1 - \beta_g^2}\left(R_e + \frac{R_\alpha}{\rho}\right) = \text{const}. \tag{38}$$

4.1 Transverse electromagnetic waves

For a transverse wave with a circular polarization, there is a solution of Eqns (35) and (36) for a constant-amplitude wave with $a(X) = a_0$ and $\varphi = 0$, i.e., $A_y = a_0 \cos(\omega\tau)$ and $A_z = a_0 \sin(\omega\tau)$. From Eqn (35), the dependence $\omega^2 = \gamma_g^2(1/\Gamma_e + \rho/\Gamma_\alpha)$ of the wave frequency on the amplitude follows, where $\gamma_g = (1 - \beta_g^2)^{-1/2}$. Using the relation between the phase and group velocity, $v_{ph} v_g = c^2$, and introducing the wave number k for which $v_{ph} = \omega/k$, we can write the dispersion equation for the frequency and wave number of the relativistically intense electromagnetic wave in non-normalized units:

$$\omega^2 = k^2 c^2 + \omega_{pe}^2\left(\frac{1}{\sqrt{1 + a_0^2}} + \frac{\rho}{\sqrt{1 + \rho^2 a_0^2}}\right). \tag{39}$$

As we see, the relativistic effects change the wave frequency, but they do not lead to the appearance of higher-order harmonics in the frequency spectrum. In the field of a circularly polarized electromagnetic wave, electrons rotate with frequency (39). The electron energy is equal to $m_e c^2(1 + a_0^2)^{1/2}$. The longitudinal component of the electron momentum vanishes, and the transverse component is $m_e c a_0$.

In a linearly polarized electromagnetic wave, the transverse and longitudinal components of the electromagnetic field and of the electron momentum are coupled to each other [72, 76]. In a wave of a small but finite amplitude, the transverse component of the electric field oscillates with the frequency $\omega \approx kc + (\omega_{pe}^2/2kc)(1 - a_0^2/2)$ and the longitudinal component oscillates with the doubled frequency, having an amplitude of the order of a_0^2.

Equations describing a plane electromagnetic wave take a particularly simple form if we make the Lorentz transformation to the reference frame moving with the group velocity. In this reference frame, the wave group velocity vanishes and the phase velocity $\bar{v}_{ph} = \bar{\omega}/\bar{k}$, by virtue of the relation $v_{ph} v_g = c^2$, becomes equal to infinity, and hence the wave number also vanishes. This means that all the values depend only on time in this reference frame [77]. Harmonic oscillations with the frequency

$$\bar{\omega} = \omega_{pe}\left(\frac{1}{\sqrt{1 + a_0^2}} + \frac{\rho}{\sqrt{1 + \rho^2 a_0^2}}\right)^{1/2}$$

correspond to a circular-polarization wave. Here, the bar denotes the values in the boosted reference frame. A linearly polarized electromagnetic wave is described by a system of equations of coupled nonlinear oscillators. Oscillations in the longitudinal direction occur at odd harmonics of the fundamental frequency and the frequency spectrum of transverse oscillations comprises the even harmonics.

The circular and linear polarizations are isolated cases: there is no change in the polarization and there is no rotation of the polarization plane. In a relativistically strong wave with elliptical polarization, which also has a longitudinal component of the electric field, rotation of the polarization plane occurs due to the nonlinearly induced birefringence [78, 79]. This process is similar to the Faraday rotation of the polarization plane of the electromagnetic wave propagating through a magnetized medium.

4.2 Longitudinal plasma waves

For a given function $a(X)$, Eqn (35) describes longitudinal waves excited by an electromagnetic pulse. In particular, if $a = a_0 = 0$, this equation describes free Langmuir oscillations. If we neglect the influence of ions for simplicity, the dependence of the relativistic Lorentz factor γ_e of the electrons in the wave on the coordinate, which we redefine for plasma waves as $X = x - v_{ph} t$ because their group velocity is equal to zero, can be represented implicitly as

$$\frac{1}{\sqrt{2}} X = \beta_{ph}\left[(\gamma_m + 1)^{1/2}\mathsf{E}(\Psi|\kappa) - (\gamma_m + 1)^{-1/2}\mathsf{F}(\Psi|\kappa)\right] - (\gamma_m - \gamma_e)^{1/2}. \tag{40}$$

Here,

$$\mathsf{F}(\Psi|\kappa) = \int_0^\Psi (1 - \kappa \sin^2\theta)^{-1/2}\,\mathrm{d}\theta,$$

$$\mathsf{E}(\Psi|\kappa) = \int_0^\Psi (1 - \kappa \sin^2\theta)^{1/2}\,\mathrm{d}\theta$$

are the elliptic integrals of the first and second kinds [80], $\Psi = \pm \arcsin\sqrt{(\gamma_m - \gamma_e)/(\gamma_m - 1)}$ is the amplitude, $\kappa = (\gamma_m - 1)/(\gamma_m + 1)$ is the modulus, and γ_m is the maximum gamma-factor value of electrons in the wave. The wavelength of longitudinal plasma waves is given by

$$\lambda_p = \frac{2^{5/2} v_{ph}}{\omega_{pe}}\left[(\gamma_m + 1)^{1/2}\,\mathsf{E}\left(\frac{\gamma_m - 1}{\gamma_m + 1}\right) - (\gamma_m + 1)^{-1/2}\,\mathsf{K}\left(\frac{\gamma_m - 1}{\gamma_m + 1}\right)\right], \tag{41}$$

where $\mathsf{K}(\kappa)$ and $\mathsf{E}(\kappa)$ are the complete elliptic integrals of the first and second kinds [80]. In the limit of a large amplitude, the wavelength dependence on the parameters is given by $\lambda_p|_{\gamma_m \to \infty} = 2^{5/2}\gamma_m^{1/2} c/\omega_{pe}$, which is equivalent to the dependence of the frequency of plasma oscillations

$$\omega_p\Big|_{\gamma_m \to \infty} = \pi \frac{\omega_{pe}}{2^{3/2}\gamma_m^{1/2}}, \qquad \omega_p\Big|_{\gamma_m \to 1} = \omega_{pe}\left[1 - 3\left(\frac{p_m}{m_e c}\right)^2\right] \tag{42}$$

in the respective limits of large and small values of the amplitudes. Here, the maximum value of the momentum of the electrons in the wave, p_m, is related to the maximum gamma-factor γ_m as $p_m = m_e c(\gamma_m^2 - 1)^{1/2}$.

4.3 General properties of plasma wave breaking

The amplitude of steady-state plasma waves for a given value of the phase velocity v_{ph} cannot be arbitrarily large. It follows from Eqn (40) that the maximum value of the Lorentz factor

γ_m associated with the maximum momentum of the electrons in the wave p_m satisfies the condition

$$\gamma_m = \sqrt{1 + \frac{p_m^2}{m_e^2 c^2}} \leqslant \gamma_{ph} = \frac{1}{\sqrt{1 - v_{ph}^2/c^2}} . \quad (43)$$

This means that the velocity of the particles cannot exceed the phase velocity of the wave. When $\gamma_m \to \gamma_{ph}$, a singularity occurs at which the particle density becomes infinite. The conservation of integral (38) implies the relation $E^2 + 2\gamma_e(m_e\omega_{pe}c/e)^2 = \text{const}$ between the electric field and the electron energy, which in turn imposes a constraint on the electric field in a nonlinear plasma wave:

$$E_{AP} = \frac{m_e\omega_{pe}c}{e}\sqrt{2(\gamma_{ph} - 1)} , \quad (44)$$

which is often referred to as the Akhiezer and Polovin limit value of the field [72].

Because strongly nonlinear wake waves play a key role in the concept of a flying relativistic mirror, we discuss the wave breaking effect below in more detail.

4.4 Breaking of plasma waves due to phase mixing

Nonlinear plasma waves break according to a completely different scenario than finite-amplitude acoustic waves or gravity waves on the surface of water (see Refs [81, 82]). For simplicity, we assume that the amplitude of the plasma wave is nonrelativistic and the ion component is immobile. Equations (35) and (36) in the one-dimensional approximation result in the equations for the electron velocity and the self-consistent electric field,

$$\frac{\partial v}{\partial t} + v\frac{\partial v}{\partial x} = -\frac{eE}{m_e} , \quad (45)$$

$$\frac{\partial E}{\partial t} + v\frac{\partial E}{\partial x} = 4\pi e n(\varepsilon x) v . \quad (46)$$

In these equations, the density of immobile ions $n(\varepsilon x)$ is assumed weakly inhomogeneous with $\varepsilon \ll 1$. Although the transformation to the Lagrangian variables gives a solution of this system in quadratures for arbitrarily large amplitude waves, we solve it by using the perturbation method, in order to find whether harmonics of different orders that appear in higher orders of the perturbation theory are in resonance with each other.

Expanding $v(x, t)$, $E(x, t)$, and $n(\varepsilon x)$ in power series in the small parameter ε, we have

$$\begin{aligned} v &= \varepsilon v^{(1)} + \varepsilon^2 v^{(2)} + \ldots , \\ E &= \varepsilon E^{(1)} + \varepsilon^2 E^{(2)} + \ldots , \\ n &= n_0 + \varepsilon n_0' x + \ldots . \end{aligned} \quad (47)$$

In the first order in the small parameter, the solution of Eqns (45) and (46) is given by

$$v^{(1)} = v_m \sin(\omega_{pe}t - kx) , \quad (48)$$

$$E^{(1)} = -\frac{m_e v_m \omega_{pe}}{e}\cos(\omega_{pe}t - kx) , \quad (49)$$

where v_m is the maximum value of the electron velocity in the wave. In the second order in the small parameter, the equations for $v^{(2)}$ and $E^{(2)}$ that follow from (45) and (46) are

$$\frac{\partial v^{(2)}}{\partial t} + e\frac{E^{(2)}}{m_e} = \frac{v_m^2 k}{2}\sin\left[2(\omega_{pe}t - kx)\right] , \quad (50)$$

$$\frac{\partial E^{(2)}}{\partial t} - 4\pi e n_0 v^{(2)} = \frac{m_e v_m^{(2)}\omega_{pe}k}{2e}\left\{1 - \cos\left[2(\omega_{pe}t - kx)\right]\right\} + 4\pi e n_0' x v_m \sin(\omega_{pe}t - kx) . \quad (51)$$

They have the solution

$$v^{(2)} = -\frac{v_m^2 k}{2\omega_{pe}}\left\{1 - \cos\left[2(\omega_{pe}t - kx)\right]\right\} + \frac{n_0' x v_m}{4n_0}\left[2\omega_{pe}t\cos(\omega_{pe}t - kx) - \sin(\omega_{pe}t - kx)\right] , \quad (52)$$

$$E^{(2)} = -\frac{m_e v_m^2 k}{2e}\sin\left[2(\omega_{pe}t - kx)\right] + \frac{\pi e n_0' x v_m}{\omega_{pe}}\left[2\omega_{pe}t\sin(\omega_{pe}t - kx) - \cos(\omega_{pe}t - kx)\right] . \quad (53)$$

As can be seen, the plasma wave harmonics are not in a resonance in a uniform plasma with $n = \text{const}$, which means that $n_0' = 0$. This follows from the fact that the group and phase velocities of the plasma wave are not equal to each other. The group velocity of the plasma wave in cold plasma vanishes, while the phase velocity is finite and equal to the ratio $v_{ph} = \omega_{pe}/k$. In a homogeneous plasma, the plane plasma wave breaks if its amplitude v_m is so large that the inequality $v_m > v_{ph}$ is satisfied. In an inhomogeneous plasma with $n_0' \neq 0$, the plasma wave, being a wave with a continuous spectrum, breaks for an arbitrarily small but finite amplitude due to phase mixing, leading to an increase in the wave number with time. Formally, the increase in the wave number is described by the second terms in the right-hand sides of Eqns (52) and (53), containing the terms proportional to the time, which corresponds to the resonance between the first and second harmonics. It is easy to show that the subsequent harmonics are also in resonance. This leads to nonlinear steepening of the wave profile and eventually to its breaking.

Phase mixing has a simple explanation. In general, the wave can be represented as $v = v_m \exp(i\psi)$, where $\psi(x, t)$ is its phase or eikonal. The wave number and frequency are respectively equal to the derivative of the eikonal with respect to the coordinate ($k = \partial\psi/\partial x$) and to minus the derivative with respect to time ($\omega = -\partial\psi/\partial t$). The equality of mixed partial derivatives $\partial^2\psi/\partial t\,\partial x = \partial^2\psi/\partial x\,\partial t$ implies the equation

$$\frac{\partial k}{\partial t} = -\frac{\partial\omega}{\partial x} . \quad (54)$$

In a stationary but inhomogeneous medium, the solution of this equation is given by the expression that describes the growth of the wave number $k = k_0 - \omega' t$, where k_0 is its initial value. Because plasma waves can be represented as an ensemble of noninteracting oscillators, the oscillators have different frequencies in a medium with inhomogeneous parameters, which leads to the growth of the phase difference between them. This phenomenon is called phase mixing. As a result of phase mixing, the wave profile is modulated such that the wavelength asymptotically decreases to the limit where the effects of dissipation, dispersion, or nonlinearity

become significant. Nonlinear effects become important when the displacement of electrons in the wave approaches the wavelength value. In a collisionless plasma, neighboring electrons overtake each other, which corresponds to wave breaking, also referred to as the particle trajectory self-intersection. Phase mixing occurs not only due to the inhomogeneity of the plasma but also because of the non-one-dimensional geometry [83]; in the limit of relativistic energies of the electron oscillations, phase mixing occurs due to the plasma wave amplitude inhomogeneity [84].

Here, we analyze the breaking of an arbitrarily large-amplitude plasma wave. In the hydrodynamic approximation, the plasma waves are described by the equations

$$\frac{\partial n}{\partial t} + r^{-s}\,\frac{\partial (r^s n v)}{\partial r} = 0\,, \tag{55}$$

$$\frac{\partial p}{\partial t} + v\,\frac{\partial p}{\partial r} = -E\,, \tag{56}$$

$$\frac{\partial E}{\partial t} + v r^{-s}\,\frac{\partial (r^s E)}{\partial r} = v \tag{57}$$

for the density, the electron momentum, and the electric field. Here, s takes the values 1, 2, 3 for planar, cylindrical, and spherical waves. Planar nonlinear plasma waves are considered in Refs [85, 86], cylindrical in [87], and spherical in Ref. [44]. The nonrelativistic case has been studied in Ref. [83]. The velocity is related to the electron momentum as $v = p/(1+p^2)^{1/2}$. It is normalized to the speed of light in the vacuum c, and the momentum unit is $m_e c$. The electron density n is normalized to the density of immobile ions n_0. The time and coordinate units are respectively ω_{pe}^{-1} and c/ω_{pe}.

Passing from the Euler variables (r, t) to the Lagrange variables (r_0, t), with the derivatives transforming as

$$\left(\frac{\partial}{\partial t}\right)_{\rm L} = \left(\frac{\partial}{\partial t} + v\,\frac{\partial}{\partial r}\right)_{\rm E}\,, \qquad \left(\left(\frac{\partial r}{\partial r_0}\right)^{-1}\,\frac{\partial}{\partial r_0}\right)_{\rm L} = \left(\frac{\partial}{\partial r}\right)_{\rm E}\,,$$

where the indices 'L' and 'E' denote the Lagrange and the Euler variables, allows solving Eqn (55) for the electron density,

$$n = \frac{r_0^s}{(r_0+\xi)^s(1+\partial\xi/\partial r_0)}\,, \tag{58}$$

and Eqn (57) for the electric field,

$$E = \frac{1}{s+1}\left[r_0 + \xi - \frac{r_0^{s+1}}{(r_0+\xi)^s}\right]. \tag{59}$$

Here and below, $\xi(r_0, t)$ is a displacement of the electron fluid element from its intial position r_0. It determines the relation between the Lagrange and the Euler coordinates, $r = r_0 + \xi(r_0, t)$. Using Eqns (58) and (59), equations of electron motion (56) can be rewritten in the Hamiltonian form with the Hamiltonian

$$\mathcal{H}(p, \xi) = (1+p^2)^{1/2} + \Pi(\xi)\,, \tag{60}$$

where the potential function $\Pi(\xi)$ is equal to $(r_0+\xi)^2/2$ for $s=0$, $(r_0+\xi)^2/4 + (r_0^2/2)\ln(r_0+\xi)$ for $s=1$, and $((r_0+\xi)^2/2 + r_0^3/(r_0+\xi))/3$ for spherical waves with $s=2$.

Using the above relations and the fact that the Hamiltonian in Eqn (60) is independent of time, $\mathcal{H} = h$, allows writing the solution of Eqns (55)–(57) in quadratures:

$$t = \int_{\xi_1}^{\xi} \frac{\bigl(h - \Pi(s)\bigr)\,{\rm d}s}{\sqrt{\bigl(h-\Pi(s)\bigr)^2 - 1}}\,. \tag{61}$$

To find the period of nonlinear oscillations, we integrate the right-hand side of Eqn (61) over a whole cycle. In the case of a spherical wave, it is shown in Ref. [44] that the oscillation period in the limit $p_{\max} \gg 1$ is equal to $T = 2\sqrt{6p_{\max}}$. In general, the period, and hence the frequency, depends on the coordinate r_0, which means that the plasma oscillations are waves with a continuous spectrum.

The wave breaking of nonlinear plasma waves corresponds to the vanishing of the Jacobian of the transformation from the Euler to the Lagrange coordinates, which is equal to

$$J = \frac{(r_0+\xi)^s}{r_0^s}\left(1 + \frac{\partial\xi}{\partial r_0}\right). \tag{62}$$

The vanishing condition is $\partial\xi/\partial r_0 = -1$. As follows from Eqn (58), the electron density tends to infinity as $J \to 0$. To estimate the characteristic time of wave breaking, we note that each element of the electron fluid undergoes periodic oscillations, and represent the periodic function describing the electron displacement in the form of a Fourier series [88]:

$$\xi(r_0, t) = \sum_{j=1}^{\infty} \xi_j(r_0)\exp\bigl({\rm i}j\Omega(r_0)t\bigr)\,, \tag{63}$$

with the frequency Ω that depends on the coordinate r_0. The dependence $\Omega(r_0)$, as mentioned above, can be due to the plasma inhomogeneity and/or inhomogeneity of the wave amplitude. Differentiating expression (63) with respect to the coordinate r_0 and time t, we obtain the displacement derivatives

$$\frac{\partial\xi(r_0,t)}{\partial r_0} = \sum_{j=1}^{\infty}\left[\frac{\partial\xi_j(r_0)}{\partial r_0} + {\rm i}t\,\frac{\partial\Omega(r_0)}{\partial r_0}\,j\,\xi_j(r_0)\right]\exp\bigl({\rm i}j\Omega(r_0)t\bigr)\,, \tag{64}$$

$$\frac{\partial\xi(r_0,t)}{\partial t} = \sum_{j=1}^{\infty}\Omega(r_0)\,j\,\xi_j(r_0)\exp\bigl({\rm i}j\Omega(r_0)t\bigr)\,. \tag{65}$$

In the limit $t \to \infty$, these equations yield an asymptotic relation between the space and time derivatives of ξ:

$$\frac{\partial\xi(r_0,t)}{\partial r_0} = t\,\frac{\partial\ln\Omega(r_0)}{\partial r_0}\,\frac{\partial\xi(r_0,t)}{\partial t}\,. \tag{66}$$

It follows that the gradient of the displacement $\partial\xi/\partial r_0$ increases with time, which corresponds to the phase mixing discussed above. In relativistically strong plasma waves, the electron velocity $\partial\xi/\partial t$ changes periodically from c in one half-cycle, to $-c$ in another, and remaines roughly constant during each half cycle. It hence follows that the dependence of the displacement on time has the form of a sawtooth oscillation: the displacement varies from $-\xi_{\max}$ to $\xi_{\max}$, being a linear function of time during the half-cycle, $\xi(t) \approx \pm ct$. This gives the relation $\Omega = \pi c/2\xi_{\max}$ between the amplitude of the oscillations and their frequency. As a result, we find the onset of wave breaking corresponding to the condition $\partial\xi/\partial r_0 = -1$:

$$t_{\rm br} \approx \left(\frac{c}{\partial\ln\Omega(r_0)/\partial r_0}\right)^{-1}. \tag{67}$$

The weaker the inhomogeneity of the wave parameters is, the longer the wave-breaking time.

4.5 Wake wave at the threshold of breaking

Relativistic plasma waves can be excited in plasma in various ways. One of the most widely used methods involves a relatively short high-intensity laser pulse with a length less than or approximately equal to the plasma wavelength, with a sufficiently large normalized wave amplitude (see Ref. [89]). Such a laser pulse propagating in collisionless plasma excites the plasma waves in a wake behind it.

Plasma wakefield excitation by a short laser pulse can also be described by systems of equations (35) and (36). We assume for simplicity that the laser pulse is given, i.e., it propagates in a plasma with a constant speed without changing shape. The solution of Eqn (36) has the form of a wave in which all functions depend on the independent variables x and t in the combination $X = x - v_{\rm ph}t$. Equation (36) under the assumption of fixed ions results in an equation for the longitudinal component of the electron momentum,

$$(\gamma_{\rm e} - p\beta_{\rm ph})'' = \frac{p}{\gamma_{\rm e}\beta_{\rm ph} - p}\,, \tag{68}$$

where the prime denotes differentiation with respect to X. The electron relativistic gamma-factor $\gamma_{\rm e}$ depends on the longitudinal and transverse components of the electron momentum with respect to the wave propagation direction, a and p, as $\gamma_{\rm e} = (1 + a^2 + p^2)^{1/2}$. Here, it is taken into account that the transverse component of the electron momentum is proportional to the corresponding component of the vector potential $a(X)$, due to the homogeneity of the configuration under consideration along the transverse direction. Equation (68) becomes singular when the denominator in the right-hand side vanishes. The singularity corresponds to the case where the electron velocity $p/\gamma_{\rm e}$ becomes equal to the wave phase velocity $\beta_{\rm ph}$, which means wave breaking. In a stationary wave, the singularity occurs at the maximum of the electron velocity $v_{\rm m} = p_{\rm m}/\gamma_{\rm m}$. We let $X_{\rm m}$ denote the wave-breaking coordinate.

To find the structure of the singularity, we expand the electron momentum and the gamma-factor near the singularity at $\delta X = X - X_{\rm m} \to 0$, assuming $\delta p = p_{\rm m} - p$ to be small. We write the electron momentum in the form

$$p = p_{\rm m} + \delta p + O(\delta p^2)\,, \tag{69}$$

where $p_{\rm m} = \beta_{\rm ph}[(1 + a_{\rm m}^2)/(1 - \beta_{\rm ph}^2)]^{1/2}$ and $\delta p/|p_{\rm m}| \ll 1$. Here, $a_{\rm m} = a(X_{\rm m})$ is the vector potential value at the wave-breaking point. Keeping the leading terms on both sides of Eqn (68), we obtain

$$(\delta p^2)'' = -\eta^2\,\frac{1}{\delta p}\,, \tag{70}$$

with $\eta^2 = 2\beta_{\rm ph}\gamma_{\rm ph}^2(1 + a_{\rm m}^2)$. Multiplying the left- and right-hand sides of the equation by $(\delta p^2)'$ and integrating over X, we find

$$\delta p\bigl(2\delta p\,(\delta p')^2 + \eta^2\bigr) = f^2\,, \tag{71}$$

where f is the integration constant. We note that because Eqn (70) has a singularity at $\delta X = 0$, the integration constant can take different values in the regions $\delta X < 0$ and $\delta X > 0$. In general, the properties of a function at a singular point are different depending on whether the product $\delta p\,\delta p'$ vanishes in the limit $\delta p \to 0$.

If the product $\delta p\,\delta p'$ tends to zero as $\delta p \to 0$, which requires the vanishing of the right-hand side of Eqn (71), then this equation with $f = 0$ implies that

$$\delta p = -\left(\frac{3}{2^{3/2}}\,\eta\,\delta X\right)^{2/3} = -\beta_{\rm ph}\gamma_{\rm ph}^3\left(\frac{3\sqrt{1 + a_{\rm m}^2}}{2\beta_{\rm ph}}\,\delta X\right)^{2/3}. \tag{72}$$

For the electron velocity, we then have

$$v = \beta_{\rm ph} - \frac{\beta_{\rm ph}}{\gamma_{\rm ph}}\left(\frac{3(1 + a_{\rm m}^2)^{1/4}}{2\beta_{\rm ph}}\,\delta X\right)^{2/3}. \tag{73}$$

In catastrophe theory, this type of singularity is called the 'cusp catastrophe' [90, 91]. In local coordinates, it can be written as the mapping $y_1 = x_1$, $y_2 = x_2^3 + x_1 x_2$.

Although the electron density tends to infinity in the vicinity of the singularity as

$$n = \frac{\beta_{\rm ph}}{\beta_{\rm ph} - v} \approx \gamma_{\rm ph}\left(\frac{3(1 + a_{\rm m}^2)^{1/4}\beta_{\rm ph}}{2\,\delta X}\right)^{2/3}, \tag{74}$$

the singularity is integrable, and hence the breaking plasma wave contains a finite number of particles.

4.6. Transverse wake wave breaking

The wave breaking regimes considered above were found in the framework of the one-dimensional approximation, under the condition that the transverse inhomogeneity scale substantially exceeds both the wavelength of the wake wave and the value of the electron displacement in the wakefield. Nonlinear wave breaking acquires new features in the three-dimensional geometry, where the relativistically strong laser pulse is relatively narrow in the transverse direction or/and in the case of a wake wave excited inside a plasma channel, e.g., inside a plasma-filled capillary. Spatially inhomogeneous wake waves have the shape of paraboloids (see Figs 3 and 4) [92, 93]. Paraboloidal structures enhance the accelerated charged particle focusing and can be used for the electromagnetic radiation focusing [35]. The curvature of constant-phase surfaces, $1/R$, increases with the distance from the driver laser pulse. The curvature radius R decreases to the value at which it becomes equal to the value of the electron displacement in the wakefield, $\xi_{\rm wf}$. After that, electron trajectory self-intersection occurs, which is equivalent to wave breaking. This process results in the injection of part of the electrons into the accelerating phase of the wakefield.

Transverse inhomogeneity of a wake wave appears due to a transverse inhomogeneity of the wake wave frequency $\omega_{\rm wf}$, which is due to its dependence on the amplitude of a relativistically strong wave, which is in turn determined by a transverse inhomogeneity of the driver laser pulse and/or the transverse inhomogeneity of the plasma density when the laser pulse propagates inside a plasma channel [94, 95]. The coordinate dependence of the wake wave frequency near the axis can be approximated by the expression $\omega_{\rm wf} \approx \omega_{\rm wf}(0) + \delta\omega_{\rm wf}(r/S)^2$, where $\delta\omega_{\rm wf}$ is the difference between the values of the frequency on the channel axis and outside. It is equal to $\delta\omega_{\rm wf} \approx \omega_{\rm wf}(0)$ if the wakewave is generated by a high-intensity laser pulse with the amplitude $a \gg 1$. The dependence of the wave phase on coordinates and time is

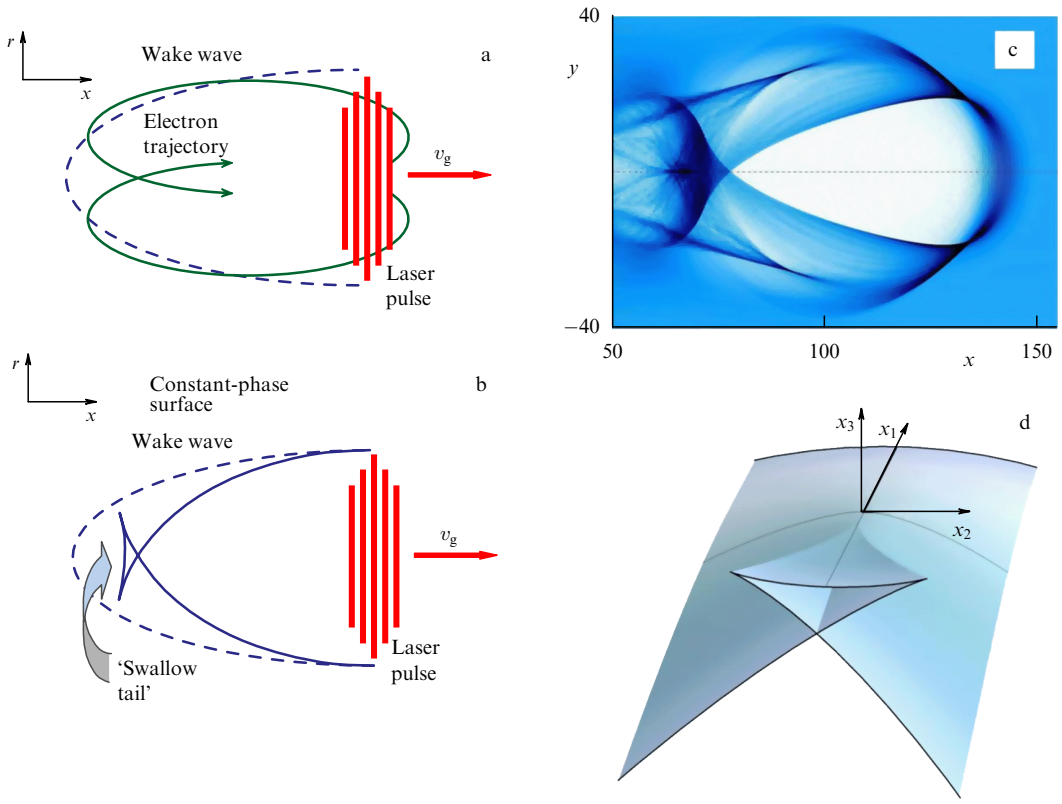

Figure 3. Wake wave breaking in the first cycle of a wave behind the driver laser pulse. (a) Ponderomotive pressure pushes the electrons in the transverse direction and forward. Under the attracting force of the electric field, which occurs due to the electric charge separation inside the cavity, the electrons far enough behind the laser pulse move into the cavity. The dashed curve shows a constant-phase surface calculated in the linear approximation. (b) Nonlinear distortion of the wake wave form corresponding to the singularity called the 'swallow tail' in catastrophe theory. (c) Distribution of the electron density in the (x, y) plane for $a = 3$ and $n_e = 0.001$ at the time $t = 155(2\pi/\omega)$. (d) The swallow-tail catastrophe.

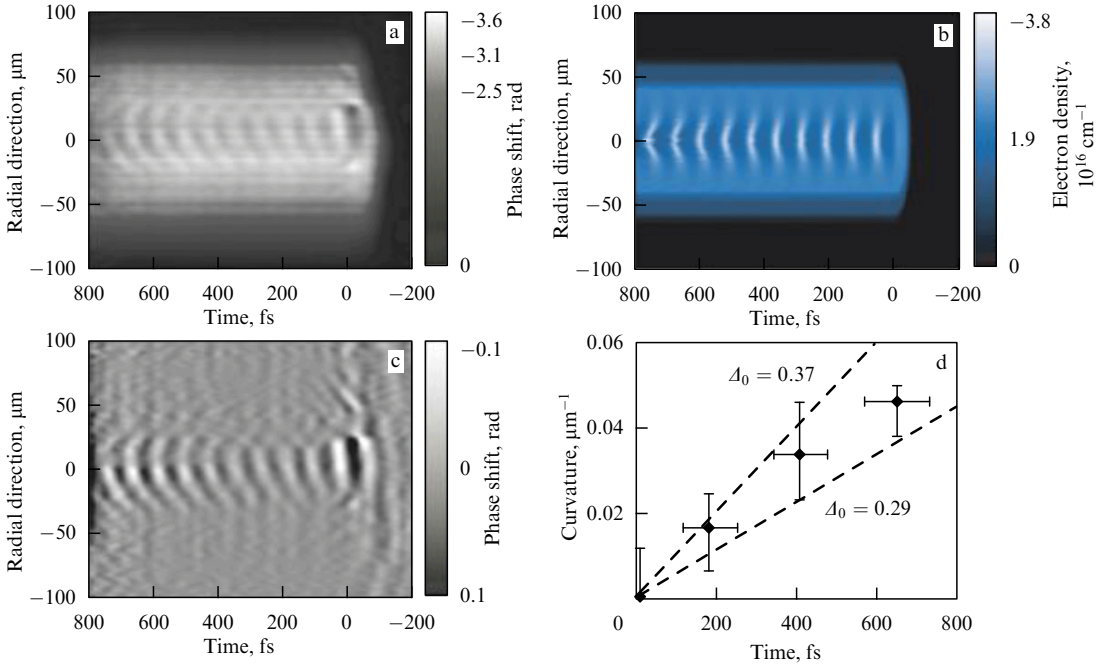

Figure 4. Nonlinear wake wave observed in the experiment in Ref. [93]. (a) Distribution of the phase in the (x, r) plane for the wake wave generated by a 30 TW laser pulse in an He plasma target with the concentration 2.2×10^{18} cm^{-3}. (b) Distribution of the electron density obtained by computer simulation. (c) The same as in frame (a) when the background plasma effect is subtracted. (d) Change in the curvature of the constant-phase surfaces obtained in the experiment and by computer simulation (dashed lines); Δ_0 is the oscillation amplitude of electrostatic potentials, normalized to c^2/e.

given by (see Ref. [96])

$$x - v_{\rm ph}t + \psi(x,r,t)\,\frac{v_{\rm ph}}{\omega_{\rm wf}(0)} = \frac{r^2}{2R}\,. \tag{75}$$

Actual localization of constant-phase surfaces in a nonlinear wake wave compared to those in a linear wave differs by the value of the electron displacement $\xi_{\rm wf}$. We can conclude that when the curvature radius R becomes equal to the displacement amplitude $\xi_{\rm wf}$, the wave breaks. This corresponds to the scenario of transverse wave breaking [96]. From Eqn (75), it is easy to see that the curvature radius decreases with the distance from the laser pulse (see also Fig. 4d). Taking this fact into account, we find that the distance between the laser pulse and the position where the first wave breaking occurs is equal to $\omega_{\rm wf}(0)S^2/(2\delta\omega_{\rm wf}\xi_{\rm wf})$. The number of cycles of a regular wake wave is $N_{\rm wf} \approx \omega_{\rm wf}^2(0)S^2/4\pi c\,\delta\omega_{\rm wf}\xi_{\rm wf}$.

Figure 3 schematically illustrates the electron trajectory self-intersection in the course of transverse wake wave breaking. The ponderomotive pressure of ultrashort laser pulses pushes the electrons away in the forward direction and transversely, forming a cavity in the electron density [96, 97]. The attracting force of the electric field, appearing due to the electric charge separation, pulls the electrons into the cavity. The dashed curves show the position of constant-phase surfaces calculated in the linear approximation.

Following Refs [96, 98], we assume that the electron displacement direction is perpendicular to the constant-phase surfaces obtained in the linear approximation. For the coordinates of a new position of the surface of constant phase in the (x,r) plane, we can write

$$x = x_0 + \frac{\xi_{\rm wf}(r_0)R}{\sqrt{R^2+r_0^2}}\,, \qquad r = r_0 - \frac{\xi_{\rm wf}(r_0)r_0}{\sqrt{R^2+r_0^2}}\,, \tag{76}$$

where $x_0 = r_0^2/2R$ and r_0 are the constant-phase surfaces obtained in the linear approximation, which are assumed to have the shape of paraboloids of revolution. Different scenarios of transverse wave breaking can be realized depending on the particular form of the function $\xi_{\rm wf}(r_0)$. For generic $\xi_{\rm wf}(r_0)$, the singularities formed during the wave break are structurally stable because they have topological properties corresponding to fundamental catastrophes [90, 91]. In the case of a homogeneous displacement $\xi_{\rm wf}$, the map $(x_0,r_0) \to (x,r)$ given by Eqn (76) transforms the paraboloid of revolution into a surface 'parallel' to it. For $\xi_{\rm wf} \geqslant R$, the cross section of this surface has a singularity corresponding to the 'swallow tail' catastrophe, which is shown in Fig. 3d. In the three-dimensional space with local coordinates (x_1,x_2,x_3), a catastrophe of that type is related to the surface on which the polynomial $y^4 + x_1y^2 + x_2y + x_3$ has multiple roots [90, 91].

In Fig. 3, we also present the results of computer simulations of the electromagnetic pulse interaction with a plasma target, which illustrates the formation of the discussed singularity. Here and below, the simulations are performed using the relativistic electromagnetic code REMP [99] based on the particle-in-cell (PIC) method. In the simulations, a laser pulse with the amplitude $a = 3$ corresponding to the radiation intensity $1.93\times10^{19}\times(0.8/\lambda\ [\mu{\rm m}])^2$ W cm^{-2} and $15\lambda \times 50\lambda$ in size propagates in a plasma slab with a thickness of 145λ and the density $n = 3\times10^{17}\times(0.8/\lambda\ [\mu{\rm m}])^2$ cm^{-3}. Figure 3c shows the electron density distribution in the (x,y) plane. We see a region where the swallow tail singularity is formed in the cavity behind the laser pulse. Also, the initial stage of the electron bunch injection into the wakefield is shown.

4.7 Bow wave

Wake plasma wave generation by a laser pulse provides one of the examples of realization of a general physical phenomenon well known in other fields of physics. For example, a moving ship leaves wake waves behind it, known also as Kelvin waves [81, 100]. In addition to these waves, the front part of the ship emits a bow wave, which, in particular, determines the outer boundary of the ship wake wave. Bow waves are well known in observations of fluid motion under conditions on Earth and in space plasma. A bow wave is formed on the day side of Earth's magnetosphere under the action of the solar wind [101]. The largest observed bow waves come from colliding galaxies [102].

Continuing the analogy between the processes specific to the dynamics of continuous media and the nonlinear interaction of intense electromagnetic radiation with plasma, it would be natural to find an analogue of the bow wave forming at the front of a laser pulse [103]. The clearest bow wave of this kind can be seen in the interaction of a strong narrow electromagnetic pulse with collisionless low-density plasma.

In Fig. 5, we present the results of PIC simulations of bow wave formation in the three-dimensional geometry. A linearly polarized laser pulse with the amplitude $a = 6.62$ and size $10\lambda \times 10\lambda \times 10\lambda$ interacts with plasma. The electron concentration is $n = 1.14\times10^{18}\times(1/\lambda\ [\mu{\rm m}])^2$ cm^{-3}.

Excitation of a high-amplitude wake wave by a laser pulse is accompanied by the formation of a cavity in the electron density in the first cycle (see Figs 5 and 6).

As can be seen in Fig. 6, the longitudinal electric field E_x is localized in the region with a size much larger than the waist of the laser pulse and that of the cavity. As a result, the electrostatic potential value φ is larger than in the case where it corresponds to only the cavity size. We also note that the cavity length is much larger than its width.

Transverse wake wave breaking leads to the emission of electron bunches in the radial directions in other cycles

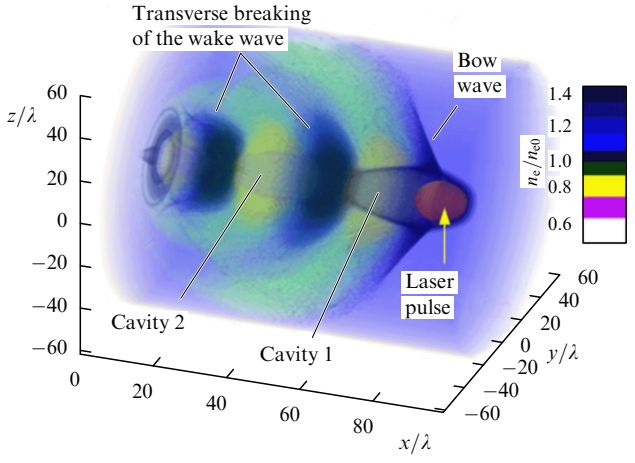

Figure 5. (Color online.) Electron density distribution in the wake behind a laser pulse. The laser pulse is shown by a surface of constant electromagnetic energy density $E^2 + B^2 = (2e/m_e\omega c)^2$ for the time $t = 100(2\pi/\omega)$.

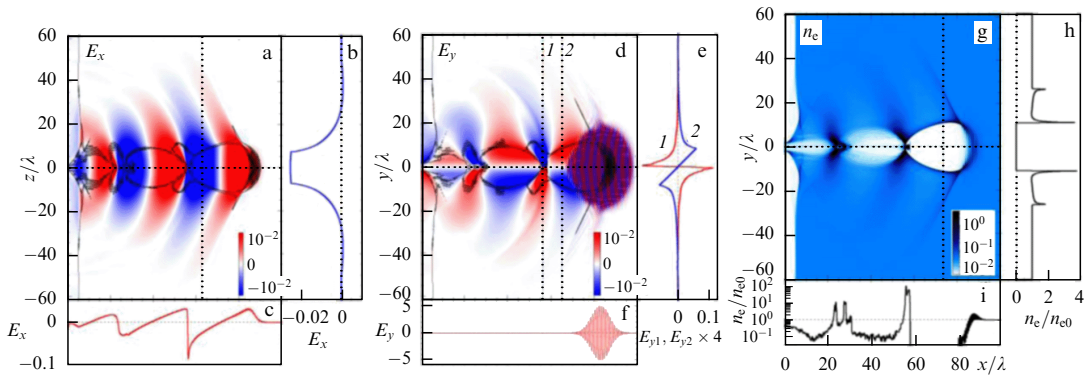

Figure 6. (Color online.) Two-dimensional slices of the electric field distribution, normalized to $mc\omega/e$: (a) E_x, (d) E_y, and (g) of the electron density at $t = 100(2\pi/\omega)$. (b, e, h) Vertical and (c, f, i) horizontal one-dimensional slices are shown by dashed lines. In (a,d), black lines show the electron density for $n_e/n_0 = 0.75$ and 1.50.

of the wake wave, enhancing the electrostatic potential there.

The form of the cavity in the electron density behind the laser pulse can be found from the fact that in a strong bow wave, all electrons in the way of the laser pulse are pushed aside, forming a multi-stream configuration in the collisionless plasma. The plasma inside the cavity is positively charged. It attracts those electrons from side regions that have not experienced the ponderomotive force action. The transverse radial component of the electric field near the axis is linearly proportional to the radius, $E_\perp = 2\pi n_0 e r$. Under the action of this field, electrons from the outer region are drawn into the cavity. It is easy to show that for a laser pulse with a radius of the order of or smaller than $2\pi ca/\omega_{pe}$, the electrons moving inwards remain nonrelativistic. The dependence of their coordinate on time is given by $r(t) = r(0)\cos(\omega_{pe}t/\sqrt{2})$. For the time equal to $t = \pi/\sqrt{2}\,\omega_{pe}$, the electrons reach the cavity axis. As a result, the cavity boundary is determined by the surface

$$r = w_0 \cos\frac{\omega_{pe}(t - x/v_{ph})}{\sqrt{2}}, \tag{77}$$

where w_0 is the laser pulse waist.

A bow wave in the laser plasma is a complex nonlinear electromagnetic object (a more detailed discussion is given in Ref. [103]). The location where the bow wave is detached from the cavity boundary, clearly seen in Figs 5 and 6g, deserves more attention. The (x, r) cross section of this region shows a strong modulation of the electron density, whose shape corresponds to a cusp-like singularity [90, 91]. We note that a bow wave was observed in the experiment presented in Ref. [104].

4.8 Wave breaking in finite-temperature plasma

The laser plasma temperature in the case of ultra-short, femtosecond laser pulses is determined by the parameters of the prepulse and pedestal interaction with the irradiated target during the time before the arrival of the main pulse. In the case typical for multi-terawatt laser radiation, plasma is formed in the process of photoionization [49, 105]. In such plasmas, the electron temperature is of the order of the quiver energy of electrons moving in the ionizing radiation, i.e., it does not exceed the keV level, which is much lower than the energy of electrons moving in the field of the main pulse, which is above the MeV level. The electron energy distribution does not correspond to the Maxwell distribution and can be approximated in the framework of the 'water bag' model, which, under circumstances different from those stated above, would be considered too artificial.

In the water bag model, the distribution function is constant, $f_e(p, x, t) = \text{const}$, in the phase-plane domain bounded by the curves $p_+(x, t)$ and $p_-(x, t)$, and vanishes outside this domain (see, e.g., Ref. [106]). The constant is proportional to the electron density and inversely proportional to the width of the distribution in the momentum space, which is related to the electron temperature.

The distribution function evolution is described by the Vlasov equations

$$\frac{\partial f_e}{\partial t} + v\frac{\partial f_e}{\partial x} - E\frac{\partial f_e}{\partial p} = 0, \tag{78}$$

$$\frac{\partial E}{\partial x} = 1 - n_e, \tag{79}$$

where all the variables are written in the dimensionless form using standard normalization. Equation (78) describes an incompressible fluid flow in the phase space.

Taking the first moment, we obtain the electron density $n_e(x, t) = g_e[p_+(x, t) - p_-(x, t)]$. Here, the constant $g_e = n_0/(p_{+,0} - p_{-,0})$ is the ratio of the initial density value to the initial width of the distribution, which is assumed to be uniform.

It follows from Eqns (78) and (79) that the functions $p_+(x, t)$, $p_-(x, t)$, and $E(x, t)$ satisfy the system of equations

$$\frac{\partial p_+}{\partial t} + \frac{p_+}{\sqrt{1 + p_+^2}}\frac{\partial p_+}{\partial x} = -E, \tag{80}$$

$$\frac{\partial p_-}{\partial t} + \frac{p_-}{\sqrt{1 + p_-^2}}\frac{\partial p_-}{\partial x} = -E, \tag{81}$$

$$\frac{\partial E}{\partial x} = 1 - g_e(p_+ - p_-). \tag{82}$$

For waves propagating with a constant velocity v_{ph}, i.e., for the solutions of Eqns (80)–(82) in terms of the independent variable $X = x - v_{ph}t$, this system can be reduced to

$$h'_+ = -E, \tag{83}$$

$$E' = 1 - \frac{p_+(h_+) - p_-(h_+ - \beta_{ph}\Delta p_0)}{\Delta p_0}, \tag{84}$$

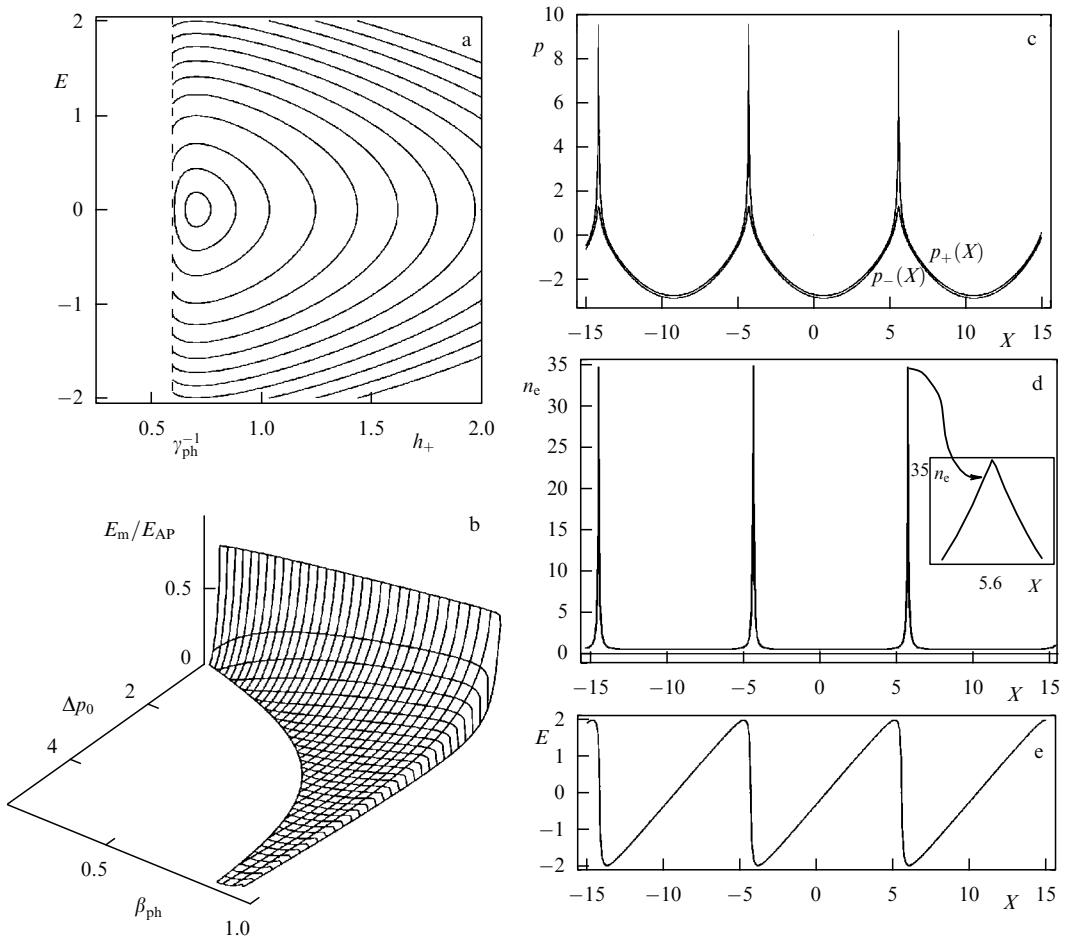

Figure 7. (a) Constant-value contours for Hamiltonian (85) on the (E, h_+) plane for $\beta_{ph} = 0.8$ and $\Delta p_0 = 0.1$. (b) Dependence of the maximum of the electric field E_m normalized to E_{AP} on the phase velocity β_{ph} and the width of the distribution function Δp_0. (c) Electron phase plane. (d) Electron density vs the coordinate X (the inset shows the density dependence on the coordinate at the wave crest). (e) Electric field vs the coordinate X.

where the prime denotes the differentiation with respect to X, $h_+ = (1 + p_+^2)^{1/2} - \beta_{ph} p_+$, $\Delta p_0 = p_{+,0} - p_{-,0}$, and $\beta_{ph} = v_{ph}/c$.

Equations (83) and (84) can be written in the Hamiltonian form. For a symmetric initial distribution with $p_{+,0} = -p_{-,0}$, the Hamiltonian function is given by [107]

$$\mathcal{H}(E, h_+) = \frac{E^2}{2} + \gamma_{ph}^2 h_+ - \frac{W(\gamma_{ph} h_+) - W\bigl(\gamma_+(h_+ + \beta_{ph}\Delta p_0)\bigr)}{2\Delta p_0}\,, \tag{85}$$

where

$$W(z) = z\sqrt{z^2 - 1} - \ln\left(z + \sqrt{z^2 - 1}\,\right). \tag{86}$$

In the limit $z \to 1$, this function tends to zero as $W(z) \approx (4\sqrt{2}/3)(z-1)^{3/2}$, and in the limit $z \to \infty$, $W(z) \approx z^2 - \ln(2z)$. In Fig. 7, we plot constant-value contours of Hamiltonian (85) in the (E, h_+) plane for $\beta_{ph} = 0.8$ and $\Delta p_0 = 0.1$.

The solutions of Eqns (83) and (84) in the limit $h_+ \to \gamma_{ph}^{-1}$ become singular, as follows from expression (85) and from the behavior of the Hamiltonian system trajectories seen in Fig. 7a. At the singularity, the electron momentum on the upper bounding curve tends to

$$p_+ \to p_{+,m} = \frac{\beta_{ph}}{\sqrt{1 - \beta_{ph}^2}}\,, \tag{87}$$

which corresponds to wave breaking when the velocity of the electrons with the momentum p_+ becomes equal to the phase velocity of the wave. At the point of wave breaking, the electron momentum on the lower bounding curve is equal to

$$p_{-,m} = p_{+,m} - \beta_{ph}\gamma_{ph}^2 \Delta h_0 - \sqrt{\gamma_{ph}^2 \Delta h_0^2 - 2\gamma_{ph}^3 \Delta h_0}\,,$$

where

$$\Delta h_0 = \sqrt{1 + p_{+,0}^2} - \sqrt{1 + p_{-,0}^2} - \beta_{ph}(p_{+,0} - p_{-,0})\,.$$

The effects of a finite temperature of the plasma decrease the value of the maximum electric field [108–110] in a stationary wave compared with the value E_{AP} given by Eqn (44). For $\Delta p_0 \ll 1/\beta_{ph}\gamma_{ph}$, the maximum field is equal to

$$E_m = E_{AP} - \frac{2(\beta_{ph}\gamma_{ph})^{3/2}}{3\sqrt{\gamma_{ph} - 1}}\,\sqrt{\Delta p_0}\,. \tag{88}$$

In the limit $\Delta p_0 \to 2\beta_{ph}\gamma_{ph}$, it vanishes (Fig. 7b).

In Figs 7c–e, we show the nonlinear wave structure: the phase plane, the electron density, and the electric field for $\beta_{ph} = 0.995$ and $\Delta p_0 = 0.25$.

In contrast to the wave breaking in cold plasma, the density at the wave-breaking point remains finite in a finite-

temperature plasma,

$$n_{e,m} = \gamma_{ph}^2 \beta_{ph} \left(\sqrt{1 + \frac{2}{\beta_{ph}\gamma_{ph}\Delta p_0}} - \beta_{ph} \right). \quad (89)$$

In the vicinity of the wave-breaking point $X = X_m$, the density dependence on the coordinate can be represented in the form [111]

$$n_e(X)\Big|_{X\to X_m} = n_{e,m} - \frac{\sqrt{n_{e,m}\gamma_{ph}^3}}{\Delta p_0} |\delta X|, \qquad \delta X = X - X_m,$$

corresponding to nonlinear waves called 'peakons' (see Fig. 7d). Among the best-known peakons are Stockes waves on a water surface [100].

5. Interaction of charged particles and electromagnetic waves with nonlinear wake waves

A number of publications have been devoted to the study of the interaction of charged particles and photons with plasma waves. Most of the publications are related to the problem of electron acceleration by wake plasma waves, which has been proposed in Ref. [89] (see also review article [33]). The interest in this problem stems from the development of a compact accelerator of high-energy electrons and positrons [33]. As demonstrated in Refs [34, 35, 44, 112, 113], wake plasma waves can also be used as mirrors moving with a relativistic velocity. This process is related to a range of problems associated with the interaction of electromagnetic waves with plasma waves, which, from a more general standpoint, includes the study of the transformation of waves of different types, parametric instabilities, and Raman scattering (see Refs [114–116] and the references therein). A detailed discussion of these problems is far beyond the scope of this paper. Below, we consider only those aspects of the electron and photon interaction with wake waves that have a direct relation to relativistic plasma mirrors.

5.1 Electron acceleration by wake waves

Nonlinear plasma waves with an amplitude close to the wave-breaking threshold play equally important roles in studying the problems related to relativistic moving mirrors and to high-energy electron acceleration. It is also important that the registration of ultrarelativistic electron beams in experimental studies of relativistic mirrors is an indication of reaching the threshold of wake wave breaking, providing the electron injection into the acceleration phase. In addition, the analysis of the energy spectrum of accelerated electrons gives information about the parameters of the wave [112, 113].

Electrons in the wake wave oscillate in a regular way. In a plasma with the electron density well below the critical one ($n_e \ll n_{cr} = m_e\omega^2/4\pi e^2$), the wake wave phase velocity v_{ph} is close to the speed of light in the vacuum, which corresponds to a large value of the relativistic Lorentz factor, $\gamma_{ph} \gg 1$. The group velocity of the wake wave is equal to zero and the phase velocity v_{ph} is equal to the group velocity of the laser pulse, $v_{g,las} = c(1 - \omega_{pe}^2/\omega_0^2)^{1/2}$, which in the limit $n_e \ll n_{cr}$ is approximately $v_{g,las} \approx c(1 - \omega_{pe}^2/2\omega_0^2)$. From these expressions, it is easy to obtain a relation between the electromagnetic pulse wavelength λ_0 and the wavelength λ_w of the wake field:

$$\lambda_w = \lambda_0 \left(\frac{\omega_0}{\omega_{pe}}\right) \left(1 - \frac{\omega_{pe}^2}{\omega_0^2}\right)^{1/2} = \lambda_0 \gamma_{ph}.$$

Assuming that the characteristic change in the electron density in the wake wave is of the order of the plasma density and considering the weakly nonlinear wave that is of interest to the discussed concept of a laser electron–positron collider [33], we can estimate the amplitude of the electrostatic potential in the wave as $\varphi_w = m_e c^2/e$. The energy of electrons accelerated by the wake wave is $(1 - v_{ph}^2/c^2)^{-1}$ times greater than $e\varphi_w$, i.e., the electron gamma-factor is $\gamma_e = 2\gamma_{ph}^2$. The electron acceleration length is

$$l_{acc} = \frac{\pi c/\omega_{pe}}{1 - v_{ph}/c},$$

which is equivalent to the expression $l_{acc} = \lambda_0 \gamma_{ph}^3$, which we use to obtain the relation between the acceleration length, the laser wavelength, and the energy of fast electrons: $l_{acc} = \lambda_0 \gamma_e^{3/2}$. For the laser wavelength $\lambda_0 = 1$ μm and the electron energy 1 TeV, i.e., for $\gamma_e = 2 \times 10^6$, we find that the acceleration length (the accelerator size) should be 1 km.

We present a description of the electron dynamics in the wake wave, limited to the one-dimensional approximation [117], for the geometry where all functions depend on the time t and one coordinate x. In the framework of classical electrodynamics, one-dimensional motion of electrons in the fields of an electromagnetic and wake plasma wave is described by the Hamiltonian

$$\mathcal{H} = \sqrt{m_e^2 c^4 + c^2 P_\parallel^2 + \left(cP_\perp + eA_\perp(x,t)\right)^2} - e\varphi(x,t), \quad (90)$$

where $P_\parallel$ and $P_\perp$ are the components of the generalized momentum, $A_\perp$ is the vector potential of the laser pulse, and φ is the wakefield scalar potential. Neglecting the influence of dispersion on the propagation of electromagnetic waves, we assume that $A_\perp$ and φ depend only on the variable $X = x - v_g t$. It is assumed here that the group velocity of the laser pulse v_g satisfies $0 < v_g < c$. The Hamiltonian in Eqn (90) has a symmetry corresponding to the Lie group with the generators $v_g\,\partial/\partial x + \partial/\partial t$, $\partial/\partial y$, and $\partial/\partial z$. The Noether theorem implies that there are integrals of motion

$$\mathcal{H} - p v_g = m_e c^2 h_0, \qquad P_\perp = P_{\perp,0}, \quad (91)$$

where constants h_0 and $P_{\perp,0}$ are determined by the initial conditions. Using the dimensionless variables introduced above, $\beta_{ph} = v_g/c$, $\Phi(X) = e\varphi(X)/m_e c^2$, $a(X) = eA_\perp(X)/m_e c^2$, and $p_x = P_\parallel/m_e c$, we write the first integral of motion as

$$h(p_x, X) \stackrel{\text{def}}{=} \sqrt{1 + p_x^2 + a^2(X)} - \varphi(X) - \beta_{ph} p_x = h_0. \quad (92)$$

It then follows that the kinetic energy acquired by an electron on the trajectory interval from X_0 to X is

$$\mathcal{E} = \gamma_{ph}^2 \Big[\varphi(X) - h_0 \pm \beta_{ph} \sqrt{\left(\varphi(X) - h_0\right)^2 - \gamma_{ph}^{-2}\left(1 + a^2(X)\right)} \Big] - 1, \quad (93)$$

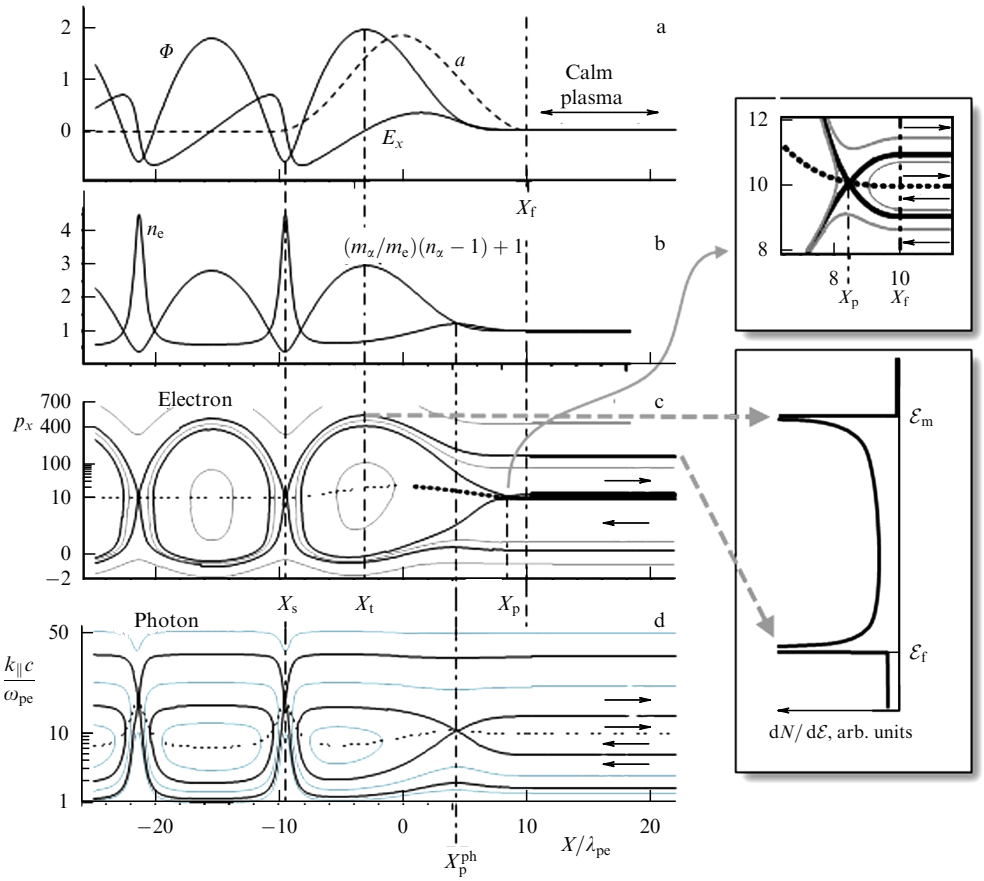

Figure 8. (a) Wake wave excited by a short laser pulse. Dependences of the dimensionless quantities Φ, a, and E_x on the coordinate $X = x - v_g t$; X_f is the coordinate of the laser pulse front. (b) Normalized density of electrons and ions. (c) Electron phase plane. X_s, X_t, and X_p are the respective coordinates of a singular point of the separatrix, its crest, and the point of intersection of the separatrix branches. The top right inset shows an enlarged fragment of Fig. c, the domain where the ponderomotive force of the laser pulse acts on electrons. The bottom inset shows the energy spectrum of the electron beam $dN/d\mathcal{E}$, which consists of the contributions from the particles at the separatrix crest and from the particles that have overtaken the laser pulse; $\mathcal{E}_m$ is the maximum energy of an electron accelerated at the front of the laser pulse. (d) Photon phase plane. The bold lines represent the separatrix and the thin lines show other trajectories in Figs c, d. Curves in Fig. c and the upper inset correspond to the dependence $p_x = \beta_{ph}\gamma_{ph}\sqrt{1 + a^2(X)}$, and in Fig. d, to the dependence $k_x c = \beta_{ph}\gamma_{ph}\omega_{pe}(X)$.

where the plus sign corresponds to the coordinate X increasing with time and the minus sign corresponds to decreasing X.

The behavior of the system with the Hamiltonian given by Eqn (92) is illustrated in Fig. 8, which presents the phase portrait for electrons with $P_{\perp,0} = 0$. The wake wave is excited by a short electromagnetic pulse of circular polarization with the envelope given by

$$a(X) = a_0\left[\exp\left(-\frac{4\ln(2)X^2}{l_p^2}\right) - \frac{1}{16}\right]\theta\left(l_p - |X|\right),$$

where $a_0 = 2$, $l_p = 10\lambda$, and $\theta(x)$ is the Heaviside function, equal to 1 for $x \geqslant 0$ and 0 for $x < 0$. The scalar potential $\varphi(X)$ satisfies Eqn (35), in the right-hand side of which the vector potential is assumed to be a given function.

Each electron trajectory $\{X(t), p_x(t)\}$ in the (X, p_x) plane corresponds to a level line of the function $h(X, p_x)$ in (92). The phase plane consists of the domains containing the trajectories of particles trapped in the wakefield and two domains corresponding to the transition particles. These areas are separated by singular trajectories, called separatrices, which merge at the singular points, which are located on the curve $p_x(X) = \beta_{ph}\gamma_{ph}\sqrt{1 + a^2(X)}$. On this curve, the radicand in the right-hand side of (93) vanishes: $(\varphi(X) - h_0)^2 = \gamma_{ph}^{-2}(1 + a^2(X))$.

We consider an electron moving along the separatrix, whose trajectory originates at a singular point X_s. Its kinetic energy reaches a maximum $\mathcal{E}_m$ when the electron position is at the crest of the separatrix at the point X_t. For a sufficiently short laser pulse with $l_p < \lambda_{wf}/2$, the points X_s and X_t in the first cycle of the wake wave correspond to a local minimum and a local maximum of the potential: $\varphi_{min} = \varphi(X_s)$ and $\varphi_{max} = \varphi(X_t)$. Hence, the maximum value of the energy acquired by the electron moving along the separatrix is

$$\mathcal{E}_m = \gamma_{ph}^2\left[(\varphi_{max} - \varphi_{min}) + \beta_{ph}\sqrt{(\varphi_{max} - \varphi_{min})^2 + 2\gamma_{ph}^{-2}(\varphi_{max} - \varphi_{min})}\right] + \mathcal{E}_{inj}, \quad (94)$$

where $\mathcal{E}_{inj} = \gamma_{ph} - 1$ is the electron energy at the point X_s. In the limit $\gamma_{ph} \gg 1$, the electron energy is given by

$$\mathcal{E}_m \approx 2\gamma_{ph}^2(\varphi_{max} - \varphi_{min}) + \gamma_{ph} - 1. \quad (95)$$

The lowest value of the scalar potential is at the point of the maximum of the electron density in the wake wave with $\varphi_{min} \geqslant -1 + 1/\gamma_{ph}$.

The value $h(X, p_x) = 1/\gamma_{ph} - \varphi_{min}$ corresponds to the separatrix separating the first-cycle trajectories of the

electrons trapped by the wakefield from the electron trajectories reflected by the potential at the point X_s. As a result of reflection, the electron acquires a speed greater than the phase velocity of the wake wave and overruns the wake wave and the laser pulse. Asymptotically as $X \to +\infty$, the electron energy tends to

$$\mathcal{E}_f = \gamma_{ph}^2 \left(|\varphi_{min}| + \beta_{ph} \sqrt{|\varphi_{min}|^2 + 2\gamma_{ph}^{-2} |\varphi_{min}|} \right) + \mathcal{E}_{inj} . \quad (96)$$

If the wakefield is excited by a strong laser pulse with $a \gg 1$, then φ_{min} tends to its lowest value $-1 + 1/\gamma_{ph}$, which gives the electron energy $\mathcal{E}_{f,m} = 2(\gamma_{ph}^2 - 1)$.

We conclude that in a weakly nonlinear wakefield, the maximum energy of the accelerated electrons is related to the electron density in the plasma by

$$\mathcal{E}_m = \gamma_e m_e c^2 = 2 m_e c^2 \gamma_{ph}^2 , \quad (97)$$

where $\gamma_{ph} = \omega_0/\omega_{pe} \equiv \lambda_p/\lambda_0 = (n_{cr}/n_0)^{1/2}$. The acceleration length is $l_{acc} = \lambda_p \gamma_{ph}^2$, i.e., $l_{acc} = \lambda_0 \gamma_{ph}^3$. It is related to the electron energy as $l_{acc} = 2\lambda_0 \gamma_e^{3/2}$, which can be represented as

$$\mathcal{E}_m = m_e c^2 \left(\frac{l_{acc}}{2\lambda_0} \right)^{2/3} = 0.3 \left(\frac{l_{acc}\ [\text{km}]}{\lambda_0\ [\mu\text{m}]} \right)^{2/3} [\text{TeV}] . \quad (98)$$

As noted above, in the mid-1950s, Enrico Fermi formulated the question about the highest particle energy that can be obtained in standard accelerators, considering an accelerator size of the order of the circumference of Earth's equator, and found the limit of 1 PeV (10^{15} eV). Substituting $l_{acc} = 40{,}000$ km for the acceleration length in expression (98), we obtain an energy of the same order. The use of a multistage wakefield accelerator [33] may increase the electron energy by several orders of magnitude.

Here, we discuss the shape of the energy spectrum of electrons accelerated by the wakefield [117, 118]. We assume that the electron beam is injected with the parameters that provide the conditions for entering a neighborhood of the point X_s in the phase plane. Then the electrons move along the separatrix with the distribution of their density given by a function $\mathcal{N}(X)$, which leads to a broadening of the spectrum from the initial energy $\mathcal{E}_0$ to the maximum energy $\mathcal{E}_m$, corresponding to the top of the separatrix. In addition, the electron energy spectrum has a singularity at the energy $\mathcal{E}_f$ (see the lower inset on the right in Fig. 8). Near the top of the separatrix, the dependence of the energy of the beam particles on the coordinate X can be approximated by a parabola:

$$\mathcal{E}(X) = \mathcal{E}_m \left[1 - \frac{(X - X_t)^2}{l_{acc}^2} \right] , \quad (99)$$

where $l_{acc} \approx \gamma_{ph}^2 \lambda_{wf}$ is the acceleration length. This implies that the spectrum of the electrons collected in the detector, equal to the integral over time, is given by

$$\left. \frac{dN}{d\mathcal{E}} \right|_{\mathcal{E} \to \mathcal{E}_m - 0} = \frac{\mathcal{N}(X)}{|d\mathcal{E}_m/dX|} \approx \frac{\mathcal{N}(X_t)\, l_{acc}}{2\sqrt{\mathcal{E}_m(\mathcal{E}_m - \mathcal{E})}} \quad (100)$$

if $\mathcal{E} < \mathcal{E}_m$. If electrons are injected in the vicinity of a singular point on the separatrix in other cycles of the wake wave, then the resulting energy spectrum contains a superposition of peaks given by Eqn (100) with different values of the maximum energy in general.

The contribution of electrons overtaking the laser pulse can be found from Eqn (93). It was shown in Ref. [117] that the spectrum is then described by the expression

$$\left. \frac{dN}{d\mathcal{E}} \right|_{\mathcal{E} \to \mathcal{E}_f + 0} \approx \frac{\mathcal{N}(X_f) X_f}{\mathcal{E} - \mathcal{E}_f} , \quad (101)$$

where $\mathcal{E}_f$ is determined by Eqn (96).

In experiments on laser wakefield acceleration by laser pulses of a multi-terawatt power, the achieved energy of electrons is of the order of 1 GeV [119] and 2 GeV [120], with the plasma size of a few centimeters. The spectrum has a quasi-mono-energetic form in the vicinity of the maximum energy.

5.2 Photon accelerator

To describe the propagation of a sufficiently short packet of electromagnetic radiation through plasma, we can use the geometrical optics approximation for the coordinate x (the center of the wave packet) and the momentum (wave vector). The equations can be written in the Hamiltonian form with the Hamiltonian

$$\omega(x, \mathbf{k}; t) = \sqrt{k^2 c^2 + \omega_{pe}^2 (x - v_{ph} t)} . \quad (102)$$

This expression is nothing more than a dispersion equation for the dependence of the wave frequency on the wave vector $k^2 = k_\parallel^2 + k_\perp^2$. In the same way as above in describing the electron motion, passing to the variable $X = x - v_{ph} t$ allows obtaining the Hamiltonian for photons:

$$\mathcal{W}(x, k_x) = \sqrt{k_x^2 c^2 + \omega_{pe}^2(X)} - \beta_{ph} k_x c . \quad (103)$$

Here, we use the conservation of the transverse momentum $k_\perp$ and assume for simplicity that it is equal to zero.

Level lines of Hamiltonian (103), which are trajectories in the phase plane, are shown in Fig. 8d. Due to the obvious similarity between the photon phase plane and the phase plane of electrons in Fig. 8c, the process of increasing the frequency of electromagnetic radiation of a short wave packet during its interaction with wake plasma waves is called 'photon acceleration' [121–126]. We note that in the case of excitation of the wake plasma wave by a short electron beam, the phase portrait of a photon is topologically equivalent to the phase portrait of a positron. On the trajectory corresponding to a fixed value of Hamiltonian (103), $\mathcal{W}(X, k_x) = w_0 = \omega_0 - \beta_{ph} k_{x,0} c$, the dependence of the photon frequency on the coordinate X is given by

$$\omega = \gamma_{ph}^2 w_0 \left[1 \pm \beta_{ph} \left(1 - \frac{\omega_{pe}^2(X)}{w_0^2 \gamma_{ph}^2} \right)^{1/2} \right] . \quad (104)$$

A photon with the initial frequency and wave number values equal to ω_0 and $k_{x,0}$ in the process of the reflection by the first or second maximum of the electron density in the wake wave undergoes a frequency upshift:

$$\tilde{\omega} = (2\gamma_{ph}^2 - 1)\, \omega_0 - 2\beta_{ph} \gamma_{ph}^2 k_{x,0} c . \quad (105)$$

The maximum value of the photon frequency $\tilde{\omega}_{max}$ reflected by the wake wave corresponds to the trajectory that lies on the separatrix separating the transient photons from the reflected ones. For that separatrix, we have $w_0 = \hat{\omega}_{pe}/\gamma_{ph}$, where $\hat{\omega}_{pe} = \omega_{pe}(X_s)$ is the maximum plasma frequency, reached at

the points of maximum electron density. From Eqn (103), we find that

$$\tilde{\omega}_{\max} = \gamma_{\rm ph}\left(\hat{\omega}_{\rm pe} + \beta_{\rm ph}\sqrt{\hat{\omega}_{\rm pe}^2 - \omega_{\rm pe,0}^2}\right), \tag{106}$$

where $\omega_{\rm pe,0} = \omega_{\rm pe}(\infty)$ is the plasma frequency in the region far ahead the laser pulse. In the limit $\hat{\omega}_{\rm pe} \gg \omega_{\rm pe,0}$ and $\beta_{\rm ph} \to 1$, the maximum photon frequency is $\tilde{\omega}_{\max} \approx 2\gamma_{\rm ph}\hat{\omega}_{\rm pe}$.

6. Electromagnetic wave reflection from caustics in the electron density distribution in nonlinear plasma waves

As has been noted above, the concept of relativistic moving mirrors is based on the idea that an electromagnetic wave can be reflected by nonlinear plasma waves near the threshold of wave breaking with small but nonexponentially small reflectivity. Below, we discuss the reflection of electromagnetic waves from the electron density maxima with a singularity in the density distribution. Following the widely used terminology, we call these singularities (singularities of the Lagrangian map) the caustics. To calculate the reflection R and transmission T coefficients, we consider the interaction of electromagnetic waves with a strongly nonuniform distribution of the electron density in a plasma wave [127]. Let the electromagnetic wave be described by the z component of the vector potential $A_z(x, y, t)$, which satisfies the wave equation

$$\frac{\partial^2 A_z}{\partial t^2} - c^2\left(\frac{\partial^2 A_z}{\partial x^2} + \frac{\partial^2 A_z}{\partial y^2}\right) + \omega_{\rm pe}^2(X)A_z = 0, \tag{107}$$

where $\omega_{\rm pe}^2(X) = 4\pi e^2 n(X)/m_{\rm e}\gamma_{\rm ph}$ is the plasma frequency with the relativistic gamma-factor equal to $\gamma_{\rm ph}$.

We perform the Lorentz transformation to a boosted reference frame moving with the phase velocity of the plasma wave. In this frame, Eqn (107) takes the form

$$\frac{{\rm d}^2 a(\zeta)}{{\rm d}\zeta^2} + \left(s^2 - v(\zeta)\right)a(\zeta) = 0, \tag{108}$$

where $s^2 = (\omega'/c)^2 - k_y^2$, $\zeta = \gamma_{\rm ph}(x - v_{\rm ph}t)$, t', k', and ω' are respectively the square of the wave number, coordinate, time, and frequency in the boosted reference frame, and $v(\zeta) = \omega_{\rm pe}^2(\zeta)/c^2$. The vector potential is normalized to $m_{\rm e}c^2/e$, and its dependence on the time t' and coordinates ζ and y is

$$a(\zeta) = \frac{eA_z(\zeta)}{m_{\rm e}c^2}\exp\left[-{\rm i}(\omega' t' - k_y y)\right]. \tag{109}$$

We represent the solution of Eqn (108) in the form

$$a(\zeta) = b_+(\zeta)\exp({\rm i}s\zeta) + b_-(\zeta)\exp(-{\rm i}s\zeta), \tag{110}$$

where the unknown functions $b_+(\zeta)$ and $b_-(\zeta)$ are the amplitudes of the reflected and transmitted waves. In the limit $\zeta \to -\infty$, the function $b_+(\zeta)$ is equal to the amplitude of the incident wave, which is set equal to unity, and $b_-(-\infty) = \rho$ is the amplitude of the reflected wave. For $\zeta \to +\infty$, the function $b_+(\zeta)$ is equal to the amplitude of the transmitted wave τ, and $b_-(\zeta)$ vanishes. Therefore, $|b_+(-\infty)|^2 = 1$, $|b_-(-\infty)|^2 = \mathsf{R}$, and $|b_+(+\infty)|^2 = \mathsf{T}$, $b_-(+\infty) = 0$.

Because we introduced two unknown functions, $b_+(\zeta)$ and $b_-(\zeta)$, instead of one, $a(\zeta)$, it is necessary to impose an additional condition on them. We choose it in the form of the requirement that the derivative ${\rm d}a/{\rm d}\zeta$ be equal to

$$\frac{{\rm d}a}{{\rm d}\zeta} = {\rm i}s\left[b_+(\zeta)\exp({\rm i}s\zeta) - b_-(\zeta)\exp(-{\rm i}s\zeta)\right], \tag{111}$$

i.e.,

$$\frac{{\rm d}b_+}{{\rm d}\zeta}\exp({\rm i}s\zeta) = -\frac{{\rm d}b_-}{{\rm d}\zeta}\exp(-{\rm i}s\zeta). \tag{112}$$

Substituting expression (110) in Eqn (108) and taking Eqns (111) and (112) into account, we obtain a system of equations for $b_+(\zeta)$ and $b_-(\zeta)$, which can be conveniently written in the form (see also Ref. [128])

$$\frac{\rm d}{{\rm d}\zeta}\begin{pmatrix} b_+ \\ b_- \end{pmatrix} = \frac{{\rm i}v(\zeta)}{2s}\begin{pmatrix} -1 & -\exp(-2{\rm i}s\zeta) \\ \exp(2{\rm i}s\zeta) & 1 \end{pmatrix}\begin{pmatrix} b_+ \\ b_- \end{pmatrix}. \tag{113}$$

We assume that the amplitude of the reflected wave is small compared with the amplitude of the incident wave, $\mathsf{R} \ll 1$, which, in particular, is satisfied if $s^2 \gg v(\zeta)$. We seek a solution of system (113) within the approach corresponding to the known approximation in quantum mechanics, with the potential energy considered a perturbation [129]. As a result, we find

$$\rho = \frac{\rm i}{2s}\int_{-\infty}^{+\infty} v(\zeta)\exp(-2{\rm i}s\zeta)\,{\rm d}\zeta. \tag{114}$$

We consider the electron density distribution typical for a plasma wave near the wave-breaking threshold. In accordance with the above analysis of the properties of breaking plasma waves, it can be approximated by the function

$$n(X) = \frac{n_0 G_{2/3}}{k_{\rm p}^{2/3}(l^2 + X^2)^{1/3}}. \tag{115}$$

In this expression, $G_{2/3}$ is a dimensionless coefficient and l is a quantitative measure of the closeness to the wave breaking threshold, which corresponds to $l = 0$. In the reference frame where the mirror is at rest, this leads to the dependence $v(\zeta) = g_{2/3}/|\sigma^2 + \zeta^2|^{1/3}$ with $g_{2/3} = G_{2/3}k_{\rm p}^{4/3}\gamma_{\rm ph}^{-1/3}$. From Eqn (74), it follows that

$$G_{2/3} = \left(\frac{2}{9}\right)^{1/3}(1 + a_{\rm m}^2)^{1/6}\gamma_{\rm ph},$$

i.e.,

$$g_{2/3} = \left(\frac{2}{9}\right)^{1/3}(1 + a_{\rm m}^2)^{1/6}k_{\rm p}^{4/3}\gamma_{\rm ph}^{2/3}.$$

Calculating integral (114) with this integrand, we find

$$\rho_{2/3}(s, l) = \frac{{\rm i}\pi^{1/2}g_{2/3}}{s^{7/6}l^{5/6}\Gamma(1/3)}\,K_{1/6}(2sl), \tag{116}$$

where $\Gamma(z)$ is the gamma-function and $K_\nu(z)$ is the modified Bessel function of the second kind [80]. In the limit of a relatively large l, $sl \gg 1$, the overbarrier reflection is exponen-

tially small:

$$\rho_{2/3}(s,l) \approx \frac{\mathrm{i}\pi}{s^{5/3}l^{2/3}\Gamma(1/3)} \exp(-2sl) . \quad (117)$$

In the opposite limit $sl \to 0$, we have nonexponentially weak reflection:

$$\rho_{2/3}(s) = \frac{\mathrm{i}3^{1/2}\Gamma(1/3)g_{2/3}}{(2s)^2} . \quad (118)$$

Accordingly, the reflection coefficient is equal to

$$\mathsf{R}_{2/3}(s) = \frac{3\Gamma^2(1/3)g_{2/3}^2}{(2s)^4} . \quad (119)$$

We emphasize that these expressions are obtained in the comoving reference frame. In the laboratory frame, expression (119) has the meaning of the reflection coefficient in terms of the number of photons.

7. Thin electron layer as a relativistic mirror

The interaction of a sufficiently wide electromagnetic pulse with a thin foil, in the case where the ponderomotive force of the pulse significantly exceeds the force caused by the electric field that occurs due to electric charge separation, can result in the formation of a dense electron layer moving in the direction of electromagnetic wave propagation. The second counter-propagating electromagnetic pulse can be partly reflected from a thin electron layer, which, due to the above-mentioned double Doppler effect, should lead to the compression of the reflected pulse and to its frequency upshift [41].

To describe the acceleration of a thin electron layer by a laser pulse, we use the known exact solution of the equations of motion of a charged particle in the field of a plane electromagnetic wave [52]. For a plane wave propagating along the x axis and described by the vector potential $\mathbf{A}_0(t - x/c)$, the transverse component of the generalized momentum of a particle is conserved:

$$\mathbf{p}_\perp - \frac{e}{c}\mathbf{A}_\perp = \mathrm{const} . \quad (120)$$

The integral of motion

$$m_\mathrm{e}c^2\gamma_\mathrm{e} - p_\parallel c = \mathrm{const} , \quad (121)$$

which is a combination of the parallel component of the electron momentum and its energy, is also conserved ($p_\parallel$ is the longitudinal component of the particle momentum). Here, m_e and c are the electron mass and the speed of light in the vacuum. We note that integral (121) is the Hamiltonian of a one-dimensional system describing a particle with the momentum $p_\parallel$ and coordinate $u = t - x/c$. In the reference frame where the electron layer is at rest before the wave arrival, the constant in the right-hand side of (121) should be set equal to $m_\mathrm{e}c^2$. The solution of Eqns (120) and (121) gives the electron kinetic energy $\mathcal{E}_\mathrm{kin} = m_\mathrm{e}c^2(\gamma_\mathrm{e} - 1)$ and the momentum

$$\mathcal{E}_\mathrm{kin} = \frac{1}{2} m_\mathrm{e}c^2 \left|\mathbf{a}_\perp(u)\right|^2 , \quad (122)$$

$$\mathbf{p}_\perp = m_\mathrm{e}c\mathbf{a}_\perp(u) , \qquad p_\parallel = \frac{1}{2} m_\mathrm{e}c \left|\mathbf{a}_\perp(u)\right|^2 . \quad (123)$$

In these expressions, $\mathbf{a}_\perp(u) = e\mathbf{A}_\perp(u)/m_\mathrm{e}c^2$ is the normalized vector potential of the wave.

The velocity of the electron motion along the x axis is

$$v_\parallel = \frac{p_\parallel}{m_\mathrm{e}\gamma} = c\,\frac{\left|\mathbf{a}_\perp(u)\right|^2}{2 + \left|\mathbf{a}_\perp(u)\right|^2} . \quad (124)$$

Generally, the particle coordinate is defined by implicit equations given in Ref. [52] [see also (9)]. For a circularly polarized wave, for example, with $\mathbf{a}_\perp(u) = a(u)[\mathbf{e}_y \cos(\omega u) + \mathbf{e}_z \sin(\omega u)]$, the coordinate x is to be found from the equation

$$\int_0^{t-x/c} \left(2 + \left|a(u)\right|^2\right) \mathrm{d}u = 2t . \quad (125)$$

If the laser pulse amplitude is constant, Eqn (125) yields the dependence of the particle position on time:

$$x(t) = x_0 + c\,\frac{|a|^2}{2 + |a|^2}\left(t - \frac{x_0}{c}\right) , \quad (126)$$

where x_0 is the coordinate value at the instant of arrival of the laser pulse, $t_0 = x_0/c$. The thickness of the electron layer is decreased by the factor $(2 + |a|^2)/2$.

To find the distribution of electrons within the layer, it is necessary to solve continuity equation (33) for the electron velocity given by Eqn (124). It is easy to find that

$$n(u) = \frac{n_0}{1 - \beta_\mathrm{M}(u)} = n_0\left(1 + \frac{\left|\mathbf{a}_\perp(u)\right|^2}{2}\right) , \quad (127)$$

where $\beta_\mathrm{M}(u) = v_\parallel(u)/c$. As a result of the interaction with a constant-amplitude laser pulse, the density increases by the factor $(2 + |a|^2)/2$, in accordance with the conclusion above that the layer is longitudinally compressed.

Using the expression for the electron velocity in Eqn (124), we find the corresponding gamma-factor of the relativistic mirror:

$$\gamma_\mathrm{M}(u) = \frac{1}{\sqrt{1 - v_\parallel^2(u)/c^2}} = \frac{2 + \left|\mathbf{a}_\perp(u)\right|^2}{2\sqrt{1 + \left|\mathbf{a}_\perp(u)\right|^2}} . \quad (128)$$

It can be seen that in the limit of a large-amplitude electromagnetic wave, when $|\mathbf{a}_\perp(u)| \to \infty$, the gamma-factor is proportional to the first power of $|\mathbf{a}_\perp|$. We note that in Refs [130, 131], where the configuration consisting of two electron layers was considered, it was concluded that the use of a two-layer configuration can significantly increase the mirror gamma-factor.

In the case where the electron layer is accelerated by a linearly polarized electromagnetic wave, we can find the parameters of the second wave reflected from the layer using the approach in Section 2.2. According to relations (6), (7), (122), and (123), the phase of the reflected wave is given by

$$\psi_\mathrm{r}(u) = \omega_0\left(u + \frac{a_0^2}{2}\,u - \frac{a_0^2}{4\Omega}\sin 2\Omega u\right) \quad (129)$$

in the configuration of a head-on collision of the wave with a mirror. The wave frequency and amplitude vary from ω_0 and E_0 to $\omega_0(1 + a_0^2)$ and $E_0(1 + a_0^2)$. In the reference frame where the mirror is at rest on average, the reflected radiation has the

form of a train of short high-frequency pulses, shown in Fig. 1b.

If the second wave propagates in the direction of motion of the electron layer (which interacts with the receding mirror), the reflected wave phase is given by

$$\psi_{\mathrm{r}}(v) = \frac{\omega_0}{\Omega}\,\frac{\arctan\left(\sqrt{1+a_0^2}\,\tan\Omega v\right)}{\sqrt{1+a_0^2}}\,. \tag{130}$$

The wave frequency and amplitude are proportional to $(1+a_0^2\sin^2\Omega v)^{-1}$, and hence vary from ω_0 and E_0 to $\omega_0(1+a_0^2)^{-1}$ and $E_0(1+a_0^2)^{-1}$. The electric field has the form of a sequence of short pulses with the width $\approx \pi/a_0\Omega$.

We find the reflection coefficient of the electromagnetic radiation from a thin electron layer similarly to how this is done in the classical scattering problem (see, e.g., Ref. [132]). We take the electron density distribution to be proportional to the Dirac delta function:

$$n(X) = n_0 l\delta(X)\,, \tag{131}$$

where l is the electron layer thickness. This approximation was used in Ref. [35] to calculate the reflection coefficient from the electron density maxima in the wake wave. Here, we use the fact that in the nonlinear wakefield, approximately half of the electrons have the speed about v_{ph}, concentrated near the maximum density, while the other half moves in the opposite direction.

In the reference frame moving with the velocity v_{ph}, Eqn (107) can be written as

$$\frac{\mathrm{d}^2 a}{\mathrm{d}\zeta^2} + \bigl(s^2 - g_\delta\delta(\zeta)\bigr)a = 0\,, \tag{132}$$

where $g_\delta = k_{\mathrm{p}}^2 l$. Integrating this equation over ζ in the interval $-\varepsilon < \zeta < \varepsilon$ and setting ε to zero, we obtain the condition for the jump of the derivative $\mathrm{d}a/\mathrm{d}\zeta$ at the boundary $\zeta = 0$:

$$\left.\frac{\mathrm{d}a}{\mathrm{d}\zeta}\right|_{+0} - \left.\frac{\mathrm{d}a}{\mathrm{d}\zeta}\right|_{-0} = g_\delta a(0)\,. \tag{133}$$

The function $a(\zeta)$ is continuous at the point $\zeta = 0$. The solution of Eqn (132) describing the wave reflection from a thin layer can be represented as

$$a(\zeta) = \mathrm{const}\begin{cases} \exp(\mathrm{i}s\zeta) + \rho\exp(-\mathrm{i}s\zeta)\,, & \zeta \geqslant 0\,,\\ \tau\exp(\mathrm{i}s\zeta)\,, & \zeta < 0\,, \end{cases} \tag{134}$$

where ρ and τ are related to each other by equations following from boundary condition (133):

$$1 + \rho(s) = \tau(s)\,, \tag{135}$$

$$\mathrm{i}s\bigl(1 - \rho(s) - \tau(s)\bigr) = g_\delta\tau(s)\,. \tag{136}$$

As a result, the reflected wave amplitude is

$$\rho(s) = -\frac{g_\delta}{2\mathrm{i}s + g_\delta} = \tau(s) - 1\,. \tag{137}$$

From this expression, we obtain the reflection coefficient for the number of photons:

$$\mathsf{R}_\delta = \frac{g_\delta^2}{4s^2 + g_\delta^2}\,. \tag{138}$$

For large values of the electron surface density $n_0 l$, i.e., for $g_\delta^2 \gg 4s^2$, the reflection coefficient is close to unity. In the opposite limit, we can neglect g_δ^2 compared with $4s^2$ in the denominator in the right-hand side of (138) and obtain

$$\mathsf{R}_\delta \approx \frac{g_\delta^2}{4s^2} \approx \frac{(n_0 l\lambda_0 r_{\mathrm{e}})^2}{\gamma_{\mathrm{e}}^2}\,. \tag{139}$$

It follows that the reflection coefficient is proportional to the square of the electron density in the surface layer, $\sim (n_0 l)^2$, i.e., the reflection is coherent. In a nonlinear wake wave, where the energy of the electrons is equal to $\gamma_{\mathrm{e}} \approx \gamma_{\mathrm{ph}} = k_0/k_{\mathrm{p}}$ and the effective layer thickness l is half the wavelength $l \approx 2\sqrt{2\gamma_{\mathrm{ph}}}/k_{\mathrm{p}}$, the reflection coefficient is inversely proportional to the cube of the parameter γ_{e}: $\mathsf{R}_\delta \approx 1/2\gamma_{\mathrm{ph}}^3$ [35].

As shown in Ref. [43], sufficiently homogeneous laser pulses are required in order to form thin electron layers continuous in the transverse direction. When this condition is not satisfied in the interaction of laser radiation with a thin foil, a cloud of ultrashort electron bunches (a swarm of electron bunches) is formed (see also Refs [133, 134]).

8. Interaction of electromagnetic waves with a receding relativistic mirror. Ion acceleration by the radiation pressure of light

In the process of interaction of a laser pulse with a receding relativistic mirror, the back-reflected electromagnetic pulse has an energy negligibly small compared to that incident on the mirror. Hence, the radiation energy is almost completely converted into the energy of ions. In this section, we consider the problem of a receding relativistic mirror, motivated by a common interest in the collective acceleration of ions and the potential for realizing a relativistic mirror for the efficient generation of hard X-rays, discussed in Section 9.

The acceleration of ions in the regime of domination of the radiation pressure of light [1] (the history of this work can be found in [4]) in the relativistic limit has the highest efficiency among the known mechanisms of laser acceleration of charged particles [135]. This ion accelerator also has the names *photon sail* and *laser piston*. This acceleration regime can be realized under the conditions where a thin target irradiated by laser light and pushed forward by the radiation pressure moves as a whole, i.e., electrons and ions move with the same average velocity. In the relativistic limit, due to the smallness of the ratio of the electron mass to the ion mass, the kinetic energy of the ions is greater than the kinetic energy of the electrons by the factor m_α/m_{e}.

8.1 Simple model of radiation pressure acceleration

We consider the interaction of electromagnetic waves with a plasma layer in the geometry where an electromagnetic wave incident on a layer propagates in the direction of its motion. Obviously, the closer the velocity of the layer v_{M} is to the speed of light c, the less the layer is transparent to radiation. If the frequency of the radiation and the plasma density in the laboratory reference frame are ω_0 and n_0, then in the comoving reference frame, where the layer is at rest, the frequency and the density are

$$\bar\omega = \omega_0\left(\frac{1-\beta_{\mathrm{M}}}{1+\beta_{\mathrm{M}}}\right)^{1/2}, \qquad \bar n = n_0(1-\beta_{\mathrm{M}}^2)^{1/2}\,. \tag{140}$$

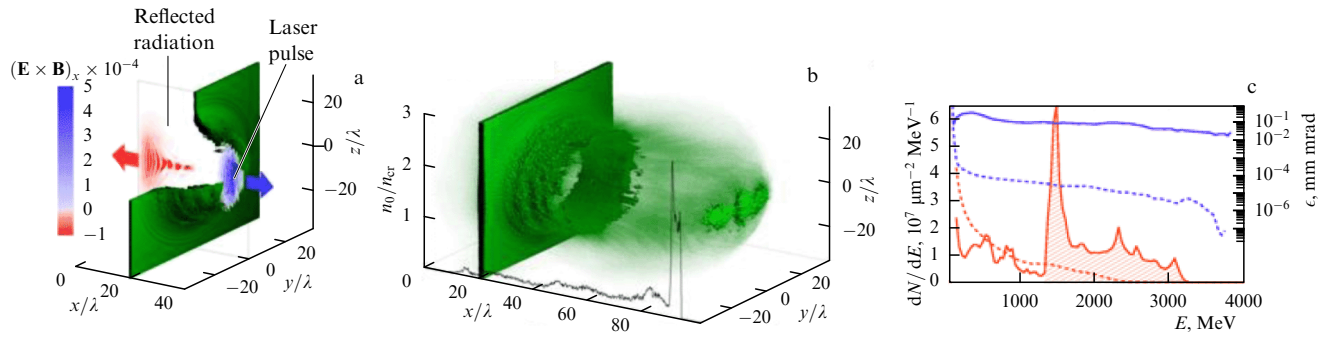

Figure 9. (Color online.) Results of a three-dimensional PIC simulation of radiation pressure acceleration [135]. An electromagnetic pulse forms a thin plasma shell that holds it. (a) The ion density distribution and the x-component of the Poynting vector $(e/m_e\omega_0 c)^2\mathbf{E}\times\mathbf{B}$ in the (x, y) plane at $z = 0$ for $t = 40\times 2\pi/\omega_0$. (b) Isosurface $n = 2n_{cr}$ of the ion density for $t = 100\times 2\pi/\omega_0$; the black curve shows the ion density distribution on the axis. (c) The ion energy spectrum (red curve) and transverse emittance of electrons ϵ (blue dashed curve) and ions (blue solid curve).

In the limit $\beta_M \to 1$ we have $\bar{\omega}\approx\omega_0/2\gamma_M$ and $\bar{n}\approx n_0/\gamma_M$, where $\gamma_M = (1-\beta_M^2)^{-1/2}$.

The plasma opacity condition is $\bar{\omega} < \bar{\omega}_{pe}$, where $\bar{\omega}_{pe} = (4\pi\bar{n}e^2/m_e)^{1/2}$, because $\bar{\omega}\propto\gamma_M^{-1}$ and $\bar{\omega}_{pe}\propto\gamma_M^{-1/2}$, is satisfied better and better in the limit $\gamma_M\to\infty$.

It hence follows that a dense ion–electron layer moving at a relativistic speed almost fully reflects the incident electromagnetic pulse and can be regarded as a perfectly reflecting mirror. Interaction with such a relativistic mirror reduces the energy of the reflected electromagnetic wave by a factor of $\approx 1/4\gamma_M^2$. As a result, the laser pulse energy transferred to the mirror is approximately $\mathcal{E}_{las}(1-1/4\gamma_M^2)$. Because the energy of the electromagnetic radiation is converted into the kinetic energy of the ions in this process, it provides a very high efficiency of this mechanism compared with other mechanisms of laser ion acceleration.

In Fig. 9, in order to illustrate the acceleration of ions in the regime of domination of the radiation pressure of light,we show the results of computer simulation by the PIC method of the radiation acceleration of ions in a three-dimensional configuration. As can be seen, in the course of interaction with a thin plasma layer, the laser pulse forms a thin shell, enclosing the laser pulse like a cocoon. The thin plasma shell holds the electromagnetic radiation inside, preventing its spreading. Ions in the front part of the shell are accelerated to an energy exceeding GeV, and have a quasi-monoenergetic spectrum (Figs 9c).

The combination of the radiation pressure acceleration and the Coulomb explosion mechanisms using a two-layer target can significantly increase the energy of the accelerated ions [136]. This allows achieving higher ion energies using a laser of a lower power and a higher repetition rate, which is of interest for the development of laser acceleration methods for generating ion beams with the parameters required in the hadron therapy of cancer [8].

Indications of the realization of the radiation-dominant regime in the interaction of laser radiation with matter were obtained in an experiment dedicated to the study of the formation of dense plasma jets ejected from a solid target irradiated by intense laser pulses [137].

8.2 Equations of motion of a deformable shell

In this section, we derive the relations required for the analysis of the acceleration and stability of a thin foil moving under the action of the radiation pressure of light [138, 139]. In describing the electromagnetic wave interaction with a foil, the foil is considered an ideally reflecting mirror.

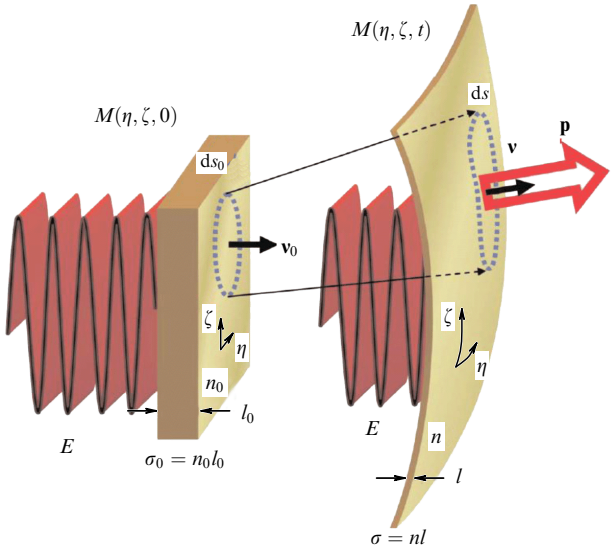

Figure 10. Thin shell evolution under the action of the electromagnetic wave radiation pressure.

In the laboratory frame, the equation of motion of a surface element of a perfectly reflecting mirror can be written as

$$\frac{d\mathbf{p}}{dt} = \mathcal{P}\frac{\mathbf{v}}{\sigma}, \tag{141}$$

where $\mathbf{p}$ is the momentum of the surface element, $\mathbf{v}$ is a unit vector directed along the normal to the mirror surface, $\mathcal{P}$ is the relativistically invariant pressure of light, and $\sigma = nl$ is the surface area density (n and l are respectively the plasma density and the foil thickness). We assume that the foil acceleration and curvature radius are small compared with the values corresponding to the electromagnetic wave frequency and wavelength. The laser–foil interaction geometry is illustrated in Fig. 10.

It is convenient to introduce the coordinates η and ζ related to the independent variables x, y, z as $x = x(\eta,\zeta,t)$, $y = y(\eta,\zeta,t)$, $z = z(\eta,\zeta,t)$. The coordinates η and ζ are markers of the surface element of the shell. We consider the surface element Δs containing the number $\Delta N = \sigma\Delta s$ of particles. This number remains constant during the motion

of the shell. The position and shape of the shell are given by the equation of the surface,

$$\mathbf{M} = \mathbf{M}(\eta, \zeta, t) = \{x(\eta, \zeta, t), y(\eta, \zeta, t), z(\eta, \zeta, t)\}. \quad (142)$$

Following the rules of differential geometry [140], we find that at a regular point of the surface, the surface element and the unit normal vector are given by $\boldsymbol{\nu}\Delta s = \partial\mathbf{M}/\partial\eta \times \partial\mathbf{M}/\partial\zeta \, \mathrm{d}\eta \, \mathrm{d}\zeta$ and

$$\boldsymbol{\nu} = \frac{\partial\mathbf{M}/\partial\eta \times \partial\mathbf{M}/\partial\zeta}{|\partial\mathbf{M}/\partial\eta \times \partial\mathbf{M}/\partial\zeta|}. \quad (143)$$

The particle number conservation gives $\sigma\Delta s = \sigma_0\Delta s_0$, where $\sigma_0 = n_0 l_0$. Hence, it follows that

$$\sigma = \frac{\sigma_0}{|\partial\mathbf{M}/\partial\eta \times \partial\mathbf{M}/\partial\zeta|}. \quad (144)$$

Using these relations, we can write equations of motion (141) in the form

$$\sigma_0 \frac{\partial p_i}{\partial t} = \mathcal{P}\varepsilon_{ijk} \frac{\partial x_j}{\partial \eta} \frac{\partial x_k}{\partial \zeta}, \quad (145)$$

$$\frac{\partial x_i}{\partial t} = c \frac{p_i}{(m_\alpha^2 c^2 + p_k p_k)^{1/2}}, \quad (146)$$

where ε_{ijk} is the unit totally antisymmetric tensor, $i = 1, 2, 3$, and summation over repeated indices is assumed.

The radiation pressure on the shell irradiated by a circularly polarized electromagnetic wave propagating along the x axis with the amplitude $E = E(t - x/c)$ is

$$\mathcal{P} = \frac{E^2}{2\pi} \frac{1-\beta}{1+\beta} = \frac{E^2}{2\pi} \frac{(m_\alpha^2 c^2 + p_x^2)^{1/2} - p_x}{(m_\alpha^2 c^2 + p_x^2)^{1/2} + p_x}. \quad (147)$$

8.3 Parameters of accelerated ion beams

Assuming that the shell moves along the x axis, with the initial conditions determining a flat mirror uniform in the y, z directions, and $y(0) = \eta$, $z(0) = \zeta$, we can write the equation for the x-component of momentum (147) as

$$\frac{\mathrm{d}p_x^{(0)}}{\mathrm{d}t} = \frac{E_0^2}{2\pi\sigma_0} \frac{m_\alpha c\gamma^{(0)} - p_x^{(0)}}{m_\alpha c\gamma^{(0)} + p_x^{(0)}}, \quad (148)$$

where $p_x^{(0)}$ depends only on the time t. The relativistic gamma-factor is equal to $\gamma^{(0)} = [1 + (p_x^{(0)}/m_\alpha c)^2]^{1/2}$.

The solution of Eqn (148) is formally equivalent to the solution to the problem of the motion of a charged particle pushed by the radiation pressure of an electromagnetic wave [52]. For the electromagnetic wave with a constant amplitude $E_0 = \text{const}$ and for the initial value of the particle momentum equal to zero, the momentum dependence on time can be written in implicit form as (see also Ref. [135])

$$\left(\frac{p_x^{(0)}}{m_\alpha c}\right)^3 + \left[1 + \left(\frac{p_x^{(0)}}{m_\alpha c}\right)^2\right]^{3/2} + \frac{3}{2}\frac{p_x^{(0)}}{m_\alpha c} - 1 = \tau, \quad (149)$$

where $\tau = E_0^2 t/2\pi\sigma_0 m_\alpha c$ is the normalized time. In the limit $\tau \to \infty$, we have

$$p_x^{(0)}(\tau) = m_\alpha c\left[\left(\frac{3\tau}{4}\right)^{1/3} - \left(\frac{6}{\tau}\right)^{1/3} + \ldots\right]. \quad (150)$$

In the case of a finite-length electromagnetic pulse, the electric field E_0 on a moving shell, i.e., at $x = x(t)$, depends on time as $E_0(t - x(t)/c)$. In this expression, the function $x(t)$ should be found from Eqn (146). We introduce the new variable $\psi = \omega_0(t - x^{(0)}(t)/c)$, equal to the phase of the electromagnetic wave at $x = x^{(0)}(t)$. Differentiating ψ with respect to time, we find

$$\frac{\mathrm{d}\psi}{\mathrm{d}t} = \omega_0 \frac{m_\alpha c\gamma^{(0)} - p_x^{(0)}}{m_\alpha c\gamma^{(0)}}. \quad (151)$$

Changing the variable from t to ψ and using the integral density of the electromagnetic wave energy flux (also referred to as the fluence of the electromagnetic wave)

$$w(\psi) = \int_0^\psi \frac{R(\psi')}{2\lambda_0} \, \mathrm{d}\psi', \quad (152)$$

where $R(\psi) = E_0^2(\psi)/\sigma_0 m_\alpha \omega_0^2$, allows representing the solution of Eqn (148) in the simple form

$$p_x^{(0)}(\psi) = m_\alpha c \frac{2w(\psi)\big(w(\psi)+1\big)}{2w(\psi)+1}. \quad (153)$$

It follows from expression (151) that the relation between t and ψ is

$$\psi + \int_0^\psi \big(2w(\psi') + w^2(\psi')\big) \, \mathrm{d}\psi' = \omega_0 t. \quad (154)$$

In the case of a constant-amplitude electromagnetic wave with $R = R_0 = E_0^2/2\sigma_0 m_\alpha \omega_0^2$, expressions (152) and (154) yield

$$w(\psi) = \frac{R_0}{\lambda_0}\psi, \quad 3\psi + 3\frac{R_0}{\lambda_0}\psi^2 + 2\left(\frac{R_0}{\lambda_0}\right)^2\psi^3 = 3\omega_0 t. \quad (155)$$

It follows that in the limit $\omega_0 t \gg \lambda_0/R_0$, the x-component of the momentum of the surface element, $p_x^{(0)}$, depends on time as

$$p_x^{(0)} \approx m_\alpha c\left(\frac{3R_0\omega_0}{\lambda_0} t\right)^{1/3}, \quad (156)$$

in agreement with Eqn (150).

We note here that the proportionality of the ion energy to time to the power one third, $t^{1/3}$, has been observed in three-dimensional computer simulations of thin foil acceleration by extremely intense electromagnetic pulses (see Ref. [135]).

It follows from Eqn (154) that the energy of accelerated ions reaches the value

$$\mathcal{E}_\alpha = m_\alpha c^2\left(1 + \frac{2w^2}{1+2w}\right). \quad (157)$$

The efficiency of transformation of the laser radiation energy to the energy of fast ions (equal to the ratio of the ion beam energy to the absorbed laser energy) is

$$\kappa_{\text{eff}} = \frac{2w}{1+2w}, \quad (158)$$

which tends to unity ($\kappa_{\text{eff}} \to 1$) in the high-fluence limit ($w \to \infty$). From this, the energy per ion is equal to the ratio of the laser pulse energy $\mathcal{E}_{\text{las}}$ to the total number of accelerated ions N_{tot}. In the opposite, nonrelativistic, limit for the ion

energy, the acceleration efficiency is

$$\kappa_{\rm eff} = 2w \approx a_0^2 \, \frac{l_{\rm las}}{l_0} \left(\frac{\omega_0}{\omega_{\rm pe}} \right)^2 \frac{m_{\rm e}}{m_\alpha} \, . \tag{159}$$

In regard to problems of controlled thermonuclear fusion within the concept of fast ignition of fusion targets by laser accelerated ions, the required acceleration efficiency should be no less than 10% if the ion energy is of the order of several tens of MeV. For that, 100 kJ laser radiation with an intensity of 10^{21} W cm^{-2} is required.

It is convenient to present the dependences obtained above in dimensional form. The ion energy dependence on the laser pulse parameters in the nonrelativistic limit $\mathcal{E}_\alpha / m_\alpha c^2 \ll 1$ is given by

$$\mathcal{E}_\alpha = 10 \left(\frac{10^{11}}{N_{\rm tot}} \right)^2 \frac{m_{\rm p}}{m_\alpha} \left(\frac{\mathcal{E}_{\rm las}}{1 \text{ J}} \right)^2 \text{[MeV]} \, , \tag{160}$$

where $m_{\rm p}$ is the mass of the proton; in the ultrarelativistic case, where $\mathcal{E}_\alpha / m_\alpha c^2 \gg 1$, we have

$$\mathcal{E}_\alpha = 100 \, \frac{10^{11}}{N_{\rm tot}} \, \frac{\mathcal{E}_{\rm las}}{1 \text{ kJ}} \text{ [GeV]} \, . \tag{161}$$

The acceleration length in the limit of an ultrarelativistic ion energy, $\mathcal{E}_\alpha / m_\alpha c^2 \to \infty$, is

$$l_{\rm acc} = \frac{l_{\rm las}}{1 - v_\alpha / c} \approx 2 \left(\frac{\mathcal{E}_\alpha}{m_\alpha c^2} \right)^2 l_{\rm las} \, . \tag{162}$$

It depends on the laser pulse duration $l_{\rm las}/c$ and on the final energy of accelerated ions $\mathcal{E}_\alpha$.

Discussing the ion beam accelerator for applications in high-energy physics, we come to the conclusion that its parameters must satisfy several conditions, in addition to the requirement of achieving the maximum energy of the particles. In particular, an important parameter such as the luminosity of the beam characterizes the number of particles produced in reactions by colliding beams in the accelerator. We note that controlling the transverse shape of colliding ion beams [138, 141] allows enhancing the beam luminosity value.

It is easy to find that the luminosity of the beam of ions accelerated in the radiation-pressure-dominated regime is given by

$$\mathcal{L} = 10^{34} \, \frac{f}{10 \text{ kHz}} \left(\frac{N_{\rm tot}}{10^{12}} \right)^2 \left(\frac{10^{-4} \text{ cm}}{\sigma_\perp} \right)^2 \text{[cm}^{-2} \text{ s}^{-1}\text{]} \, . \tag{163}$$

Here, $N_{\rm tot}$ is the number of particles in each beam, $\sigma_\perp$ is the transverse size of the beam, and f is the laser repetition rate. The product of the luminosity and the reaction cross section gives the reaction rate. As we can see, the luminosity can be increased by increasing the number of particles per bunch $N_{\rm tot}$ and/or by increasing the laser repetition rate f, or by decreasing the transverse size of the ion beam $\sigma_\perp$.

8.4 Instability of an accelerated shell

The accelerated thin shell is unstable with respect to the development of a mode corresponding to the well-known Rayleigh–Taylor instability [142, 143]. This instability plays a fundamental role in space plasmas and in applications to problems of inertial confinement fusion. In space plasmas and in laser plasma, the Rayleigh–Taylor instability affects the scenario of the interaction of intense radiation with matter. In the case of a thin shell, it can cause its breakup into individual clumps [144, 145].

The thin-shell stability [139] can be analyzed using system of equations (145), (146). Linearizing these equations around the unperturbed solution given by Eqns (148), (149), and (153), we obtain

$$\frac{\partial}{\partial \psi} \left(p_x^{(0)} \, \frac{\partial \xi_x^{(1)}}{\partial \psi} \right) = \frac{R(\psi)}{2\pi} \left(\frac{\partial \xi_y^{(1)}}{\partial \eta} + \frac{\partial \xi_z^{(1)}}{\partial \zeta} \right) , \tag{164}$$

$$\frac{\partial}{\partial \psi} \left(\frac{1}{p_x^{(0)}} \, \frac{\partial \xi_y^{(1)}}{\partial \psi} \right) = - \frac{R(\psi)}{2\pi m_\alpha c} \, \frac{\partial \xi_x^{(1)}}{\partial \eta} \, , \tag{165}$$

$$\frac{\partial}{\partial \psi} \left(\frac{1}{p_x^{(0)}} \, \frac{\partial \xi_z^{(1)}}{\partial \psi} \right) = - \frac{R(\psi)}{2\pi m_\alpha c} \, \frac{\partial \xi_x^{(1)}}{\partial \zeta} \, , \tag{166}$$

where the perturbations $\xi_x^{(1)}(\eta, \zeta, \psi)$, $\xi_y^{(1)}(\eta, \zeta, \psi)$, and $\xi_z^{(1)}(\eta, \zeta, \psi)$, leading to shell deformation in the transverse direction, are assumed to be small. We seek the solution in the framework of the WKB approximation. We represent the functions $\xi_i^{(1)}(\eta, \zeta, \psi)$ in the form

$$\xi_i^{(1)}(\eta, \zeta, \psi) \propto \exp \left(\int_0^\psi \Gamma(\psi') \, {\rm d}\psi' - {\rm i}q\eta - {\rm i}r\zeta \right) \tag{167}$$

under the assumption of a slow dependence of the growth rate $\Gamma(\psi)$ on ψ: $(\partial \Gamma(\psi)/\partial \psi)/\Gamma^2(\psi) \ll 1$. Substituting dependence (167) in system (164)–(166) and solving the algebraic dispersion equation, we obtain the instability growth rate

$$\Gamma(\psi) = (q^2 + r^2)^{1/4} \left(\frac{R(\psi)}{2\pi} \right)^{1/2} . \tag{168}$$

Using expression (155), we find that for a constant-amplitude electromagnetic wave, the perturbations depend on time as

$$\xi_i^{(1)}(\eta, \zeta, t) \propto \exp \left[\left(\frac{t}{\tau_{\rm r}} \right)^{1/3} - {\rm i}q\eta - {\rm i}r\zeta \right] , \tag{169}$$

where the characteristic time of the instability development in the ultrarelativistic limit is

$$\tau_{\rm r} = \omega_0^{-1} (2\pi)^{3/2} \, \frac{R_0^{1/2}}{6(q^2 + r^2)^{3/2} \lambda_0^2} \, .$$

Taking into account that $R_0 = E_0^2 / (2\sigma_0 m_\alpha \omega_0^2)$, we see that the characteristic time of the instability is proportional to the square root of the ratio of the radiation pressure to the ion mass. In other words, the higher the ion mass is, the faster the instability develops, and the higher the radiation pressure is, the slower the perturbations grow.

The expansion of plasma in the transverse direction along the surface of the shell can lead to a slowdown in the nonlinear stage of instability, characterized by the formation of cusp singularities and of high-density plasmoids.

Nonlinear evolution of the instability of a thin shell is illustrated in Fig. 11, which presents the results of computational experiments. A thin plasma slab with a width of $25\lambda_0$ and thickness of $0.5\lambda_0$ with the density corresponding to the ratio $\omega_{\rm pe}/\omega_0 = 16$ is irradiated by an s-polarized laser pulse with the electric field directed along the z axis. The laser radiation is a superposition of a 'Gaussian' pulse and a

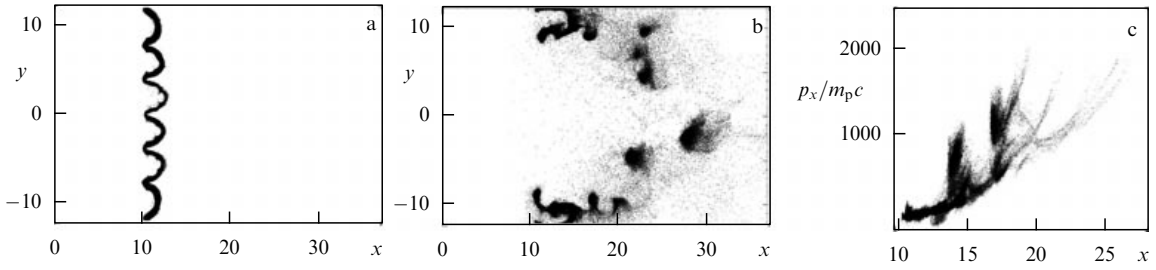

Figure 11. Ion density distribution in the xy plane at the time (a) $t = 75$ and (b) $t = 92$. (c) Ion phase plane (x, p_x).

wide, relatively weak pulse whose intensity is sinusoidally modulated in the y-direction. The dimensionless amplitude of the laser pulse is $a_0 = 320$, which for the wavelength $\lambda_0 = 1$ μm corresponds to the intensity $I \approx 1.4 \times 10^{23}$ W cm^{-2} ($R_{\max}/\lambda_0 = 200$). This corresponds to the parameters that are expected for the extremely high-power lasers like ELI (Extreme Light Infrastructure) and HiPER (High Power laser Energy Research facility) [146–148].

The Rayleigh–Taylor instability, which develops in a thin foil under the action of radiation pressure, was observed in the experiment in [149]. It manifested itself in the modulation of the energy spectrum and the spatial distribution of accelerated ions.

8.5 Regime of 'unlimited' acceleration

The expansion of the plasma along the surface of the shell (notably, it may be a result of the instability discussed in Section 8.4) can lead to a substantial increase in the energy of ions accelerated by the radiation pressure [138, 141] because, due to the shell expansion, the number of ions in the region of interaction with the electromagnetic pulse is reduced, which leads to an increase in their energy. To show this, we consider the case where the shell moves in the longitudinal direction with a momentum $p_x/m_\alpha c \gg 1$, with relatively small transverse components of the momentum corresponding to expansion of the shell, $p_y/p_x \ll 1$ and $p_z/p_x \ll 1$. Using these conditions, we seek the solution of Eqns (145) and (146) assuming that the transverse coordinates and momenta are linear functions of the Lagrangian coordinates η and ζ:

$$y = \Lambda_y(t)\eta\,, \qquad z = \Lambda_z(t)\zeta\,, \tag{170}$$

$$p_y = \pi_y^{(0)}\eta\,, \qquad p_z = \pi_z^{(0)}\zeta\,. \tag{171}$$

Relations (171) with constant $\pi_y^{(0)}$ and $\pi_z^{(0)}$ describe the free expansion of the shell with uniform deformation and correspond to the local approximation of solutions in the near-axial region. It follows from Eqn (146) that the functions Λ_y and Λ_z satisfy the equations

$$\frac{\mathrm{d}\Lambda_y}{\mathrm{d}t} = \frac{\pi_y^{(0)}}{m_\alpha\gamma}\,, \qquad \frac{\mathrm{d}\Lambda_z}{\mathrm{d}t} = \frac{\pi_z^{(0)}}{m_\alpha\gamma} \tag{172}$$

with the initial conditions $\Lambda_y(0) = 1$ and $\Lambda_z(0) = 1$. Here, the ion gamma-factor is $\gamma = [1 + (p_x/m_\alpha c)^2]^{1/2}$. For simplicity, we assume that $\Lambda_y = \Lambda_z = \Lambda$ and $\pi_y^{(0)} = \pi_z^{(0)} = \pi^{(0)}$. The surface density changes according to the relation $nl = n_0 l_0/\Lambda^2$. Substituting these expressions in Eqn (145) for the longitudinal component of the momentum and changing the variable to ψ, we obtain the equation for the deformation parameter $\Lambda(t)$:

$$\frac{\mathrm{d}^2\Lambda}{\mathrm{d}\psi^2} = h^2\Lambda^2\,. \tag{173}$$

If a solution of this equation is known, we can find the longitudinal component of the momentum by integrating the equation

$$\frac{\mathrm{d}p_x}{\mathrm{d}\psi} = \frac{m_\alpha v_E^2}{\omega_0 l_0}\,\frac{m_\alpha c\gamma}{m_\alpha c\gamma + p_x}\,\Lambda^2\,, \tag{174}$$

where $v_E^2 = E^2/2\pi n_0 m_\alpha$ and $h^2 = E^2\pi^{(0)}/2\pi n_0 l_0 m_\alpha^2\omega_0^2 c$.

We assume that the laser pulse with a duration t_{las} has a constant amplitude equal to E_0 in the interval $0 < \psi < \omega_0 t_{\mathrm{las}} = \psi_{\mathrm{m}}$ and zero outside it, i.e., the coefficient h in Eqn (173) is constant inside this interval. The solution of Eqn (173) is then given by the Weierstrass elliptic function $\wp(u; \{g_2, g_3\})$ [80]:

$$\Lambda(\psi) = \wp\bigl(\tilde{\psi}^* - \tilde{\psi}; \{g_2, g_3\}\bigr)\,, \tag{175}$$

where we set $\tilde{\psi} = 6^{1/2}\psi/h$ and g_2 and g_3 are constant, $g_2 = 0$ and $g_3 = 1 - \Lambda'(0)$. The value $\tilde{\psi}^*$ is determined by the minimal positive solution of the equation $\wp(\tilde{\psi}^*; \{0, g_3\}) = 1$. The Weierstrass elliptic function $\wp(u; \{g_2, g_3\}) = z$ gives the value of z for which [80]

$$u = \int_{-\infty}^{z} \frac{\mathrm{d}t}{(4t^3 - g_2 t - g_3)^{1/2}}\,. \tag{176}$$

We discuss the limit cases. For the shell that is not expanding, i.e., for $\Lambda = 1$, it follows from Eqn (174) that asymptotically as $t \to \infty$, the ion momentum depends on time as

$$p_x(t) = m_\alpha c\left(\frac{t}{\tau_{1/3}}\right)^{1/3} + \ldots\,, \tag{177}$$

which corresponds to expression (156). Here, $\tau_{1/3} = 4l_0 c/(3v_E^2)$. It is easy to show that for a shell that expands along only one axis, the dependence of the longitudinal momentum on time is given by $p_x(t) = m_\alpha c(t/\tau_{1/2})^{1/2} + \ldots$, with $\tau_{1/2} = (m_\alpha l_0 c/3v_E^2\pi_y^{(0)})^{1/2}$. For expansion along both axes, Eqn (174) yields the dependence $p_x(t) = m_\alpha c(t/\tau_{3/5})^{3/5} + \ldots$, where $\tau_{3/5} = [48 m_\alpha^2 l_0 c/125 v_E^2(\pi^{(0)})^2]^{1/3}$. It can be seen that the surface density decreases as $nl \propto t^{-4/5}$, and the longitudinal component of the momentum, $p_x \propto t^{3/5}$, increases more rapidly than in the case of a shell that is not expanding or expanding along only one direction.

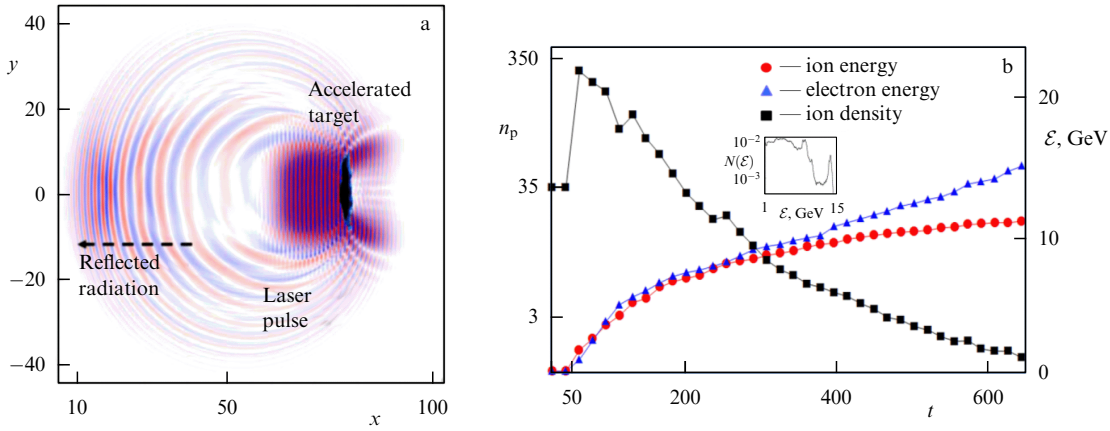

Figure 12. (a) The laser pulse, the reflected wave, and the accelerated plasma target are shown as a superposition of the distribution of the z-component of the electric field and of the ion density in the plane (x, y) for $t = 112.5$. (b) Dependence of the ion and electron energy and of the ion density n/n_{cr} on time. The inset shows the energy spectrum of ions at $t = 600$.

We calculate the value of the phase ψ (the coordinate of the ions relative to the electromagnetic pulse), equal to the integral

$$\psi = \omega_0 \int_0^t \left(1 - \frac{p_x(t')}{m_\alpha c \gamma(t')}\right) \mathrm{d}t' . \tag{178}$$

Substituting the dependence of the momentum on time in the integrand in the form $p_x(t) = m_\alpha c (t/\tau_k)^k$, which for $k = 1/3$, $1/2$, and $3/5$ corresponds to the relations found above, we obtain

$$\frac{\psi}{\omega_0 \tau_k} = \frac{t}{\tau_k} - \frac{(t/\tau_k)^{1+k}}{1+k}\, {}_2F_1\left[\frac{1+k}{2k}, \frac{1}{2}, \frac{1+3k}{2k}; -\left(\frac{t}{\tau_k}\right)^{2k}\right], \tag{179}$$

where ${}_2F_1(\alpha, \beta, \gamma; z)$ is the Gauss hypergeometric function [80]. Asymptotically, in the limit as $t \to \infty$, it follows from this expression that

$$\frac{\psi}{\omega_0 \tau_k} \to \frac{(t/\tau_k)^{1-2k}}{2(1-2k)} + \frac{1}{\pi^{1/2}} \Gamma\left(\frac{2k-1}{2k}\right) \Gamma\left(\frac{k+1}{2k}\right). \tag{180}$$

For $k = 1/2$, Eqn (180) gives the dependence

$$\frac{\psi}{\omega_0 \tau_{1/2}} \to \frac{t - \sqrt{t(t+\tau_{1/2})}}{\tau_{1/2}} + \ln \frac{t^{1/2} + \sqrt{t+\tau_{1/2}}}{\tau_{1/2}^{1/2}}, \tag{181}$$

and hence the phase tends to infinity logarithmically with time.

If the index k is larger than $1/2$, then in the limit $t \to \infty$, the first term in the right-hand side of (180) tends to zero and the phase tends to a finite value equal to the second term. When the ion momentum dependence on time is given by $p_x(t) = m_\alpha c (t/\tau_{3/5})^{3/5} + \ldots$, the index is $k = 3/5$. In this case, we have

$$\psi \underset{t\to\infty}{\to} 2.804 \omega_0 \tau_{3/5} .$$

As can be seen, the phase shift between the position of the ions and the laser pulse does not increase. In a long laser pulse, the ions become trapped, and their energy increases formally without a bound due to the decreasing number of accelerated particles. We note here that the examples of unlimited acceleration are well known for electrons accelerated by an electromagnetic wave propagating along a magnetic field in the autoresonant regime [150], when an electron is trapped in an electrostatic wave propagating perpendicularly to the magnetic field [151–154], and in the case of an electron acceleration by a wake wave in an inhomogeneous plasma [28, 29]. To satisfy the conditions of the trapping of ions in the accelerating phase, the laser pulse must be sufficiently long, with $t_{las} > 2.804\tau_{3/5}$.

Figure 12 shows the results of a computer simulation of the interaction of strong laser radiation with an ellipsoidal target $1.0\lambda_0 \times 7.5\lambda_0$ in size. The initial plasma density corresponds to the ratio $\omega_{pe}/\omega_0 = 6$. A laser pulse $25\lambda_0 \times 25\lambda_0$ in size with the amplitude $a_0 = 125$ compresses the target in the longitudinal direction. The target expands transversely, and, as a result, the radiation pressure of the laser pulse accelerates the target in accordance with the scenario described above. The wavelength of the reflected light increases with time, as it should for a wave reflected from a receding mirror that moves with acceleration. At the initial stage of the interaction, the plasma density increases due to the longitudinal compression of the target, and then it decreases monotonically. For the time $t = 600$, the ion energy reaches 14 GeV, and the electron energy becomes equal to 27 GeV. For a target not extending in the transverse direction, the ion energy would be equal to 3 GeV. In the inset in Fig. 12b, which shows the energy spectrum of ions at $t = 600$, the spectrum is seen to have a quasi-mono-energetic form.

9. Model of a double-sided relativistic mirror

An accelerated double-sided mirror (Fig. 13) allows increasing the value of the coefficient of reflection of counter-propagating electromagnetic waves compared with other approaches for making a relativistic mirror. The role of the mirror is played by a thin layer of dense plasma accelerated to relativistic velocities by the radiation pressure of a laser pulse [135], in accordance with the scenario presented above. The relativistic plasma layer interacting with a counter-propagating electromagnetic wave exhibits properties of flying, oscillating, and sliding relativistic mirrors [36, 38], not only compressing the reflected wave in the longitudinal direction but also generating higher-order harmonics, whose frequency

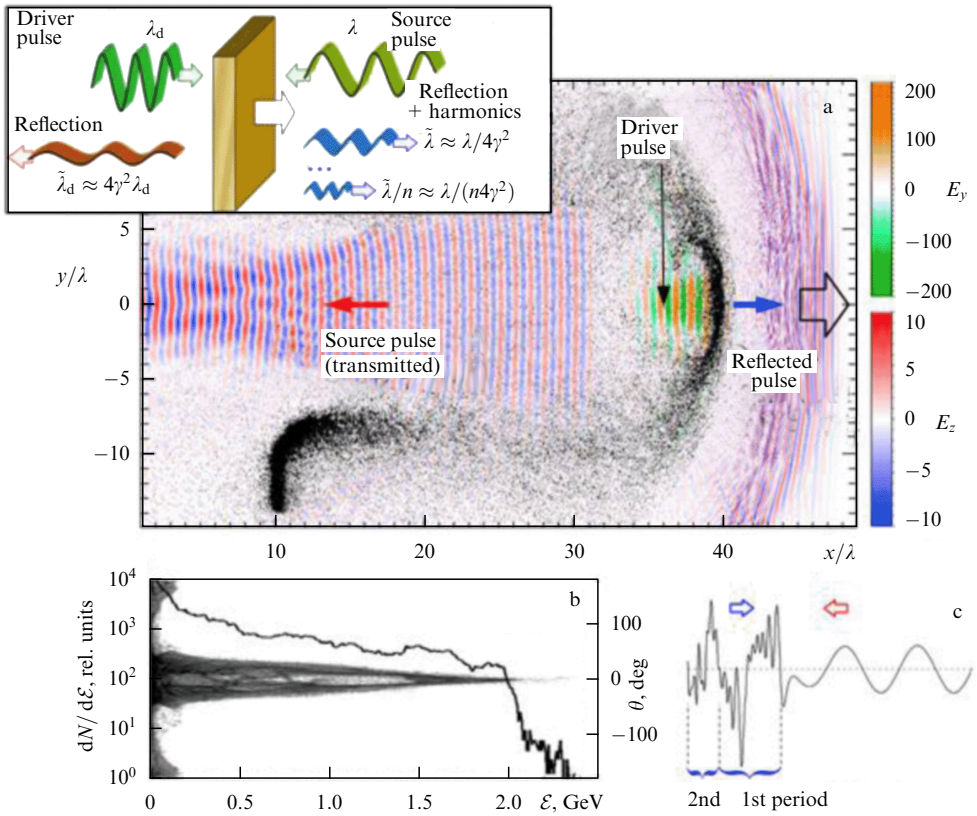

Figure 13. (Color online.) (a) The E_y and E_z components of the electric field in the driver and source laser pulses and the ion concentration distribution (shown in black). Inset: accelerated double-sided mirror [135]. (b) Energy spectrum (solid curve) and angular distribution of ions (gray scale). (c) Profile of the z-component of the electric field of the reflected wave: presented are the first two periods, which are superimposed on the field of the wave incident on the mirror.

due to the Doppler effect increases by the same factor of approximately $4\gamma^2$.

Computer simulations [45] of the interaction of an intense laser pulse with a thin foil (Fig. 13 a) show that the foil is accelerated to relativistic energies, as can be seen from the energy spectrum of the ions in Fig. 13b. The accelerated plasma layer reflects the counter-propagating electromagnetic pulse, which is compressed in the longitudinal direction, and its frequency spectrum becomes modulated (Fig. 13c). As the mirror velocity $c\beta$ increases, the frequency of the reflected wave increases in accordance with the dependence $\omega_0(1+\beta)/(1-\beta)$. This leads to a more and more modulated profile of the reflected laser pulse (Fig. 14a).

The frequency spectrum of the reflected radiation has a complex structure. It comprises not only the frequency of the fundamental mode, increased in accordance with the instantaneous mirror velocity value, but also higher-order harmonics. In Fig. 14b, we show the modulus of the spectrum $|I_\omega(t)|$ calculated for the E_z component of an electromagnetic wave propagating along the x axis for each instant of time. The frequency spectrum of the reflected wave is modulated as a result of the accelerated motion of the mirror, as shown in Fig. 14b.

When the speed of the mirror exceeds a certain threshold in the comoving reference frame, where the mirror is at rest, the average distance between the electrons becomes larger than the wavelength of the incident radiation. As a result, the reflection loses its coherence, and the intensity of the reflected wave is no longer proportional to the square of the number of electrons in the mirror. Instead, it becomes linearly proportional to the number of particles. But even in this less favorable regime, the interaction of electromagnetic waves with a relativistic mirror can provide a high efficiency of X-ray generation in the process of nonlinear backward Thomson scattering, due to the large number of electrons in a solid target.

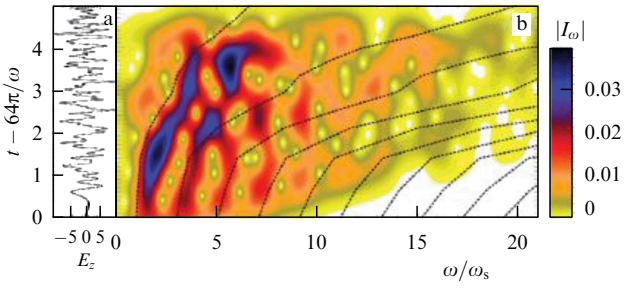

Figure 14. (Color online.) (a) The dependence of the electric field component E_z, taken on the x axis, representing reflected light (in the x-direction); (b) Time sweep of the corresponding frequency spectrum. Dotted lines demonstrate the time dependence of the frequency of odd harmonics, multiplied by $(1+\beta_M)/(1-\beta_M)$, where β_M corresponds to the time-dependent instantaneous velocity of a relativistic double-sided mirror; ω_s is the frequency of the pulse incident on the accelerating two-sided mirror.

We estimate the brightness of the reflected light from the mirror in the two limit cases: for a relatively small, but relativistic velocity, and in the limit of large velocities. When the condition $2\gamma < (n\lambda_s^3)^{1/6}$ is satisfied, the coherent regime of

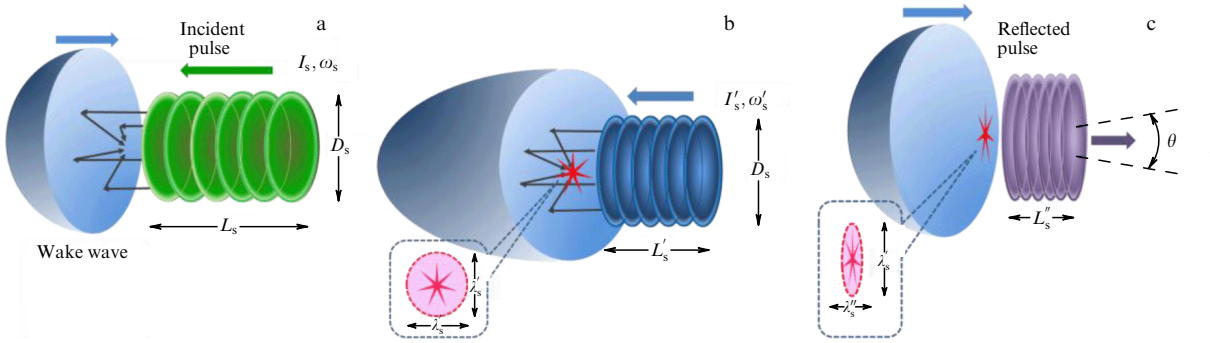

Figure 15. The concept of a flying relativistic mirror [35]. (a) Laboratory frame of reference. Before reflection from the mirror, the laser pulse propagates from right to left. (b) Reference frame where the mirror is at rest. The incident laser pulse has the length $L' \approx L_s/2\gamma_M$ and the wave length $\lambda' \approx \lambda_s/2\gamma_M$. After reflection from a parabolic mirror, the radiation is focused on a region of size $\approx \lambda'$. (c) Laboratory reference frame. The reflected pulse is compressed by a factor of $4\gamma_M^2$; its wavelength becomes $\lambda'' \approx \lambda_s/4\gamma_M^2$. Moving the focal region produces an ellipsoid with the longitudinal dimension λ'' and transverse dimension λ'. Radiation is collimated within the angle $\theta \approx 1/\gamma_M$.

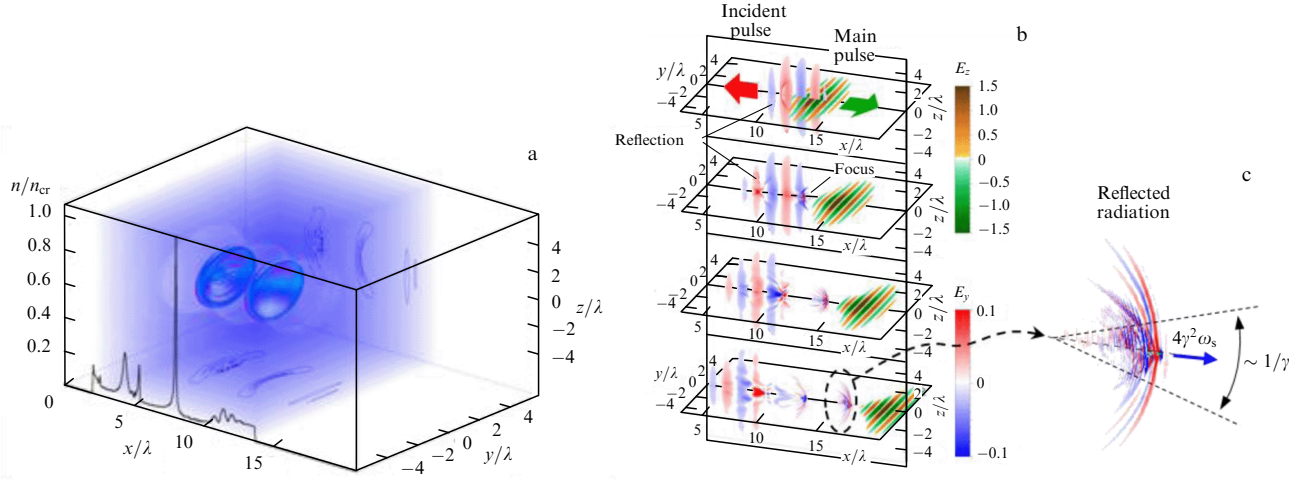

Figure 16. (Color online.) The results of a three-dimensional particle-in-cell computer simulation are shown. (a) Paraboloidal thin shells of relativistic electrons in the wake wave left behind a strong short laser pulse. (b) Colliding laser pulses having mutually perpendicular polarizations. (c) Inset: the reflected pulse with a shortened wavelength is compressed in the longitudinal direction and focused in the transverse direction.

reflection is in effect. The brightness is given by

$$B_M \approx \frac{\mathcal{E}_s(\hbar\omega_r)^3\lambda_s}{4\pi^5\hbar^4c^3}\,, \tag{182}$$

where $\hbar\omega_r$ is the energy of a reflected photon and $\mathcal{E}_s$ is the energy of an electromagnetic pulse incident on the mirror. For large values of γ, the interaction becomes incoherent. Assuming that the electromagnetic radiation is generated by Thomson scattering, we find that the brightness is

$$B_T \approx \frac{a_d\mathcal{E}_s(\hbar\omega_r)^2r_e\lambda_s^2}{8\pi^4\hbar^3c^2\lambda_d^3}\,. \tag{183}$$

For example, when an electromagnetic pulse incident on a mirror with a wavelength $\lambda_s = 0.8$ μm, i.e., $\hbar\omega_s = 1$ eV, has the energy $\mathcal{E}_s = 10$ J, then the reflected light has the brightness $B_M \approx 0.8 \times 10^{40}$ photon/mm^2 mrad^2 s, which is orders of magnitude greater than the brightness of any existing X-ray sources or sources proposed in a terrestrial laboratory [155]. For the same parameters of the electromagnetic pulse incident on a mirror and for the driver pulse parameters $\lambda_d = 0.8$ μm, $a_d = 300$, i.e., $I \approx 10^{23}$ W cm^{-2} and $\hbar\omega_r = 10$ keV ($\gamma = 40$), we obtain $B_T \approx 3 \times 10^{32}$ photon/mm^2 mrad^2 s.

10. Compact source of high-brightness X-rays based on the mechanism of a relativistic flying mirror

10.1 Relativistic flying mirror in nonlinear wake waves

The use of relativistic flying mirrors produced in the interaction of short laser pulses with subcritical-concentration plasmas was suggested in Refs [34, 35] (Fig. 15). In the framework of this concept, relativistic mirrors are related to the thin layers of relativistic electrons generated in nonlinear plasma waves, which are excited in plasma by a short strong laser pulse. Constant-density surfaces in the wake of nonlinear waves have the form of paraboloids of revolution. The counter-propagating laser pulse is partially reflected by these relativistic mirrors. This results in a frequency upshift of the reflected pulse, shortening in the longitudinal direction, and focusing by paraboloidal mirrors in the transverse direction, providing an intensification of reflected radiation, despite the fact that the reflection coefficient is relatively small (Fig. 16).

A relativistic flying mirror with a sufficiently large reflection coefficient for counter-propagating radiation is formed in the process of wake wave breaking. The phase velocity of the wake wave $v_{\rm ph}$ equals the group velocity of the driver laser pulse $v_{\rm g} = \partial\omega/\partial k$, which, in accordance with the dispersion equation $\omega = (k^2c^2 + \omega_{\rm pe}^2)^{1/2}$ for transverse (electromagnetic) waves, is given by $v_{\rm g} = c[1 - (\omega_{\rm pe}/\omega_0)^2]^{1/2}$. In a low-density plasma, where the laser frequency ω_0 is much higher than the Langmuir frequency, $\omega_0 \gg \omega_{\rm pe}$, the group velocity of electromagnetic waves is close to the speed of light in the vacuum. At the threshold of wave breaking, the velocity of the electrons in the wake wave becomes comparable to the wake wave phase velocity $v_{\rm ph}$, which is equivalent to the condition for the electron energy $\mathcal{E}_{\rm e} = m_{\rm e}c^2\gamma_{\rm e}$ and the relativistic gamma-factor corresponding to $v_{\rm ph}$. Wave breaking occurs if

$$\gamma_{\rm e} \geqslant \gamma_{\rm ph} \equiv \left(1 - \frac{v_{\rm ph}^2}{c^2}\right)^{-1/2} = \frac{\omega_0}{\omega_{\rm pe}}\,. \tag{184}$$

As a result of plasma wave breaking, a singularity in the electron density distribution occurs, which breaks the geometrical optics approximation and increases the reflection coefficient [34, 35]. If there is no wave breaking, the reflectivity is exponentially weak.

In the simplest model where the singularity is approximated by a delta function, the reflection coefficient R_δ is given by formula (139). In terms of the number of photons, it depends on the plasma density as

$$\mathsf{R}_\delta \sim \frac{1}{2}\,\gamma_{\rm ph}^3 = \frac{(\omega_{\rm pe}/\omega_0)^3}{2} = \frac{(n/n_{\rm cr})^{3/2}}{2}$$

in the limit $\gamma_{\rm ph} \gg 1$.

With the pulse compression in the transverse direction as a result of focusing by a parabolic mirror with the diameter D_0 taken into account, we obtain the reflected wave intensity

$$I_{\rm r} \approx 32 I_0 \left(\frac{D_0}{\lambda_0}\right)^2 \gamma_{\rm ph}^3\,. \tag{185}$$

Accordingly, the energy and power are $\mathcal{E}_{\rm r} \approx 2\mathcal{E}_0/\gamma_{\rm ph}$ and $\mathcal{P}_{\rm r} \approx 8\mathcal{P}_0\gamma_{\rm ph}$.

As an example, we consider the parameters required to achieve the Schwinger limit for an electromagnetic wave reflected by a flying mirror. We assume that a laser pulse of the amplitude $a_0 = 15$ interacts with plasma with a density of 10^{18} cm^{-3}. The relativistic gamma-factor $\gamma_{\rm ph}$ associated with the wake wave and determined by Eqn (184) equals 45, which corresponds to the frequency upshift by a factor of 810. The intensity and the transverse size of the exciting wake wave laser pulse are assumed to be 4×10^{20} W cm^{-2} and 40 μm. For the counter-propagating laser pulse with the intensity 2×10^{19} W cm^{-2} and beam diameter $D_0 = 40$ μm, the intensity of the radiation partially reflected from the mirror according to Eqn (185) is of the order of 5×10^{28} W cm^{-2}, which corresponds to the Schwinger limit. These parameters correspond to the laser pulse energies of 10 kJ and 50 J. Laser systems capable of generating short pulses of tens of kilojoules of energy are under development in the framework of the ELI project [146].

If such intensity values are achieved, this will allow producing electron–positron pairs from the vacuum. We note that the effects of transverse inhomogeneity of the electromagnetic wave in the focal region and the effects of nonmonochromaticity can significantly increase the electron–positron pair creation probability in the vacuum (see, e.g., Ref. [30]).

The Kerr constant of a nonlinear vacuum, given by Eqn (195), for radiation with a wavelength of 1 μm is approximately 10^{-27} cm^2 erg^{-1}. Nonlinear effects of quantum electrodynamics lead to a mutual focusing of two electromagnetic beams propagating in opposite directions [156, 157]. The critical power corresponding to this process, $\mathcal{P}_{\rm c} = cE_{\rm QED}^2 D_0^2/4\pi$, is given by

$$\mathcal{P}_{\rm c} = \frac{45}{14}\,\frac{cE_{\rm QED}^2\lambda_0^2}{\alpha}\,. \tag{186}$$

It follows from this expression that for $\lambda_0 = 1$ μm, the threshold power is $\mathcal{P}_{\rm c} \approx 2.5 \times 10^{24}$ W. Taking into account that a pulse reflected from a relativistic mirror has a wavelength that is shorter by a factor of $4\gamma_{\rm ph}^2$ and its power is higher by a factor of $8\gamma_{\rm ph}$ than those of a wave incident on the mirror, we find that the effects of the nonlinear quantum electrodynamical vacuum can occur for laser pulses with a power of 50 PW.

The use of spherical Langmuir waves as a relativistic mirror can allow a much higher intensification of the reflected radiation [44]. Owing to the spherical geometry, the reflected wave with a wavelength $\approx \lambda_0/4\gamma_{\rm ph}^2$ is focused in the volume $\lambda_0^3/48\gamma_{\rm ph}^6$, which gives the radiation intensity $I_{\rm r} \approx I_0\gamma_{\rm ph}^4$ for the reflection coefficient $\mathsf{R}_{2/3} \sim 1/\gamma_{\rm ph}^4$ and $I_{\rm r} \approx I_0\gamma_{\rm ph}^5$ for $\mathsf{R}_\delta \sim 1/\gamma_{\rm ph}^3$.

10.2 Experimental demonstration of a relativistic flying mirror

Proof-of-principle experiments on the flying relativistic mirror concept were reported in Refs [112, 113], where the generation of soft X-rays with a narrow energy spectrum was observed. The frequency upshift factor reached the value 100.

In the first experiment that demonstrated the concept of a 'relativistic flying mirror' in a laser plasma, two short laser pulses collided at an angle of 45° in a supersonic gas jet [112]. The configuration of the experiment is shown in Fig. 17. The laser used in this experiment generates radiation pulses with the wavelength 820 nm, energy 210 mJ, and duration 76 fs; hence, it has 2.75 TW of power.

The horizontally polarized driver laser pulse is focused by an off-axis parabolic mirror with a focal length of 645 mm in the supersonic gas jet, ejected out of the nozzle of a rectangular cross section with the size of the long side equal to 10 mm, and with the short side equal to 1.26 mm. The laser pulse propagates along the direction of the short side of the nozzle. The second pulse (the source pulse) is focused by a plano-convex lens with a focal length of 200 mm, which is placed on a five-axle movable lens holder, which provides a spatial overlay with the first pulse driver. The source pulse propagates at the angle $\theta = 45°$ in order to avoid laser damage by the radiation propagating in the opposite direction relative to the pulse driver. The driver pulse has a $1/e^2$ focus diameter equal to 27 μm and an intensity of 5×10^{17} W cm^{-2}. The source pulse energy is 6.3% of the driver energy, which corresponds to the intensity $\approx 10^{17}$ W cm^{-2}.

During the interaction of the driver laser pulse with the gas jet, the gas is ionized. The driver excites the wake plasma wave that accelerates the electrons to ultra-relativistic

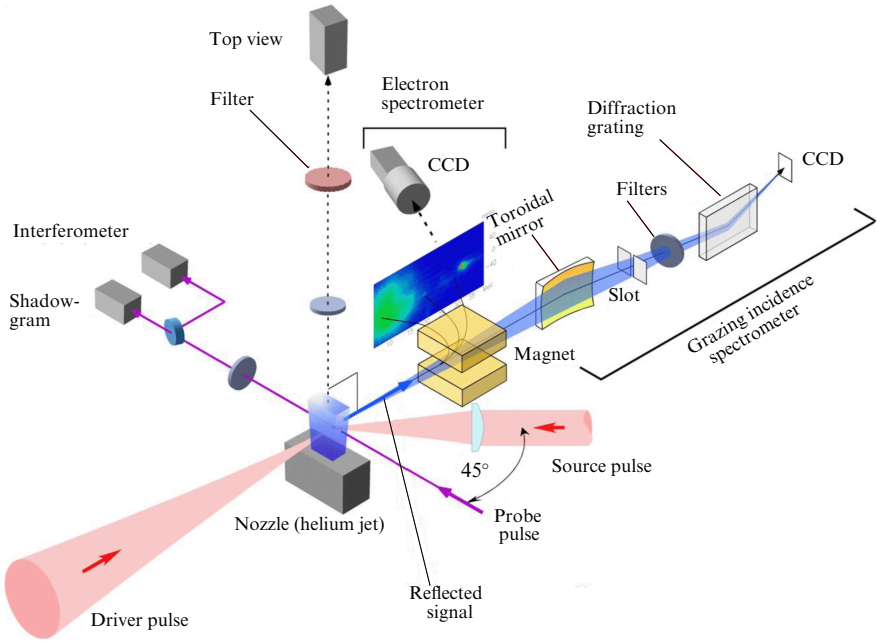

Figure 17. Configuration of the proof-of-principle experiments for the flying relativistic mirror concept [112, 113]. A strong driver pulse excites a plasma wake wave. As a result of wake wave breaking, relativistic mirrors are generated. The second, weaker source laser pulse that propagates at the angle $\theta = 45^\circ$ is focused on the place where the wake wave breaks. The third probe laser pulse is used for high-precision alignment. A permanent magnet is used to deflect relativistic electrons accelerated by the wake wave. The electron beam forms an image on a phosphor screen, showing the electron energy spectrum, which is measured by using a CCD (charge-coupled device). The signal reflected by the nonlinear wake wave is measured by a grazing incidence spectrometer sensitive to radiation in the soft X-ray range having a wavelength from 5 to 15 nm.

energies (see the discussion of electron wakefield acceleration in review article [33] and in the references therein). A permanent magnet is used to bend the relativistic electron beam, which forms an image on a phosphor screen, showing the electron energy spectrum measured by using a CCD (charge-coupled device).

In the configuration of the counter-crossing of two laser pulses at the angle $\theta = 45^\circ$, the frequency of the light reflected from the relativistic mirror should be increased by the factor $\omega_r/\omega_s \approx 3.4\gamma_{ph}^2$. The plasma density in the target is approximately 5×10^{19} cm^{-3}. For this plasma density, the wake wave gamma-factor is $\gamma_{ph} \approx 6.5$ and the theoretically predicted frequency upshift factor is 140.

For the above parameters of laser radiation and the target plasma, the driver pulse excites a wake wave with an amplitude large enough to exceed the wave-breaking threshold. However, the excess over the wave-breaking threshold is not too great, and the regular wake wave structure is not destroyed. Evidence of this regime is the observation of quasi-mono-energetic spectra of ultrarelativistic electrons with an energy of 20 MeV accelerated by the wake wave. In accordance with the theory of wakefield acceleration whose results are presented in Section 4, the injection of electrons into the accelerating phase of the wakefield is the result of nonlinear plasma wave breaking leading to a multi-stream electron flow. At the next stage, the electrons are accelerated by the electric field of the wake wave, forming a narrow band in the vicinity of the separatrix in the phase plane (longitudinal coordinate x, longitudinal momentum p_x), which results in the characteristic shape of the electron energy spectrum (see Fig. 8).

Another indication of the nonlinear character of the wake is the detection of upshifted and downshifted maxima in the frequency spectrum of radiation scattered at an angle of 60°, corresponding to the stimulated backward Raman scattering (SRS). In addition, an analysis of the interferogram reveals channel formation in the plasma density, which, in accordance with the wake excitation by an electromagnetic wave, is also unstable against relativistic self-focusing, which leads to a redistribution of the electron density.

Further development of the theory of the relativistic flying mirror and experiments with laser light of a higher power [158] have allowed the demonstration of high-efficiency regimes that can allow developing highly effective sources in the energy range corresponding to hard X-rays. In this case, a laser with an energy of 0.5 J and a power of 15 TW is used. Here, in contrast to the experiments discussed above, the configuration of two colliding pulses was realized, which provided an increase of several orders of magnitude in the number of reflected photons in the spectral range corresponding to soft X-rays. To detect the reflected radiation, the spectrometer had a relatively large aperture for collecting a sufficiently large number of photons from a representative solid angle. Various methods were used to ensure the collision of pulses to occur at a location predetermined with high accuracy at the desired time. A detailed description of the experiment can be found in [113, 158, 159]. The observed spectrum in the extreme ultraviolet region is presented in Fig. 18b.

The number of photons of hard electromagnetic radiation registered in the experiment allows us to conclude that agreement with theoretical predictions for the reflection coefficient defined by formula (119) was achieved.

In addition to the problem of relativistic mirror reflectivity, it is of particular interest to determine whether the mirror has a high-quality reflective surface, i.e., whether it is smooth enough. In the experiment presented in Ref. [158], the observed radiation in the wavelength range 12 to 20 nm

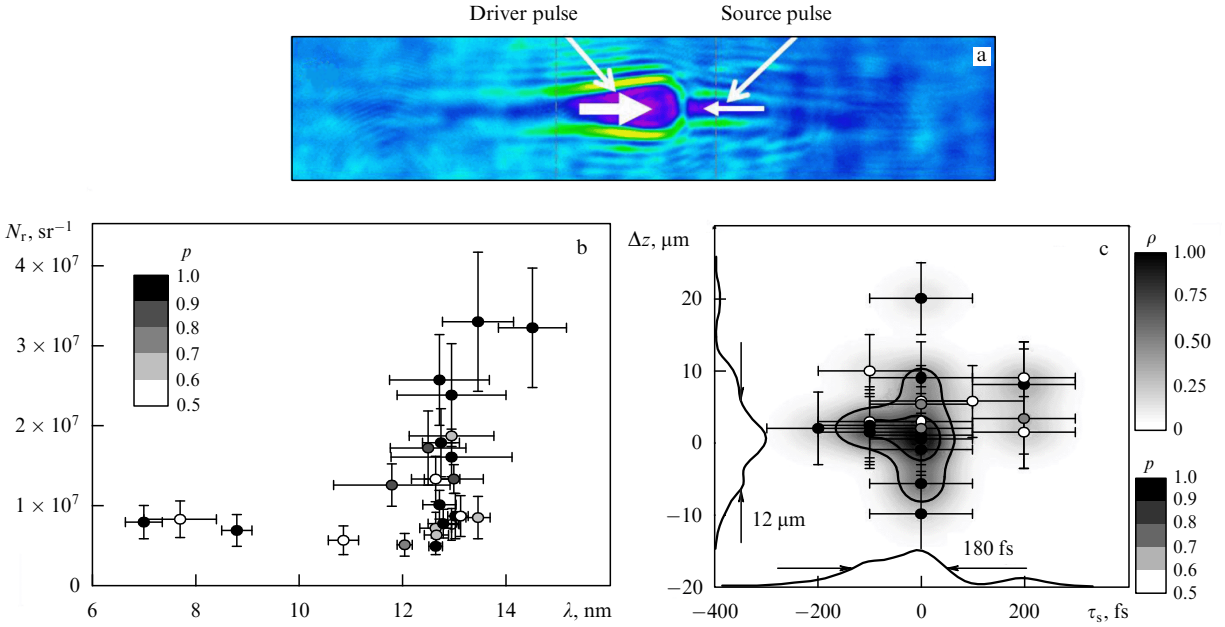

Figure 18. (a) Shadowgram image of two colliding laser pulses. (b) The wavelength and the number N_r of reflected photons measured in 24 different shots; p is the probability that the registered signal is not noise. The length of vertical bars characterizes the measurement error, and the horizontal bar shows the spectrum width. (c) The dependence of the number of reflected photons on the laser pulse delay time τ_s and on the deviation of the laser pulse in the vertical direction Δz. Gray scale shows the normalized density of the reflected photons ρ in units (srad μm ps)$^{-1}$; the distance between the contours is 0.33 [112].

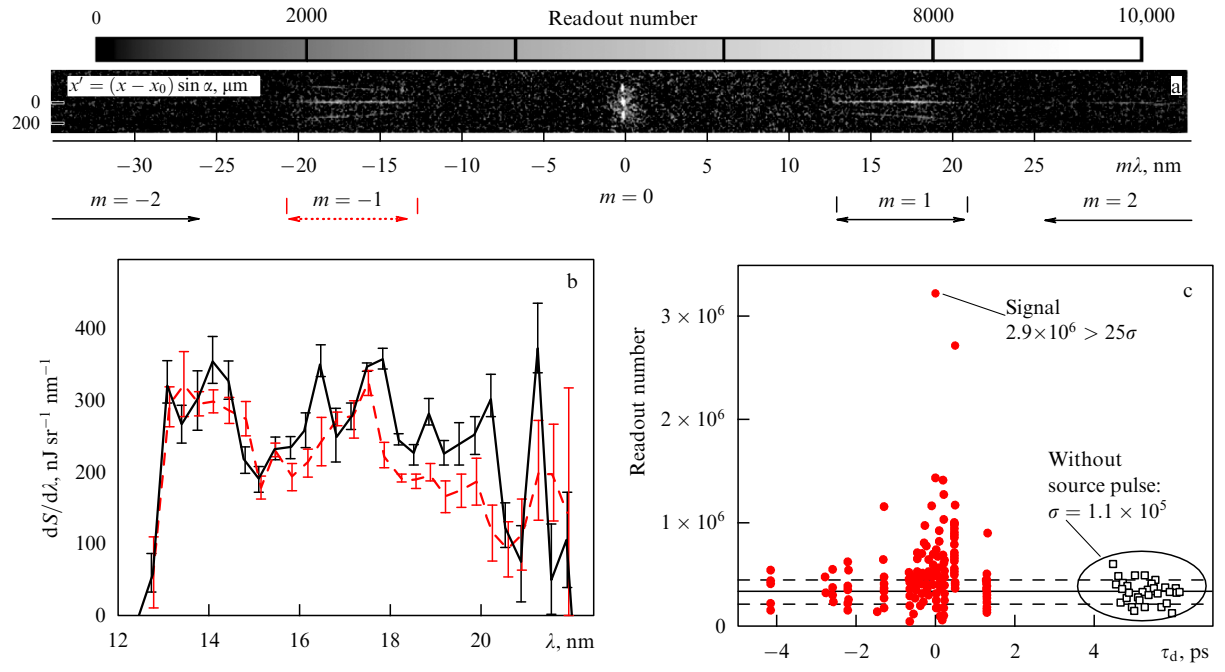

Figure 19. (Color online.) The radiation reflected from a relativistic flying mirror with the gamma-factor $\gamma_{ph} = 6 \pm 1$. (a) The original CCD image obtained by using a normal-incidence spectrograph. (b) The spectrum of the reflected radiation $dS/d\lambda$ in the diffraction order $m = 1$ (black curve) and in the order $m = -1$ (red curve). (c) The dependence of the CCD in the diffraction order $m = 1$ on the time delay τ_d between laser pulses (red dots) and in the absence of the second source pulse (black dots) [158]; σ is the detector noise level.

within the observation angles in the range 9° to 17° (Fig. 19) had a sufficiently smooth spectral distribution. Because the frequency upshift factor depends on the angle at which the reflected light propagates and on the local angle of reflection from the mirror surface, this shows that the radiation is reflected from a smooth surface has a curvature. This is also consistent with the predictions of the theory, which is important for further research aimed at the demonstration of the sharp focusing of X-rays in order to reach the high limits of their intensity.

11. Other schemes to develop a compact high-intensity X-ray source based on the use of relativistic mirrors

There are several other schemes to develop compact X-ray sources of high intensity based on the use of relativistic mirrors formed in the process of nonlinear interaction of laser radiation with plasma, whose implementation will create exciting opportunities for experiments on nonlinear electrodynamics of continuous media in the relativistic regime. Nonlinear interaction of Langmuir waves with regular nonlinear structures in collisionless plasma, such as relativistic electromagnetic solitons, electron vortices, and plasma waves, are considered in Refs [38, 43] as a way toward generating ultra-short electromagnetic pulses of high amplitude. These X-ray pulses are generated due to a partial reflection of a low-frequency electromagnetic field from a relativistic mirror. This process is accompanied by a frequency upshift due to the double Doppler effect. This effect also leads to a strong field compression and to electromagnetic pulse formation on a scale much smaller than that of the original nonlinear structure.

Dense electron layers accelerated to a relativistic velocity by laser radiation interacting with a thin plasma foil are also considered as relativistic mirrors capable of generating beams of coherent X-ray and gamma radiation of high brightness [41].

12. Parameters characterizing the interaction of strong electromagnetic radiation with matter

The purpose of further studies of the physical processes associated with relativistic mirrors is to design and build a compact source of hard electromagnetic radiation with a photon energy and intensity large enough to conduct experiments in previously inaccessible regimes of interaction of electromagnetic fields with matter. In this section, we present the parameters that characterize the main regimes of laser–matter interaction, depending on the intensity of the electromagnetic wave.

In this review, we consider the nonlinear electrodynamics of plasma in the limit of relativistic particle energies. The behavior of an electron in the field of an electromagnetic wave is determined by the dimensionless parameter $a = eE/m_e\omega c$, which is the normalized wave amplitude. This value is associated with a relativistic invariant, as is clearly seen from its representation in the form

$$a = e\,\frac{\sqrt{A^\mu A_\mu}}{m_e c^2}\,. \tag{187}$$

If $a > 1$, the electron energy becomes relativistic. Its longitudinal momentum exceeds the transverse momentum by a factor of $a/2$. Therefore, the relativistic limit is reached at the values of the dimensionless amplitude of the wave

$$a_0 = \frac{eE_0}{m_e\omega_0 c} = \frac{eE_0\lambda\!\!\!^{-}_0}{m_e c^2} \tag{188}$$

of the order of unity, which corresponds to the intensity $I \approx 1.37 \times 10^{18}$ W cm^{-2} for the radiation wavelength λ_0 equal to one micron. The electric field of such a wave is able to produce work equal to $m_e c^2$ over the distance $\lambda\!\!\!^{-}_0 = c/\omega_0 = \lambda_0/2\pi$.

When a long enough electromagnetic pulse propagates in plasma, the average longitudinal momentum of electrons is equal to zero. The solution of the problem of the nonlinear electromagnetic wave dynamics in collisionless plasmas obtained by Akhiezer and Polovin in Ref. [72] shows that the transverse component of the momentum and the kinetic energy of the electron in the wave are respectively equal to $m_e c a_0$ and $m_e c^2[(1 + a_0^2)^{1/2} - 1]$.

With a further increase in the electromagnetic wave intensity, its interaction with a sufficiently dense plasma is characterized by radiation loss effects [160–163]. The energy loss rate by an electron rotating in the field of a circularly polarized wave is given by

$$\dot{\mathcal{E}}^{(-)} = \varepsilon_{\rm rad} m_e c^2 \omega_0 a_0^2 (1 + a_0^2)\,, \tag{189}$$

where we introduce the dimensionless parameter

$$\varepsilon_{\rm rad} = \kappa_{\rm p}\,\frac{r_e}{\lambda\!\!\!^{-}_0} \tag{190}$$

characterizing the radiation losses. The coefficient $\kappa_{\rm p}$ depends on the electromagnetic wave polarization. For circular polarization, it is equal to 3/8, while for linear polarization, it is 1/8. In expression (190), $r_e = e^2/m_e c^2 \approx 2.8 \times 10^{-13}$ cm is the classical electron radius.

Because the electromagnetic wave cannot transfer energy to the particle with a rate greater than

$$\dot{\mathcal{E}}^{(+)} = eE_0 c = m_e c^2 \omega_0 a_0\,, \tag{191}$$

we can use the condition of the balance between incoming and radiated energy per unit time, $\dot{\mathcal{E}}^{(+)} = \dot{\mathcal{E}}^{(-)}$, to find the threshold value of the amplitude of the electromagnetic wave above which the influence of radiation losses cannot be ignored. In dimensionless form, the threshold amplitude of the wave is

$$a_{\rm rad} = \varepsilon_{\rm rad}^{-1/3}\,. \tag{192}$$

For a circularly polarized wave with $\lambda_0 = 0.8$ μm, it is equal to $a_{\rm rad}^{\rm c} = 408$, which corresponds to the radiation intensity $I^{\rm c} = 4 \times 10^{23}$ W cm^{-2} and $a_{\rm rad}^{\rm l} = 713$ with $I^{\rm l} = 7 \times 10^{23}$ W cm^{-2}, if the wave is linearly polarized.

When the intensity threshold $I \approx 10^{25}$ W cm^{-2} is exceeded, which corresponds to the normalized amplitude

$$a_{\rm QM} = \frac{e^2 m_e c}{\hbar^2 \omega_0}\,, \tag{193}$$

it is necessary to consider quantum mechanical processes such as the recoil effect in Compton scattering [162], leading to the phenomenon of 'quantum diffusion', known in the physics of particle accelerators, and to electron–positron pair creation in the interaction with an electromagnetic wave of gamma photons emitted by ultra-relativistic electrons [163–169]. These processes principally alter the scenario of the interaction of laser radiation with plasmas.

When the limit intensity $I \approx 10^{29}$ W cm^{-2} is reached, the electric field of the laser radiation becomes comparable in magnitude with the critical field of quantum electrodynamics

$$E_{\rm s} = \frac{m_e c^2}{e\lambda\!\!\!^{-}_{\rm C}}\,, \tag{194}$$

where $\lambda\!\!\!^{-}_{\rm C} = \hbar/m_{\rm e}c$ is the Compton wavelength. The condition implied by (194) means that the electric field $E_{\rm s}$ over a length equal to the Compton wavelength $\lambda\!\!\!^{-}_{\rm C}$ produces work equal to $m_{\rm e}c^2$. This electric field, first mentioned in Refs [170–172], corresponds to the dimensionless amplitude $a_{\rm s} = m_{\rm e}c^2/\hbar\omega_0$. In the limit when the laser field approaches $E_{\rm s}$, nonlinear effects of quantum electrodynamics lead to the creation of electron–positron pairs in the vacuum, and the vacuum therefore behaves as a nonlinear optical medium with a refractive index that depends on the electric field strength [173]. The effective value of the Kerr constant of the vacuum is (the refractive index in a Kerr nonlinear medium can be represented in the form $n = n_0 + \lambda_0 K|E|^2$)

$$K_{\rm QED} = \frac{7\alpha\lambda\!\!\!^{-3}_{\rm C}}{90\pi m_{\rm e}c^2\lambda_0}\,, \tag{195}$$

where $\alpha = e^2/\hbar c$ is the fine structure constant.

Expression (193) corresponds to the electric field $E_{\rm QM} = em_{\rm e}^2c^2/\hbar^2 = \alpha E_{\rm s}$, i.e., it is less than the critical field of quantum electrodynamics by a factor of approximately 1/137.

The creation of electron–positron pairs in the vacuum can occur for an intensity of the electromagnetic wave well below 10^{29} W cm^{-2} due to the multi-photon Breit–Wheeler process [167, 169, 174]. Here, we do not discuss the theoretically and experimentally well-established process of pair creation in collisions of electrons with nuclei and positrons [173, 175], on which much attention was focused in regard to the problems of laser-produced plasmas [176–178]. In our case, pairs are generated due to the interaction of sufficiently high-energy gamma rays with an electromagnetic wave. The probability of this process is determined by the dimensionless parameter

$$\chi_\gamma = \frac{\sqrt{\left(F^{\mu\nu}\hbar k_\nu\right)^2}}{m_{\rm e}cE_{\rm s}} \approx a\,\frac{\hbar^2\omega\omega_\gamma}{m_{\rm e}^2c^4}\,, \tag{196}$$

which is a relativistic invariant. In this expression, $F_{\mu\nu}$ is the four-tensor of the electromagnetic field, k_ν is the four-vector of the photon, ω_γ is its frequency, ω is the frequency of the electromagnetic wave, and a is its amplitude. For small values of this parameter, the pair production probability is exponentially suppressed. In a high-intensity laser field, the electron emits high-energy photons as a result of multi-photon Compton scattering. This process is characterized by the relativistically invariant parameter

$$\chi_{\rm e} = \frac{\sqrt{\left(F^{\mu\nu}p_\nu\right)^2}}{m_{\rm e}cE_{\rm s}} = \frac{1}{E_{\rm s}}\sqrt{\left(\gamma_{\rm e}\mathbf{E} + \frac{\mathbf{p}\times\mathbf{B}}{m_{\rm e}c}\right)^2 - \left(\frac{\mathbf{p}\,\mathbf{E}}{m_{\rm e}c}\right)^2}\,, \tag{197}$$

which is approximately

$$\chi_{\rm e} \approx \frac{E}{E_{\rm s}}\,\frac{p_\perp}{m_{\rm e}c}\,,$$

where $p_\perp$ is the component of the electron momentum. In the limit $\chi_{\rm e} \gg 1$, the electron emits photons for which $\chi_{\rm e} \approx \chi_\gamma$. Hence, the condition of an avalanche-type regime of pair production requires the condition $\chi_{\rm e} \gg 1$, which can be satisfied in the limit of the intensity values above 10^{25} W cm^{-2}. This threshold may be decreased if a laser beam interacts with pre-accelerated ultra-relativistic electrons. In the experiments in [174], positrons were registered in the collision of a 50 GeV beam of electrons with a laser pulse with an intensity of the order of 10^{17} W cm^{-2}.

To conclude this section, we note that the peak value of laser intensity reached by now is greater than 10^{22} W cm^{-2} [179].

13. Conclusion

In the framework of the relativistic flying mirror concept, it is possible to develop a compact source of high-brightness, ultrafast X- and gamma rays with a tunable energy of photons. In laser plasma, when the infrared photons of laser light are reflected by a mirror, their energy is in the ultraviolet or X-ray range. In other words, this is a high-power X-ray laser. As a part of this concept, the possibility of developing a compact high-energy ion accelerator based on high-power laser interaction with a receding mirror is also considered.

These facts significantly expand the range of applications of laser relativistic plasma toward applications requiring a large number of photons in a short pulse, on the one hand, and short bunches of high-energy ions, on the other hand.

The development of this scientific field will create new areas of research and new applications, opening up new horizons for nuclear physics [6], laboratory astrophysics [48, 180, 181], controlled thermonuclear fusion [7], biology and medicine [47], and fundamental physics [29, 135].

We appreciate the support from MEXT (Japan) under the grant 23740413, 2011 and the RFBR grants 10-02-01016-a,d 11-02-12250-ofi-m, and 12-02-00287a.

The authors are grateful for the fruitful discussions to K Akimoto, P Bolton, M Borghesi, V Yu Bychenkov, A V Gordeev, H Daido, G Dunne, E Yu Echkina, A G Zhidkov, V A Ivanov, I N Inovenkov, T Kawachi, F Califano, F F Kamenets, S Kar, Y Kato, T Kimura, H Kiriyama, J Koga, K Kondo, G Korn, H Kotaki, V V Kulagin, M Lobet, V Lontano, J M Lee, W P Leemans, A Macchi, N Matlis, G Mourou, T Nakamura, C H Nam, N B Narozhnyi, P Nickles, D Neely, K Nishihara, A V Panchenko, F Pegoraro, T A Pikuz, V S Popov, E N Ragozin, V I Ritus, W Rozmus, J Rocca, A A Rukhadze, A S Sakharov, H Suk, T Tajima, V I Telnov, A Ya Faenov, D Farina, Yu Fukuda, D Habs, J Hajdu, T Heinzl, V N Tsytovich, A V Cherepenin, C Schroeder, and E Esarey.

References

1. Veksler V I *Sov. J. Atom. Energy* **2** 525 (1957) [*Atom. Energ.* **2** 427 (1957)]
2. Lebedev P N *Ann. Physik* **6** 433 (1901)
3. Eddington A S *Mon. Not. R. Astron. Soc.* **85** 408 (1925)
4. Tsander F A *Tekhnika Zhizn'* (13) 15 (1924)
5. Bolotovskii B M, Lebedev A N *Phys. Usp.* **50** 847 (2007) [*Usp. Fiz. Nauk* **177** 889 (2007)]
6. Ledingham K D W, Galster W *New J. Phys.* **12** 045005 (2010)
7. Roth M et al. *Phys. Rev. Lett.* **86** 436 (2001)
8. Bulanov S V, Khoroshkov V S *Plasma Phys. Rep.* **28** 453 (2002) [*Fiz. Plazmy* **28** 493 (2002)]
9. Einstein A *Ann. Physik* **17** 891 (1905)
10. Davies P C W, Fulling S A *Proc. R. Soc. Lond. A* **356** 237 (1977)
11. Hawking S W *Nature* **248** 30 (1974)
12. Unruh W G *Phys. Rev. D* **14** 870 (1976)
13. Mostepanenko V M, Trunov N N *Sov. Phys. Usp.* **31** 965 (1988) [*Usp. Fiz. Nauk* **156** 385 (1988)]
14. Landecker K *Phys. Rev.* **86** 852 (1952)
15. Ostrovskii L A *Sov. Phys. Usp.* **18** 452 (1975) [*Usp. Fiz. Nauk* **116** 315 (1975)]
16. Dodonov V V *Adv. Chem. Phys.* **119** 309 (2001)

17. Granatstein V L et al. *Phys. Rev. A* **14** 1194 (1976)
18. Pasour J A, Granatstein V L, Parker R K *Phys. Rev. A* **16** 2441 (1977)
19. Semenova V I *Radiophys. Quantum Electron.* **10** 599 (1967) [*Izv. Vyssh. Uchebn. Zaved. Radiofiz.* **10** 1077 (1967)]
20. Lampe M, Ott E, Walker J H *Phys. Fluids* **21** 42 (1978)
21. Belov S N, Rukhadze A A *Kratk. Soobshch. Fiz.* (5) 8 (1978)
22. Savage R L (Jr.), Joshi C, Mori W B *Phys. Rev. Lett.* **68** 946 (1992)
23. Mori W B et al. *Phys. Rev. Lett.* **74** 542 (1995)
24. Hashimshony D, Zigler A, Popadopoulos K *Phys. Rev. Lett.* **86** 2806 (2001)
25. Higashiguchi T et al. *Appl. Phys. Lett.* **90** 111503 (2007)
26. Askar'yan G A, Manzon B M *JETP Lett.* **31** 259 (1980) [*Pis'ma Zh. Eksp. Teor. Fiz.* **31** 283 (1980)]
27. Bakunov M I et al. *Astropart. Phys.* **33** 335 (2010)
28. Bulanov S V et al., in *Reviews of Plasma Physics* Vol. 22 (Ed. V D Shafranov) (New York: Kluwer Acad./Plenum Publ., 2001) p. 227
29. Mourou G A, Tajima T, Bulanov S V *Rev. Mod. Phys.* **78** 309 (2006)
30. Marklund M, Shukla P K *Rev. Mod. Phys.* **78** 591 (2006)
31. Belyaev V S et al. *Phys. Usp.* **51** 793 (2008) [*Usp. Fiz. Nauk* **178** 823 (2008)]
32. Fortov V E *Phys. Usp.* **52** 615 (2009) [*Usp. Fiz. Nauk* **179** 653 (2009)]
33. Esarey E, Schroeder C B, Leemans W P *Rev. Mod. Phys.* **81** 1229 (2009)
34. Bulanov S V et al. *Kratk. Soobshch. Fiz.* (6) 9 (1991)
35. Bulanov S V, Esirkepov T, Tajima T *Phys. Rev. Lett.* **91** 085001 (2003)
36. Bulanov S V, Naumova N M, Pegoraro F *Phys. Plasmas* **1** 745 (1994)
37. Teubner U, Gibbon P *Rev. Mod. Phys.* **81** 445 (2009)
38. Naumova N M et al. *Phys. Rev. Lett.* **92** 063902 (2004)
39. Bulanov S S et al. *Phys. Rev. E* **73** 036408 (2006)
40. Pirozhkov A S et al. *Phys. Plasmas* **13** 013107 (2006)
41. Kulagin V V et al. *Phys. Plasmas* **14** 113101 (2007)
42. Meyer-ter-Vehn J, Wu H-C *Eur. Phys. J. D* **55** 433 (2009)
43. Bulanov S S et al. *Phys. Lett. A* **374** 476 (2010)
44. Bulanov S S et al. *Phys. Plasmas* **19** 020702 (2012)
45. Esirkepov T Zh et al. *Phys. Rev. Lett.* **103** 025002 (2009)
46. Mourou G, Tajima T *Science* **331** 41 (2011)
47. Neutze R et al. *Nature* **406** 752 (2000)
48. Bulanov S V et al. *Eur. Phys. J. D* **55** 483 (2009)
49. Popov V S *Phys. Usp.* **47** 855 (2004) [*Usp. Fiz. Nauk* **174** 921 (2004)]
50. Bolotovskii B M, Stolyarov S N *Sov. Phys. Usp.* **32** 813 (1989) [*Usp. Fiz. Nauk* **159** 155 (1989)]
51. Birrell N D, Davies P C W *Quantum Fields in Curved Space* (Cambridge: Cambridge Univ. Press, 1982)
52. Landau L D, Lifshitz E M *The Classical Theory of Fields* (Oxford: Pergamon Press, 1980) [Translated from Russian: *Teoriya Polya* (Moscow: Nauka, 1988)]
53. Van Meter J R, Carlip S, Hartemann F V *Am. J. Phys.* **69** 783 (2001)
54. Mikhel'son V A *Zh. Russ. Fiz. Chim. Obshch. Ch. Fiz.* **31** (7) 119 (1899)
55. Miller M A, Sorokin Yu I, Stepanov N S, in *Fizicheskii Entsiklopedicheskii Slovar'* (Encyclopedic Dictionary of Physics) (Ed.-in-Chief A M Prokhorov) (Moscow: Sov. Entsiklopediya, 1984) p. 185
56. Frank I M *Izv. Akad. Nauk SSSR Ser. Fiz.* **6** 3 (1942)
57. Rosanov N N *Opt. Spectrosc.* **107** 768 (2009) [*Opt. Spektrosk.* **107** 808 (2009)]
58. Ostrovskii L A *Izv. Vyssh. Uchebn. Zaved. Radiofiz.* **2** 833 (1959)
59. Freidman G I *Sov. Phys. JETP* **14** 165 (1962) [*Zh. Eksp. Teor. Fiz.* **41** 226 (1961)]
60. Rupasov V I *Sov. J. Quantum Electron.* **12** 1383 (1982) [*Kvantovaya Elektron.* **9** 2127 (1982)]
61. Rosanov N N *JETP Lett.* **88** 501 (2008) [*Pis'ma Zh. Eksp. Teor. Fiz.* **88** 577 (2008)]
62. Rozanov N N *JETP* **108** 140 (2009) [*Zh. Eksp. Teor. Fiz.* **135** 154 (2009)]
63. Rosanov N N *Opt. Spectrosc.* **106** 430 (2009) [*Opt. Spektrosk.* **106** 487 (2009)]
64. Rosanov N N *Opt. Spectrosc.* **106** 609 (2009) [*Opt. Spektrosk.* **106** 680 (2009)]
65. Rosanov N N *Opt. Spectrosc.* **106** 742 (2009) [*Opt. Spektrosk.* **106** 823 (2009)]
66. Rosanov N N *Opt. Spectrosc.* **106** 901 (2009) [*Opt. Spektrosk.* **106** 989 (2009)]
67. Rosanov N N, Vysotina N V, Shatsev A N *JETP Lett.* **93** 308 (2011) [*Pis'ma Zh. Eksp. Teor. Fiz.* **93** 341 (2011)]
68. Rozanov N N *Phys. Usp.* **48** 167 (2005) [*Usp. Fiz. Nauk* **175** 181 (2005)]
69. Rosanov N N *JETP Lett.* **95** 609 (2012) [*Pis'ma Zh. Eksp. Teor. Fiz.* **95** 689 (2012)]
70. Ginzburg V L *The Propagation of Electromagnetic Waves in Plasmas* (Oxford: Pergamon Press, 1970) [Translated from Russian: *Rasprostranenie Elektromagnitnykh Voln v Plazme* (Moscow: Nauka, 1967)]
71. Vysotina N V, Rosanov N N, Shatsev A N *Opt. Spectrosc.* **112** 291 (2012) [*Opt. Spektrosk.* **112** 320 (2012)]
72. Akhiezer A I, Polovin R V *Sov. Phys. JETP* **3** 696 (1956) [*Zh. Eksp. Teor. Fiz.* **30** 915 (1956)]
73. Farina D, Bulanov S V *Phys. Rev. Lett.* **86** 5289 (2001)
74. Farina D, Bulanov S V *Phys. Rev. E* **64** 066401 (2001)
75. Kozlov V A, Litvak A G, Suvorov E V *Sov. Phys. JETP* **49** 75 (1979) [*Zh. Eksp. Teor. Fiz.* **76** 148 (1979)]
76. Lehmann G, Spatschek K H *Phys. Plasmas* **17** 072102 (2010)
77. Chian A C-L *Phys. Rev. A* **24** 2773 (1981)
78. Chakraborty B, Khan M, Bhattacharyya B *Phys. Rev. A* **28** 1047 (1983)
79. Smetanin I V et al. *Phys. Lett. A* **320** 438 (2004)
80. Gradshteyn I S, Ryzhik I M *Table of Integrals, Series, and Products* (New York: Academic Press, 1965) [Translated from Russian: *Tablitsy Integralov, Summ, Ryadov i Proizvedenii* (Moscow: Fizmatgiz, 1963)]
81. Whitham G B *Linear and Nonlinear Waves* (New York: Wiley, 1974)
82. Kadomtsev B B, Karpman V I *Sov. Phys. Usp.* **14** 40 (1971) [*Usp. Fiz. Nauk* **103** 193 (1971)]
83. Dawson J M *Phys. Rev.* **113** 383 (1959)
84. Drake J F et al. *Phys. Rev. Lett.* **36** 196 (1976)
85. Akhiezer A I et al. *Elektrodinamika Plazmy* (Electrodynamics of Plasma) (Moscow: Nauka, 1974)
86. Sengupta S et al. *Phys. Rev. E* **79** 026404 (2009)
87. Gorbunov L M et al. *Plasma Phys. Res.* **36** 345 (2010) [*Fiz. Plazmy* **36** 375 (2010)]
88. Brantov A V et al. *Phys. Plasmas* **15** 073111 (2008)
89. Tajima T, Dawson J M *Phys. Rev. Lett.* **43** 267 (1979)
90. Poston T, Stewart I *Catastrophe Theory and Its Applications* (London: Pitman, 1978) [Translated into Russian: *Teoriya Katastrof i ee Prilozheniya* (Moscow: Mir, 1980)]
91. Arnold V I *Catastrophe Theory* (Berlin: Springer-Verlag, 1986) [Translated from Russian: *Teoriya Katastrof* (Moscow: Izd. MGU, 1983)]
92. Bulanov S V, Sakharov A S *JETP Lett.* **54** 203 (1991) [*Pis'ma Zh. Eksp. Teor. Fiz.* **54** 208 (1991)]
93. Matlis N H et al. *Nature Phys.* **2** 749 (2006)
94. Ehrlich Y et al. *Phys. Rev. Lett.* **77** 4186 (1996)
95. Bobrova N A et al. *Phys. Rev. E* **65** 016407 (2002)
96. Bulanov S V et al. *Phys. Rev. Lett.* **78** 4205 (1997)
97. Pukhov A, Meyer-ter-Vehn J *Appl. Phys. B* **74** 355 (2002)
98. Kando M et al. *JETP* **105** 916 (2007) [*Zh. Eksp. Teor. Fiz.* **132** 1052 (2007)]
99. Esirkepov T Zh *Comput. Phys. Commun.* **135** 144 (2001)
100. Lamb H *Hydrodynamics* (Cambridge: The Univ. Press, 1932)
101. Meyer-Vernet N *Basics of the Solar Wind* (Cambridge: Cambridge Univ. Press, 2007)
102. Appleton P N et al. *Astrophys. J. Lett.* **639** L51 (2006)
103. Esirkepov T Zh, Kato Y, Bulanov S V *Phys. Rev. Lett.* **101** 265001 (2008)
104. Sylla F et al. *Phys. Rev. Lett.* **108** 115003 (2012)
105. Keldysh L V *Sov. Phys. JETP* **20** 1307 (1965) [*Zh. Eksp. Teor. Fiz.* **47** 1945 (1964)]
106. Davidson R C *Methods in Nonlinear Plasma Theory* (New York: Academic Press, 1972)
107. Bulanov S V et al. *Phys. Plasmas* **19** 113102 (2012); *Phys. Plasmas* **19** 113103 (2012)
108. Katsouleas T, Mori W B *Phys. Rev. Lett.* **61** 90 (1988)

109. Schroeder C B, Esarey E *Phys. Rev. E* **81** 056403 (2010)
110. Trines R M G M, Norreys P A *Phys. Plasmas* **13** 123102 (2006)
111. Solodov A A, Malkin V M, Fisch N J *Phys. Plasmas* **13** 093102 (2006)
112. Kando M et al. *Phys. Rev. Lett.* **99** 135001 (2007)
113. Pirozhkov A S et al. *Phys. Plasmas* **14** 123106 (2007)
114. Silin V P *Parametricheskoe Vozdeistvie Izlucheniya Bol'shoi Moshchnosti na Plazmu* (Parametric Effects of High-Power Radiation on the Plasma) (Moscow: Nauka, 1973)
115. Kruer W L *The Physics of Laser Plasma Interactions* (Redwood City, Calif.: Addison-Wesley, 1988)
116. Silin V P, Rukhadze A A *Elektromagnitnye Svoistva Plazmy i Plazmopodobnykh Sred* (The Electromagnetic Properties of Plasma and Plasma Environments) (Moscow: LIBROKOM, 2012)
117. Esirkepov T, Bulanov S V, Yamagiwa M, Tajima T *Phys. Rev. Lett.* **96** 014803 (2006)
118. Andreev N E, Gorbunov L M, Kuznetsov S V *IEEE Trans. Plasma Sci.* **24** 448 (1996)
119. Leemans W P et al. *Nature Phys.* **2** 696 (2006)
120. Hafz N A M et al. *Nature Photon.* **2** 571 (2008)
121. Wilks S C et al. *Phys. Rev. Lett.* **62** 2600 (1989)
122. Mironov V A et al. *Phys. Rev. A* **42** 4862 (1990)
123. Siders C W et al. *Phys. Rev. Lett.* **76** 3570 (1996)
124. Dias J M et al. *Phys. Rev. Lett.* **78** 4773 (1997)
125. Mendonça J T *Theory of Photon Acceleration* (Bristol: IOP, 2001)
126. Murphy C D et al. *Phys. Plasmas* **13** 033108 (2006)
127. Panchenko A V et al. *Phys. Rev. E* **78** 056402 (2008)
128. Berry M V *J. Phys. A Math. Gen.* **15** 3693 (1982)
129. Landau L D, Lifshitz E M *Quantum Mechanics. Non-Relativistic Theory* (Oxford: Pergamon Press, 1977) [Translated from Russian: *Kvantovaya Mekhanika. Nerelyativistskaya Teoriya* (Moscow: Nauka, 1989)]
130. Wu H-C et al. *Phys. Rev. Lett.* **104** 234801 (2010)
131. Wu H-C et al. *Phys. Rev. ST Accel. Beams* **14** 070702 (2011)
132. Scott A *Nonlinear Science. Emergence and Dynamics of Coherent Structures* 2nd ed. (Oxford: Oxford Univ. Press, 2003)
133. Naumova N et al. *Phys. Rev. Lett.* **93** 195003 (2004)
134. Popov K I et al. *Phys. Plasmas* **16** 053106 (2009)
135. Esirkepov T et al. *Phys. Rev. Lett.* **92** 175003 (2004)
136. Bulanov S S et al. *Phys. Rev. E* **78** 026412 (2008)
137. Kar S et al. *Phys. Rev. Lett.* **100** 225004 (2008)
138. Bulanov S V et al. *Phys. Rev. Lett.* **104** 135003 (2010)
139. Pegoraro F, Bulanov S V *Phys. Rev. Lett.* **99** 065002 (2007)
140. Byushgens S S *Differentsial'naya Geometriya* (Differential Geometry) (Moscow: LKI, 2008)
141. Bulanov S V et al. *Phys. Plasmas* **17** 063102 (2010)
142. Chandrasekhar S *Hydrodynamic and Hydromagnetic Stability* (Oxford: Clarendon Press, 1961)
143. Inogamov N A *Astrophys. Space Phys. Rev.* **10** 1 (1999)
144. Ott E *Phys. Rev. Lett.* **29** 1429 (1972)
145. Manheimer W, Colombant D, Ott E *Phys. Fluids* **27** 2164 (1984)
146. Mourou G A et al. (Eds) *ELI — Extreme Light Infrastructure Science and Technology with Ultra-Intense Lasers WHITEBOOK* (Berlin: THOSS Media GmbH, 2011)
147. Korzhimanov A V et al. *Phys. Usp.* **54** 9 (2011) [*Usp. Fiz. Nauk* **181** 9 (2011)]
148. Dunne M *Nature Phys.* **2** 2 (2006)
149. Palmer C A J et al. *Phys. Rev. Lett.* **108** 225002 (2012)
150. Milant'ev V P *Phys. Usp.* **40** 1 (1997) [*Usp. Fiz. Nauk* **167** 3 (1997)]
151. Katsouleas T, Dawson J M *Phys. Rev. Lett.* **51** 392 (1983)
152. Bulanov S V, Sakharov A S *JETP Lett.* **44** 543 (1986) [*Pis'ma Zh. Eksp. Teor. Fiz.* **44** 421 (1986)]
153. Dieckmann M E, Bret A, Shukla P K *New J. Phys.* **10** 013029 (2008)
154. Kichigin G N *JETP* **92** 895 (2001) [*Zh. Eksp. Teor. Fiz.* **119** 1038 (2001)]
155. Hartemann F V, Siders C W, Barty C P J *Phys. Rev. Lett.* **100** 125001 (2008)
156. Rozanov N N *JETP* **76** 991 (1993) [*Zh. Eksp. Teor. Fiz.* **103** 1996 (1993)]
157. Rozanov N N *JETP* **86** 284 (1998) [*Zh. Eksp. Teor. Fiz.* **113** 513 (1998)]
158. Kando M et al. *Phys. Rev. Lett.* **103** 235003 (2009)
159. Kawase K et al. *Appl. Phys. Express* **3** 016101 (2010)
160. Zel'dovich Ya B *Sov. Phys. Usp.* **18** 79 (1975) [*Usp. Fiz. Nauk* **115** 161 (1975)]
161. Zhidkov A et al. *Phys. Rev. Lett.* **88** 185002 (2002)
162. Bulanov S V et al. *Plasma Phys. Rep.* **30** 196 (2004) [*Fiz. Plazmy* **30** 221 (2004)]
163. Di Piazza A et al. *Rev. Mod. Phys.* **84** 1177 (2012)
164. Breit G, Wheeler J A *Phys. Rev.* **46** 1087 (1934)
165. Nikishov A I, Ritus V I *Sov. Phys. Usp.* **13** 303 (1970) [*Usp. Fiz. Nauk* **100** 724 (1970)]
166. Ritus V I *Tr. Fiz. Inst. Akad. Nauk SSSR* **111** 5 (1979)
167. Bell A R, Kirk J G *Phys. Rev. Lett.* **101** 200403 (2008)
168. Fedotov A M et al. *Phys. Rev. Lett.* **105** 080402 (2010)
169. Bulanov S S et al. *Phys. Rev. Lett.* **105** 220407 (2010)
170. Sauter F *Z. Phys.* **69** 742 (1931)
171. Heisenberg W, Euler H *Z. Phys.* **98** 714 (1936)
172. Schwinger J *Phys. Rev.* **82** 664 (1951)
173. Berestetskii V B, Lifshitz E M, Pitaevskii L P *Quantum Electrodynamics* (Oxford: Butterworth-Heinemann, 1999) [Translated from Russian: *Kvantovaya Elektrodinamika* (Moscow: Nauka, 1980)]
174. Bamber C et al. *Phys. Rev. D* **60** 092004 (1999)
175. Bisnovatyi-Kogan G S, Zel'dovich Ya B, Syunyaev R A *JETP Lett.* **12** 45 (1970) [*Pis'ma Zh. Eksp. Teor. Fiz.* **12** 64 (1970)]
176. Wilks S C et al. *Astrophys. Space Sci.* **298** 347 (2005)
177. Cowan T E et al. *Laser Part. Beams* **17** 773 (1999)
178. Chen H et al. *Phys. Rev. Lett.* **105** 015003 (2010)
179. Yanovsky V et al. *Opt. Express* **16** 2109 (2008)
180. Remington B A, Drake R P, Ryutov D D *Rev. Mod. Phys.* **78** 755 (2006)
181. Bulanov S V et al. *Nucl. Instrum. Meth. Phys. Res. A* **660** 31 (2011)